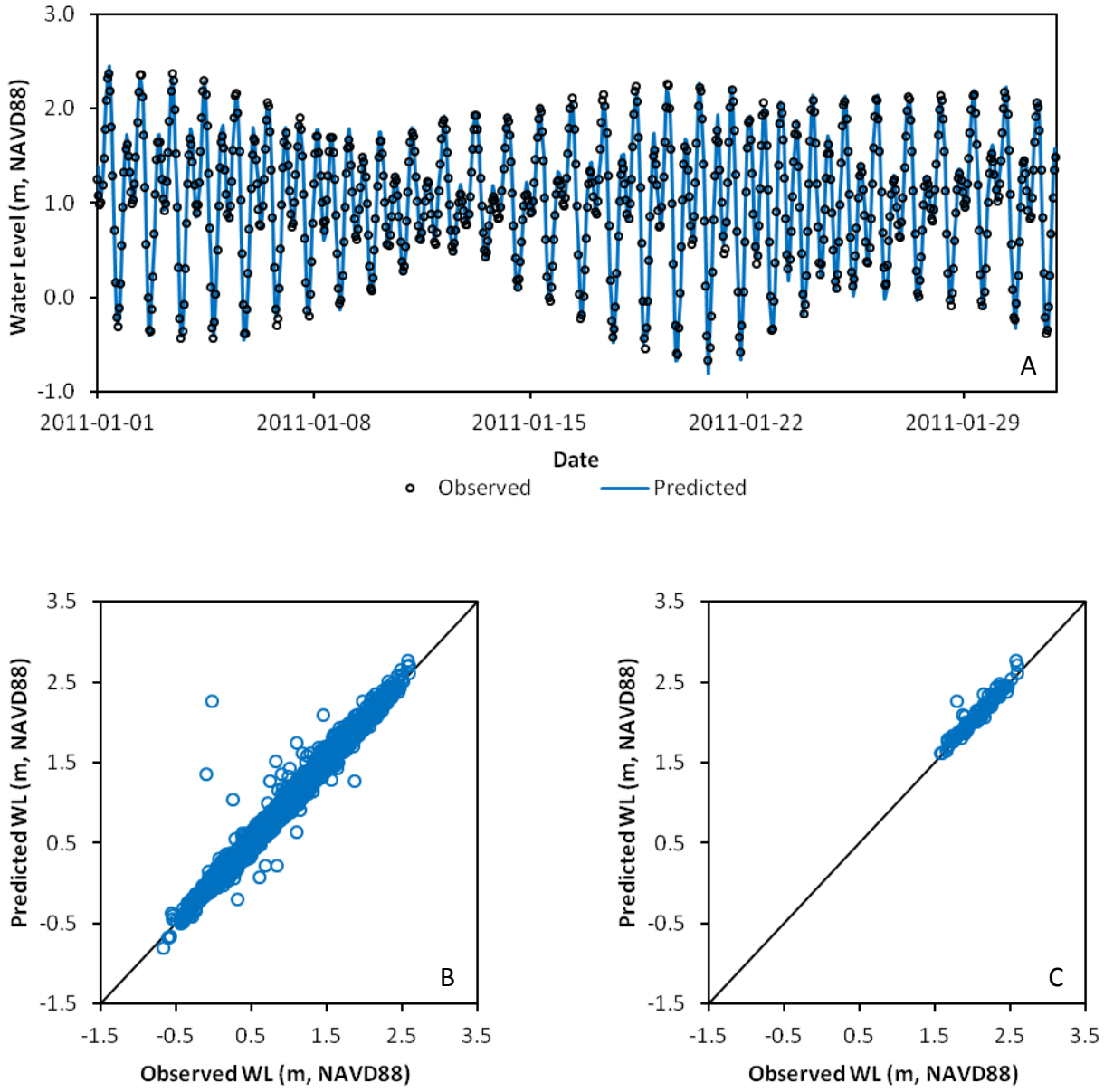

Figure 5-4 Time series and correlation plots of observed and predicted water levels (WL) for Fields Landing NOAA tide gauge (9418723). Tidal observations were from NOAA and were adjusted for vertical land motion (VLM) estimates (Table 5-1). Plot A is a time series for January 2011, plot B is the correlation between predicted and observed hourly water levels, and plot C is the correlation between predicted and observed daily maximum water levels. The data points that significantly deviate from the 1:1 line in the correlation plots are associated with tsunami events in the North Spit and Crescent City tidal records.

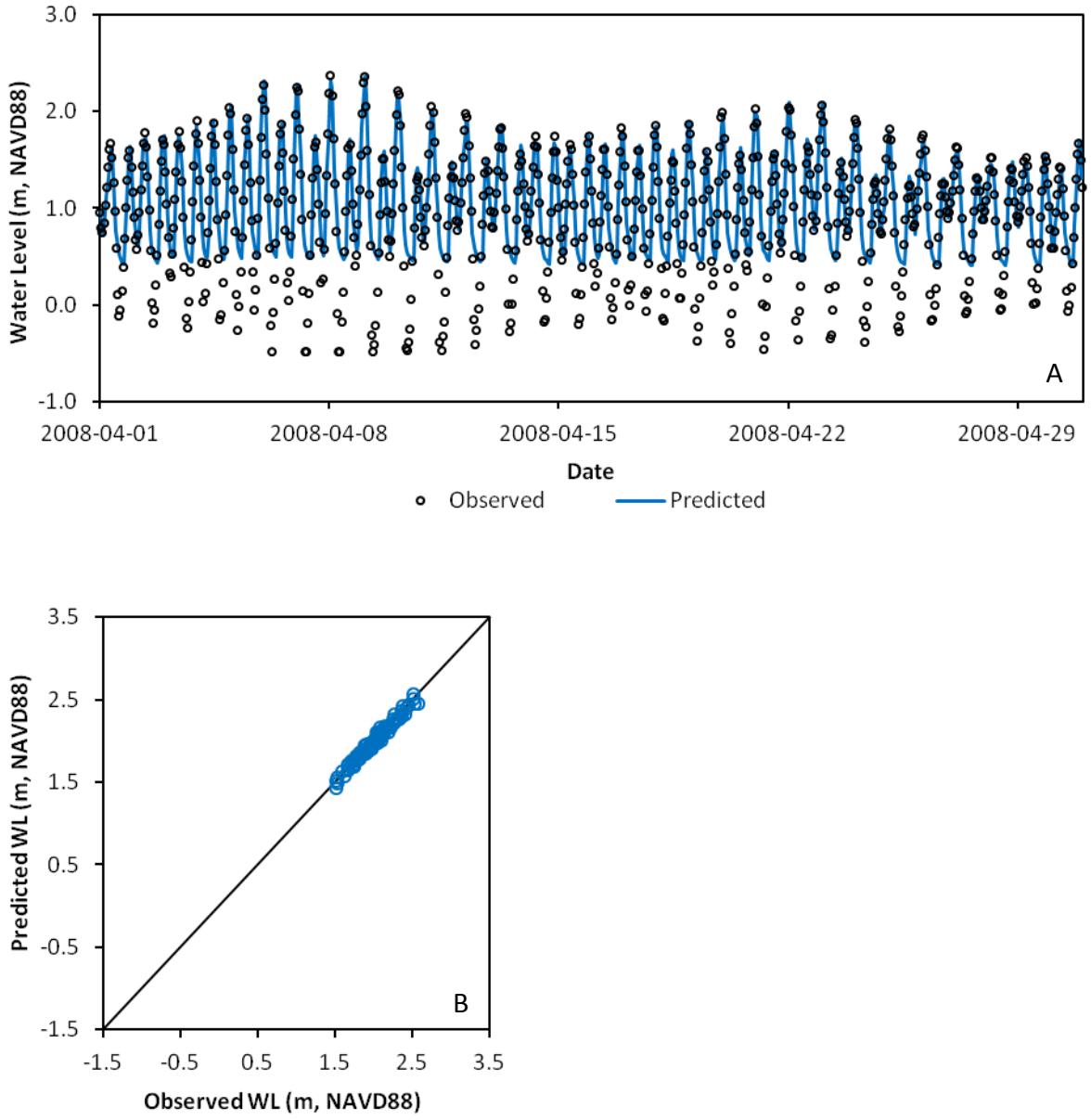

Figure 5-5 Time series and correlation plot of observed and predicted water levels (WL) for Mad River Slough NOAA tide gauge (9418865). Tidal observations were from NHE and CG (2013) and were adjusted for vertical land motion (VLM) estimates (Table 5-1). Plot A is a time series for April 2008, and plot B is the correlation between predicted and observed daily maximum water levels. The 2D model grid resolution did not allow for a full simulation of the tidal range, and an hourly water level correlation was not provided for this gauge.

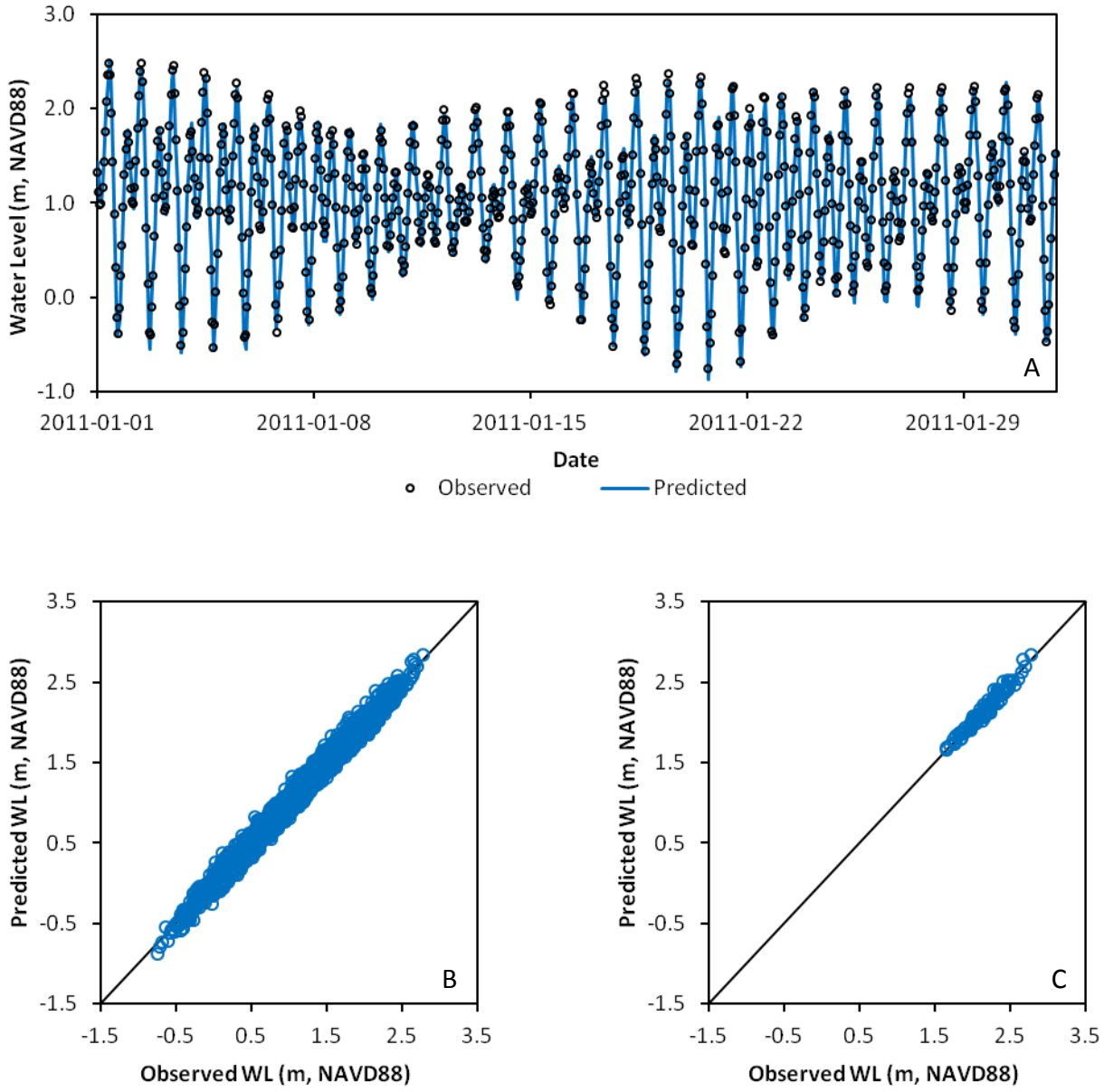

Figure 5-6 Time series and correlation plots of observed and predicted water levels (WL) for Samoa NOAA tide gauge (9418817). Tidal observations were from NOAA and were adjusted for vertical land motion (VLM) estimates (Table 5-1). Plot A is a time series for January 2012, plot B is the correlation between predicted and observed hourly water levels, and plot C is the correlation between predicted and observed daily maximum water levels.

6 Sea Level Rise Inundation Vulnerability Mapping

This section summarizes the development of the Humboldt Bay inundation vulnerability mapping conducted for this study. Five SLR scenarios were assessed (Table 4-6 and Figure 4-6); Year 2012 existing sea levels and half-meter increments of 0.5, 1.0, 1.5 and 1.5-m SLR above year 2000. The inundation vulnerability maps show areas surrounding Humboldt Bay that are vulnerable to inundation from existing and future sea levels. The purpose of the inundation vulnerability maps is to provide supporting information for Humboldt Bay sea level rise vulnerability and adaptation planning efforts in a user-friendly format.

The inundation maps indicate areas vulnerable to inundation, not areas that are currently inundated. The inundation maps show areas surrounding Humboldt Bay landward of Mean High Water (MHW) that are vulnerable to existing and future sea levels and are currently protected from inundation by the bay's shoreline (e.g. natural shoreline, levees, road and railroad grades, or other barriers). MHW was chosen as the water level to define the boundary between areas currently inundated and areas vulnerable to inundation.

Post-Processing 2D Hydrodynamic Model Results

Each of the five 100-yr long SLR scenarios (Table 4-6) were modeled with the Humboldt Bay 2D hydrodynamic model. For each SLR scenario, predicted water levels (in meters, referenced to NAVD88) were output every 15-minutes for the 100-yr simulation at each grid cell within the model domain. Approximately 5.47 billion data points of 15-min water levels were generated over the entire model domain for each 100-yr simulation. A flowchart of the general modeling procedure for each 100-yr long SLR scenario is shown in Figure 6-1.

Data post-processing for each SLR scenario consisted of multiple analyses using Excel and Visual Basic for Application (VBA) programs. The general data processing steps for each 100-yr long SLR scenario are as follows:

1. A 100-yr long hourly water level record was created at each grid cell from the predicted 100-yr 15-min water level results.
2. Estimates of mean higher high water (MHHW), mean monthly maximum water (MMMW) and mean annual maximum water (MAMW) were determined at each grid cell using the entire 100-yr hourly water level record.
3. A 100-yr annual maximum series was created at each grid cell from the predicted 100-yr 15-min water level results.
4. Probabilities of exceedance of extreme high water level events were generated at each grid cell using a generalized extreme value (GEV) analysis on the 100-yr annual maximum series.
5. All post-processed water level results for each grid cell from steps 2 and 4 were compiled into a single data file for each 100-yr long SLR scenario.

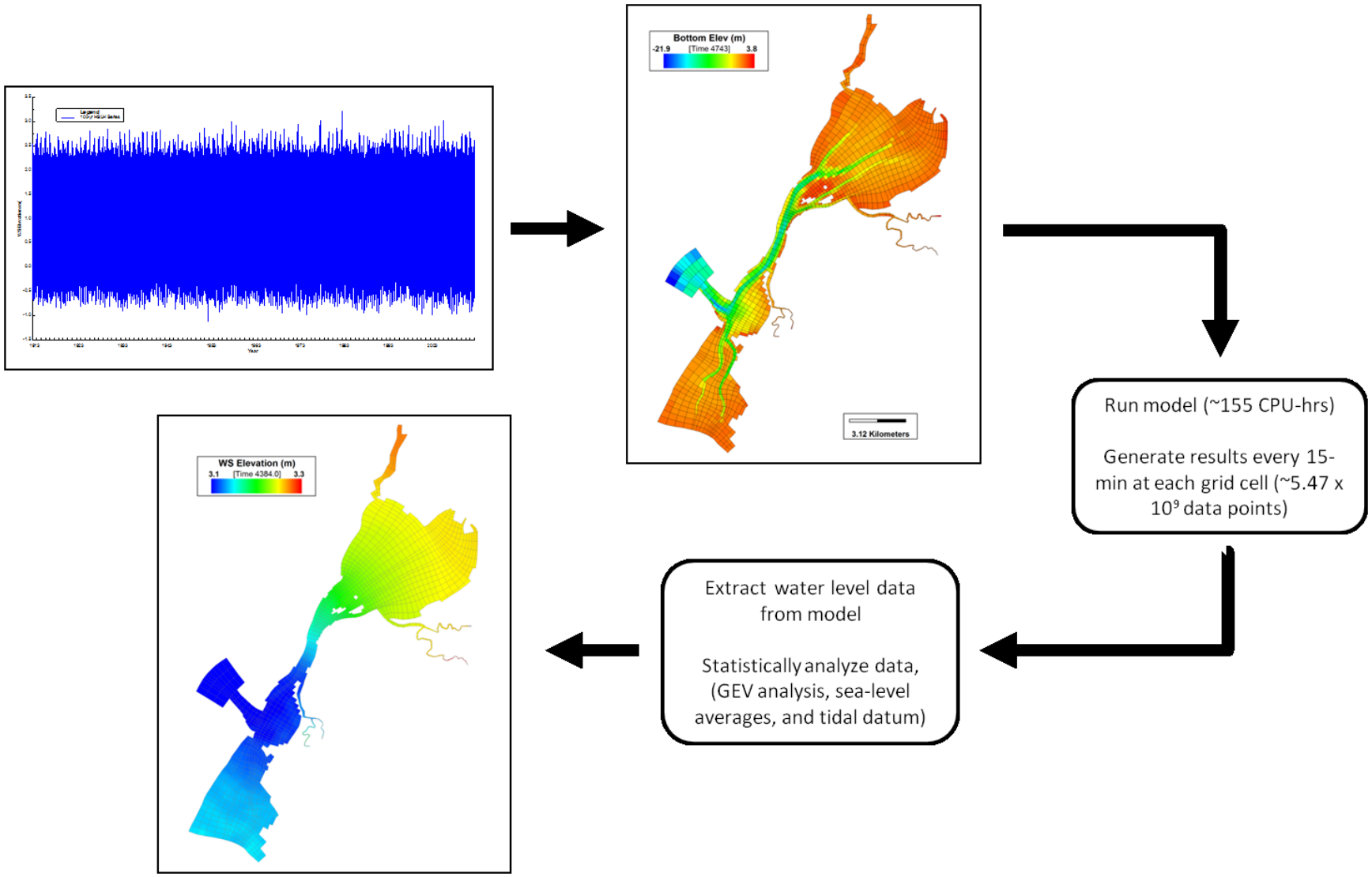

Figure 6-1 General hydrodynamic modeling procedure for each 100-yr long SLR scenario.

6. The post-processed water levels for MHHW, MMMW, MAMW, and the 10-yr and 100-yr extreme high water level events for each simulated 100-yr long SLR scenario was remapped onto the model grid and model grid boundary using EFDC_Explorer7.1. A water surface elevation points file containing the northing, easting, and water surface elevation (x,y,z) was generated at the model grid centroids and the model grid boundary.

Figure 6-2 shows the resulting 100-yr water surface elevations in Humboldt Bay for Year 2012 existing sea levels.

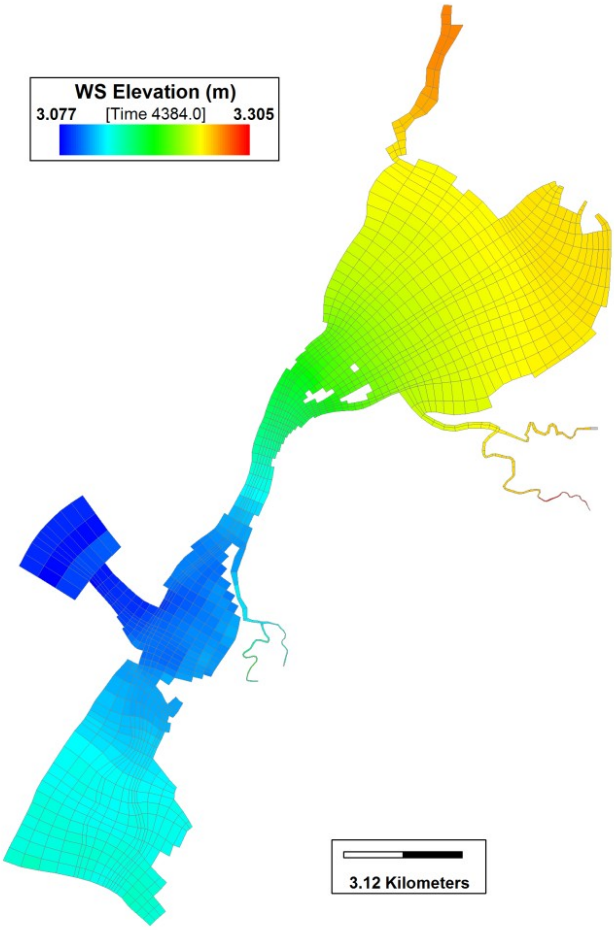

Figure 6-2 Predicted 100-yr extreme high water surface elevations in Humboldt Bay for Year 2012 existing sea levels.

Inundation Vulnerability Mapping

Mapping of areas surrounding Humboldt Bay vulnerable to inundation from each 100-yr long SLR scenario (Table 4-6 and Figure 4-6) were developed for MHHW, MMMW, MAMW, and the 10-yr and 100-yr extreme high water level events. The inundation maps were generated

using ArcGIS. A flowchart of the general inundation mapping procedure is shown in Figure 6-3 and summarized as follows:

1. The Humboldt Bay project DEM (PWA, 2014) was input into ArcGIS.
2. A line was created along the 7-m contour and densified with points approximately every 137 m (7-m line).
3. A line representing the model grid boundary was created, and densified with points approximately every 137 m (model-boundary line).
4. The water surface elevation point files generated in Step 6 of the hydrodynamic model post-processing were input into ArcGIS, and a triangulated irregular network (TIN) was created from the points. The TIN was then clipped along the model-boundary line.
5. Water surface elevations were then mapped horizontally to the 7-m line from the closest points within the TIN created in Step 4.
6. A new water surface elevation TIN (inundation TIN) was created from the 7-m line from Step 5 and the original TIN from Step 4.
7. The inundation TIN from Step 6 and the Humboldt Bay DEM were differenced using the ArcGIS Spatial Analyst cut/fill routine. The resulting fill polygons represented the raw inundation polygons.
8. Within ArcGIS, the raw inundation polygons were cleaned, then aggregated (joined) with a 2-m tolerance, and then generalized with a 5-m tolerance to create the final inundation polygons.
9. The inundation polygons from Step 8 were then clipped to the Humboldt Bay MHW polygon (the MHW polygon is described below) to remove areas currently inundated below MHW. The resulting polygons represent the areas vulnerable to inundation, landward of the MHW line.
10. The final step was to create the inundation map coverages. Inundation shapefiles and kmz files were created from the final inundation polygons. The horizontal projection of the inundation maps is UTM Zone 10, WGS84.

By repeating steps 4 through 10, twenty-five separate inundation vulnerability maps were created for MHHW, MMMW, MAMW, and the 10-yr and 100-yr recurrence interval extreme high water level events for each 100-yr long SLR scenario. The twenty-five inundation maps were provided as both kmz and shapefiles. The raw inundation polygons from Step 7 above are available upon request from NHE. Figure 6-4 shows the 100-yr extreme high water level inundation for Year 2012 existing sea levels, and the 2.0-m SLR scenario.

In summary, the inundation vulnerability maps represent areas surrounding Humboldt Bay, landward of MHW, that are vulnerable to inundation from existing and future sea levels, but are currently protected from inundation by the bay's shoreline.

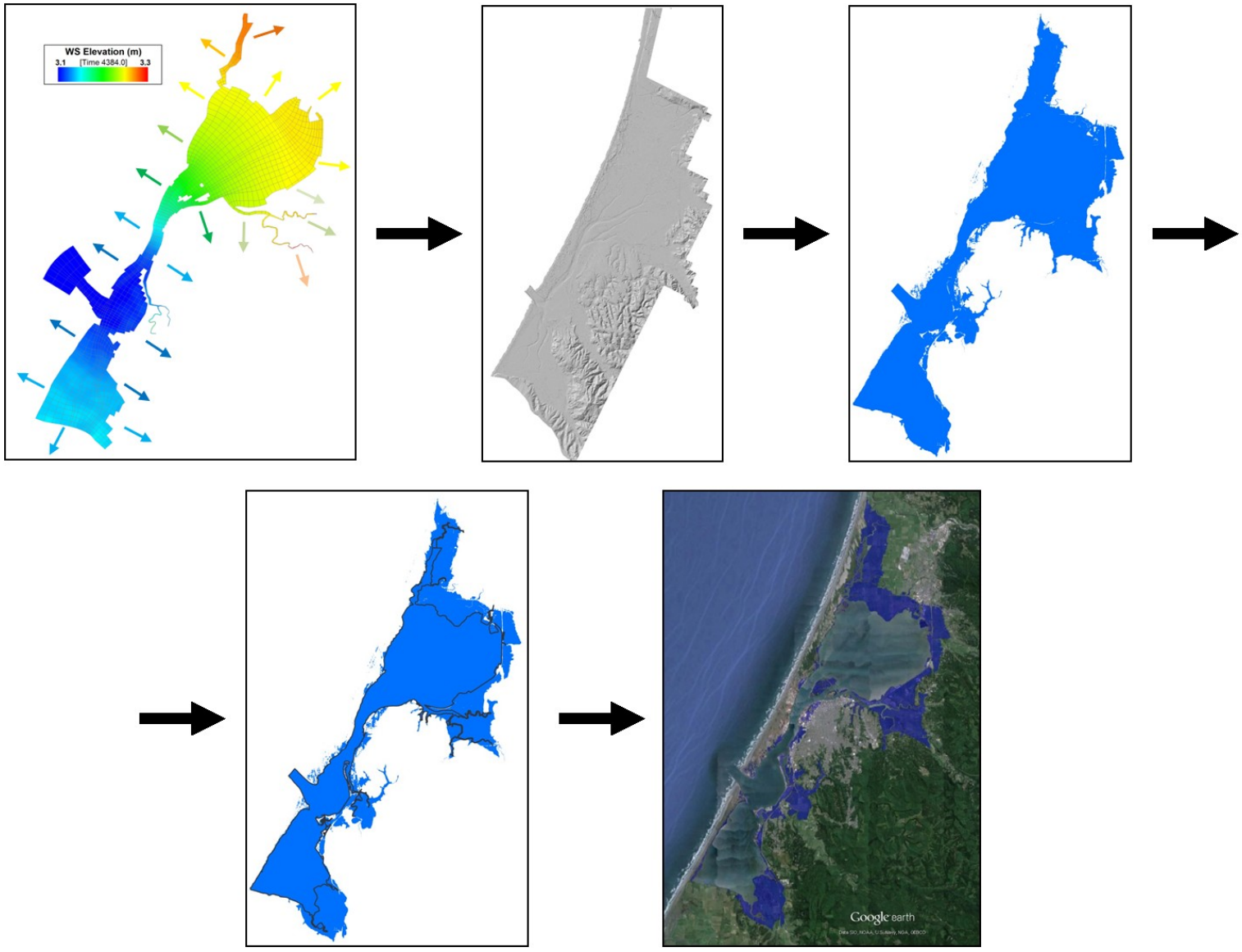

Figure 6-3 General Inundation mapping procedure for each mapped water level from the 100-yr long SLR scenarios.

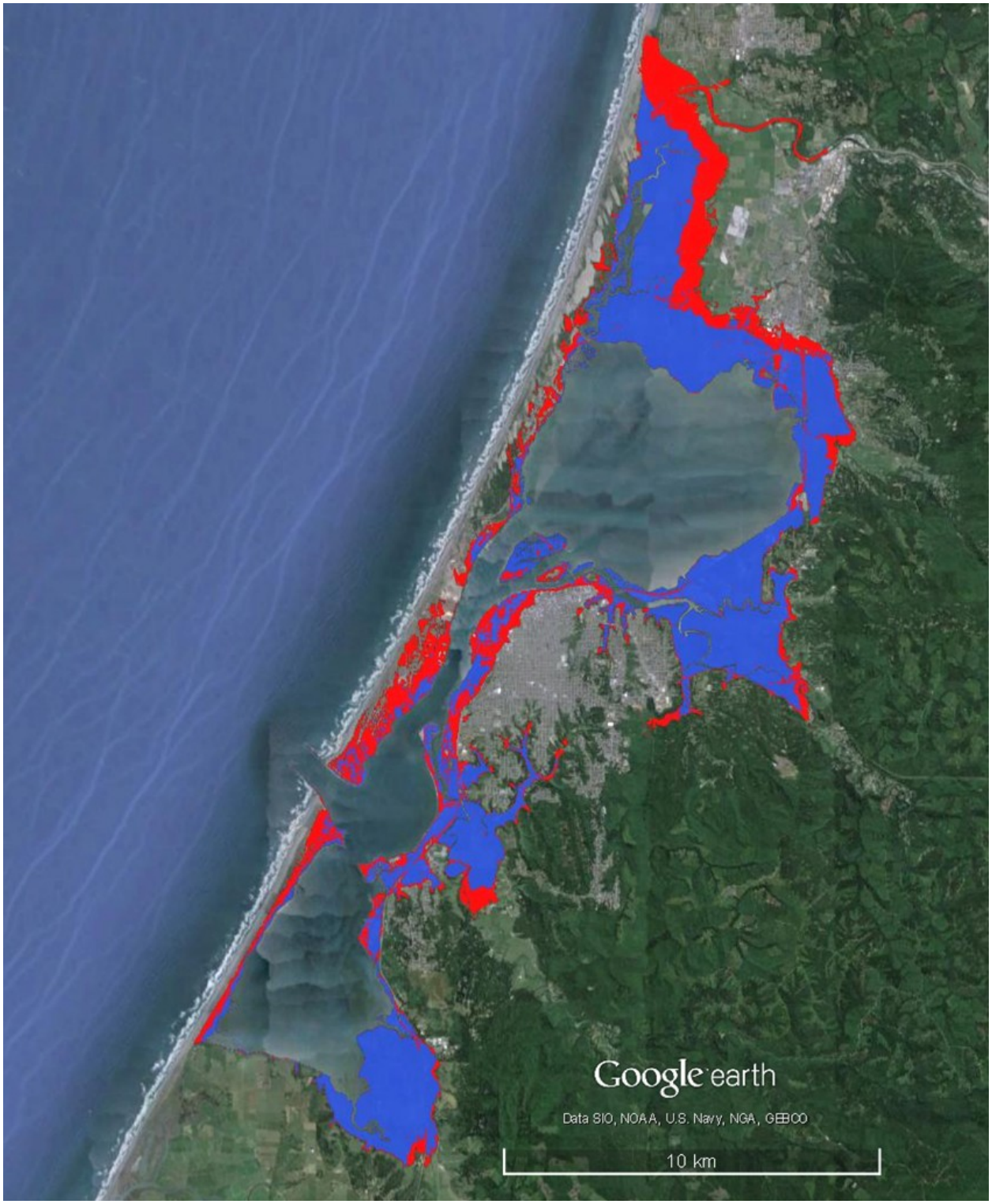

Figure 6-4 Areas surrounding Humboldt Bay vulnerable to inundation from 100-yr extreme high water levels for Year 2012 existing sea levels (blue) and 2.0-m sea level rise scenario (red).

Humboldt Bay Year 2012 Mean High Water Map

A MHW map was not available for Humboldt Bay. Consequently, a MHW map of Humboldt Bay was produced for the inundation mapping and made available as part of this project. The MHW map was created by subtracting the average difference (21.7 cm) between MHHW and MHW for all NOAA tide gauges in Humboldt Bay (Table 6-1), from the MHHW water levels at each grid cell generated for the year 2012 existing sea levels simulation. The resulting MHW grid cell water levels were then mapped to the Humboldt Bay project DEM, and MHW polygons were created following a similar procedure as the inundation mapping outlined above. The MHW polygons were provided as both shapefiles and kmz files. The developed Humboldt Bay MHW coverage (Figure 6-5) coincides well with the Laird (2013) mapped shoreline file.

Table 6-1 Humboldt Bay NOAA tide gauges Mean Higher High Water(MHHW) and Mean High Water (MHW) tidal datum for 1983-2001 National Tidal Datum Epoch.

NOAA Tide Gauge	Mean Higher High Water (cm, STND)	Mean High Water (cm, STND)	Difference (cm)
Bucksport	287.3	264.9	22.4
Eureka	615.5	595.1	20.4
Fields Landing	264.3	242.6	21.7
Freshwater Slough	240.1	218.2	21.9
Hookton Slough	284.6	262.5	22.1
Mad River Slough	284.7	262.6	22.1
North Spit	652.4	630.7	21.7
Red Bluff	311.3	289.8	21.5
Samoa	276.7	254.8	21.9
Upper Mad River Slough	550.1	528.3	21.8
Average Difference			**21.7**

Figure 6-5 Humboldt Bay Mean High Water (MHW) shoreline coverage for Year 2012 existing sea levels developed to support inundation vulnerability mapping.

Inundation Vulnerability Mapping Distribution Files

The inundation vulnerability maps for each 100-yr long SLR scenario were provided as kmz files, which can be opened in Google Earth, and shapefiles, which can be imported into GIS software such as ArcGIS. Also included as a kmz file and shapefile was the MHW shoreline for Humboldt Bay, which shows areas of the bay currently inundated below MHW.

The inundation maps and MHW shoreline kmz files and shapefiles were provided in a file structure with individual folders named for each SLR scenario or shoreline, and contained within a separate folder for the kmz files or shapefiles. For example, the folder named YEAR2000+0.5MSLR_140326 within the folder named Generalized_KMZ_Files contains the separate inundation map kmz files for the Year 2000 + 0.5 m SLR scenario generated on 26 March 2014. Each individual inundation map file name contains the SLR scenario, corresponding inundation water level, and the date of production. For example, file YEAR2000+0.5MSLR_10YR_140326.kmz is the 10-year recurrence interval extreme high water level inundation for the Year 2000 + 0.5 m SLR scenario, and was generated on 26 March 2014.

The inundation files may be updated in the future, so users should check to make sure they have the most updated version of the inundation maps. All inundation maps have the date of production in the file name so that it is clear when an update occurs. It will be left to the user to ensure that the most recent version of the inundation maps is used.

7 Discussion

This section provides a general discussion pertaining to the Humboldt Bay sea level rise modeling and inundation vulnerability mapping conducted in this study, specifically with regards to limitations of the inundation vulnerability mapping, modeling approach, estimated or predicted water levels resulting from SLR, areas vulnerable to inundation, and the developed inundation vulnerability maps. The 100-yr HSLH series and the 2D model water level predictions are discussed in detail in Section 4 and Section 5, respectively.

The Humboldt Bay EFDC 2D hydrodynamic model was developed to predict water levels over a 100-yr long period (1913-2012) in Humboldt Bay for five SLR scenarios. The 2D model was forced by a 100-yr HSLH series, adjusted for each SLR scenario. Modeling results indicate that the 2D model predicts observed water levels in Humboldt Bay reasonably well. Estimates of average water levels (MHHW, MMMW and MAMW) and annual extreme high water level events (e.g. 10- and 100-yr events) were determined from the 100-yr long record of predicted water levels at each grid cell for each SLR scenario. Inundation maps of areas surrounding Humboldt Bay, vulnerable to inundation from Year 2012 existing sea levels and SLR rise scenarios of 0.5, 1.0, 1.5 and 2.0-m, were developed for MHHW, MMMW, MAMW, and the 10- and 100-year recurrence interval extreme high water level events.

Inundation Vulnerability Map Limitations

The inundation vulnerability maps developed for this study identify areas surrounding Humboldt Bay landward of existing MHW that are currently vulnerable to tidal inundation, and areas that are vulnerable to future sea levels. Most of the areas vulnerable to inundation from future SLR are currently protected from inundation by some type of shoreline barrier, such as levees or railroad and road grades, which would only be inundated if these barriers were overtopped or breached. The inundation vulnerability maps identify areas surrounding Humboldt Bay and its adjoining tributary and slough channels where ground elevations are below the adjacent water surface elevations for MHHW, MMMW, MAMW and the 10- and 100-yr extreme high water level events predicted from the 2D model.

The 2D model was driven solely by the 100-yr HSLH series and did not account for internally-generated wind wave effects on water levels in Humboldt Bay, which could raise or lower predicted water levels. The 2D model did not account for tributary flooding, which could increase predicted water levels in the local vicinity of the tributaries. Furthermore, the hydrodynamics of water flooding across the vulnerable areas, such as a levee breach, were not accounted for in the modeling, which could raise or lower predicted water levels in these areas. Incorporating tributary flooding, wind wave effects, and lateral flooding into the hydrodynamic model was beyond the scope and funding of this project, but could be included in future efforts.

All inundation maps assume that the Humboldt Bay project DEM (PWA, 2014) ground elevations remain fixed in time, relative to the acquisition date and processing of each individual topographic/bathymetric data set, and any data point adjustments to the DEM made during development. The effects of erosion, sediment and organic material accretion, subsidence, or VLM, all of which could raise or lower ground surfaces and change the inundation footprint over time, have not been included in this study.

Humboldt Bay Predicted Water Levels for Existing and Future Sea Levels

Hydrodynamic Model and Ocean Boundary Condition

To account for the observed sea level height variability in the Humboldt Bay region, the 2D model was driven by a 100-yr HSLH series (developed for Crescent City tide gauge) that was detrended to remove the effects of SLR and VLM (see Section 4). The Crescent City tide gauge had a much longer period of record than the North Spit gauge (Table 4-1). The detrended series represented a stationary 100-yr HSLH series, relative to the middle of the current 1983-2001 NTDE (midnight on 2 July 1992), retaining the sea level height variability observed at the Crescent City tide gauge.

Due to the inherent uncertainty in predicting future SLR rates, the 2D modeling, analysis, and resulting inundation mapping conducted for this study did not use a SLR projection for a specified time period (e.g. NRC (2012)), but instead modeled SLR scenarios by adjusting the entire stationary 100-yr HSLH series by fixed elevation increases, or "steps". Each modeled SLR scenario created a 100-yr long record of predicted water levels within Humboldt Bay relative to year 2000. Since the 100-yr HSLH series boundary condition accounted for the long-term sea level height variability at the Crescent City tide gauge, and was stationary relative to each SLR scenario, the 100-yr period of predicted water levels could directly be used to estimate average water levels (e.g. MHHW) and extreme high water level events (e.g. 100-yr event) at each model grid cell within Humboldt Bay. This general modeling approach provided a robust set of water level predictions associated with each simulated SLR scenario that were not tied to the specific timeline of a SLR projection.

SLR Scenarios and SLR Projections

The SLR scenarios modeled in this study were not tied to a SLR projection timeline, however, the SLR scenarios were developed in the context of published SLR projections. Projections of SLR are typically referenced to a start time. For example, the NRC (2012) SLR projections are relative to year 2000. The SLR scenarios developed for this study were relative to year 2000 (Table 4-6 and Figure 4-6), so that comparisons could be made with the NRC (2012) SLR projections, or other projections with a year 2000 base date. To adjust the SLR scenarios relative to year 2000, the 100-yr HSLH series was adjusted from the middle of the current 1983-2001 NTDE (midnight on 2 July 1992) to year 2000 by adding 1.82 cm, using the ReMSL rise rate of 2.28 mm/yr (Burgette et al., 2009) applied over 8 years.

The only SLR scenario assessed in this study tied to a specific year was the year 2012 existing sea levels scenario, which was developed to represent current conditions in Humboldt Bay for 100-yr long water level predictions and inundation vulnerability mapping. The Year 2012 existing sea levels scenario was adjusted from year 2000 to 2012 by adding 2.74 cm, using the ReMSL rise rate of 2.28 mm/yr over 12 years (Table 4-6).

Figure 7-1 shows the five SLR scenarios compared to the range of modified NRC (2012) SLR projections for Humboldt Bay (refer to Chapter 2 for discussion of the modified NRC (2012) SLR projections). The SLR projections trend through specific years between 2000 and 2100. In contrast, the half-meter SLR increments are not targeted to specific years and can be applied to any year within the 2000 to 2100 period, or beyond. For example, the 2.0-m SLR scenario is above the highest modified NRC (2012) SLR projection estimate at year 2100.

Humboldt Bay Relative Sea Level Rise Rates

Relative or local sea level (RSL) rise represents the combined effects of GMSL or ReMSL rise and VLM at a specific tide gauge. Due to the observed downward VLM, Humboldt Bay has the highest reported RSL rise rates (Table 2-3) on the west coast of the United States (Patton et al., 2014). For example, RSL rise rates for Mad River Slough, North Spit, and Hookton Slough are approximately 3.4, 4.6 and 5.8 mm/yr, respectively.

The VLM in Humboldt Bay significantly increases the RSL rise rates above the ReMSL rise rate of 2.28 mm/yr, with both the North Spit and Hookton Slough RSL rates being more than twice the ReMSL rate. These higher RSL rise rates indicate that the global rise in sea levels will affect Humboldt Bay faster than other parts of U.S. west coast; and within the bay, the south end will be affected sooner than the north end.

Incorporating VLM into the SLR modeling was beyond the scope of this project and may not be currently feasible with the available data. However, the Humboldt Bay project DEM ground elevations used for the SLR modeling and inundation vulnerability mapping remained fixed in time relative to acquisition dates and processing as discussed previously. The predicted water levels and inundation mapping for the SLR scenarios can therefore be considered to represent the combined effect of SLR and VLM. For example, the 0.5-m SLR scenario inundation map represents the inundation footprint of a combined 0.5 m of SLR and VLM. Based on the varying rates of VLM across the bay, the 0.5-m SLR scenario inundation footprint occurs non-uniformly at a point in time due to the different VLM rates in Humboldt Bay.

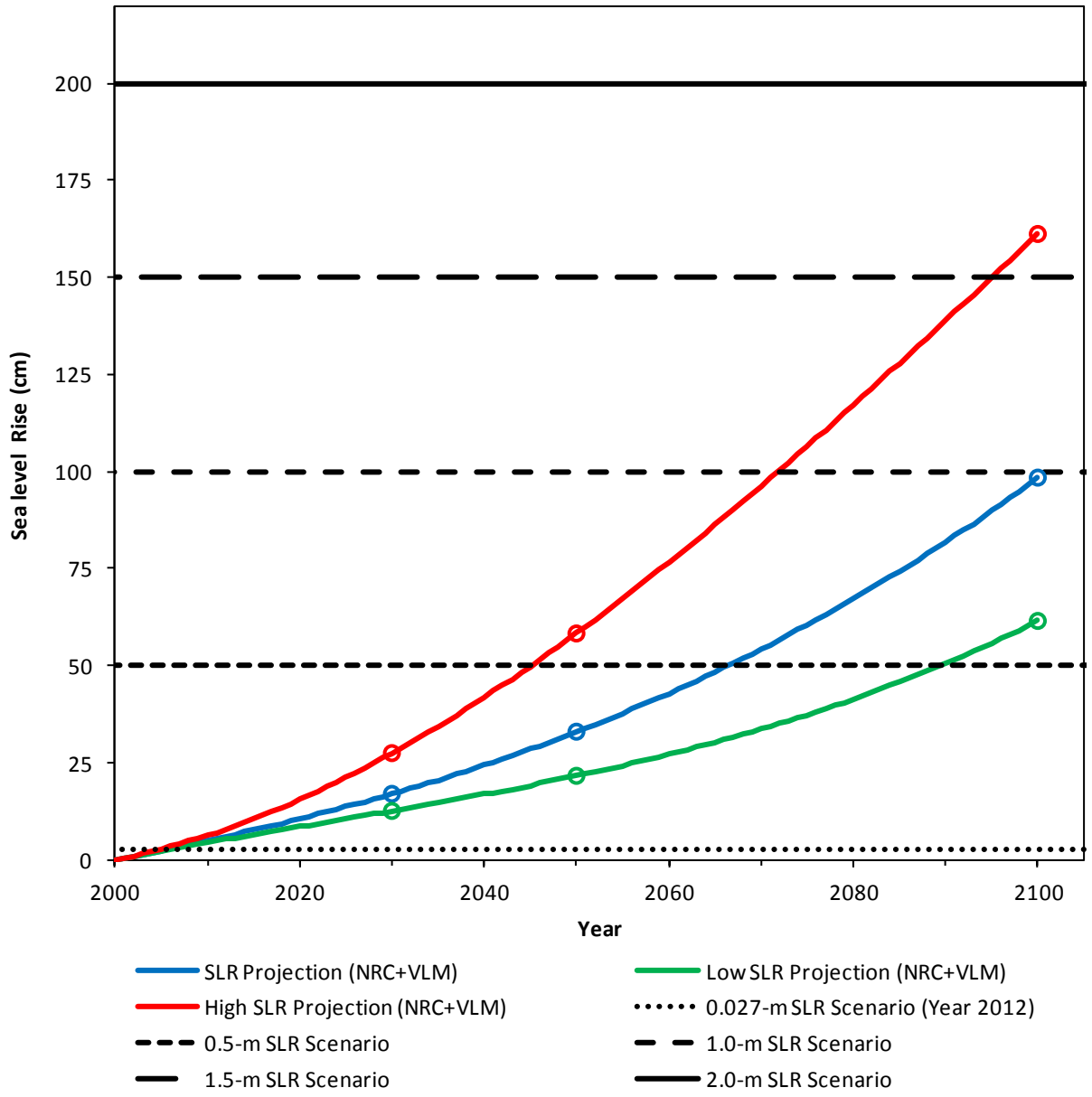

Figure 7-1 Humboldt Bay SLR scenarios used in this study compared to the modified NRC (2012) SLR projections for Humboldt Bay. The NRC projections were adjusted to account for the North Spit VLM rate of -2.33 mm/yr (Patton et al, 2014).

Effects of SLR on Humboldt Bay Predicted Water Levels

Similar to Knowles (2010), bay-wide average water levels were predicted for each SLR scenario to demonstrate the range of bay water levels relative to existing sea levels, and the effect of SLR during extreme high water level events in Humboldt Bay. Figure 7-2 shows the bay-wide

average MHHW, MMMW, MAMW and the extreme high water level events for Year 2012 existing sea levels, including an average mean sea level (MSL) estimate. The MSL estimate was determined from the MSL tidal datum (1983-2001 NTDE) reported for all the NOAA tide gauges in Humboldt Bay, and adjusted to year 2012 by adding 4.56 cm, using the 2.28 mm/yr ReMSL rise rate over 20 years.

The SLR projections estimate how MSL will change as sea levels increase. However, extreme sea level events are the cause of most damage to the California coast (Cayan et al., 2008; NRC, 2012), making it critical to understand the effects of SLR on extreme events. Figure 7-2 demonstrates the importance of considering extreme events when planning for SLR, compared to using average water levels such as MHHW. For example, the 100-yr extreme event is approximately 2 meters higher than MSL, 1 meter higher than MHHW, and 0.5 meter higher than MAMW. Furthermore, the 2-yr extreme event is approximately equal to MAMW, and the 1-yr event is only slightly greater than MMMW, showing how, on average, the more frequent extreme events are related to average water levels in the bay.

Figure 7-3 shows the predicted bay-wide average extreme high water level events for Year 2012 existing sea levels, and the half-meter increment SLR scenarios of 0.5, 1.0, 1.5 and 2.0-m relative to year 2000. Over time, SLR increases the extreme high water level events. Furthermore, as sea levels rise, the frequency of inundation of fixed water levels increases. For example, the 1.1-yr extreme event under the 0.5-m SLR scenario relative to year 2000, is approximately equal to the 100-yr event today, which is consistent with Knowles (2009) SLR study in San Francisco Bay.

To put this into perspective for Humboldt Bay, since 1912 the bay has seen approximately 46 cm of sea level rise using the North Spit RSL rise rate of 4.6 mm/yr applied over 100 years. Therefore, what was a 100-yr extreme event in 1912 is today about the 1-yr event, or about the monthly average high tide (Figure 7-2). Using Hookton Slough RSL rise rate of 5.8 mm/yr, it would only take approximately 85 years for the 100-yr event to equal the 1-yr event. This helps to explain why many Humboldt Bay levees are currently so vulnerable to overtopping by high water level events (Laird, 2013), as many of the bay's levees were constructed in the early 1900s.

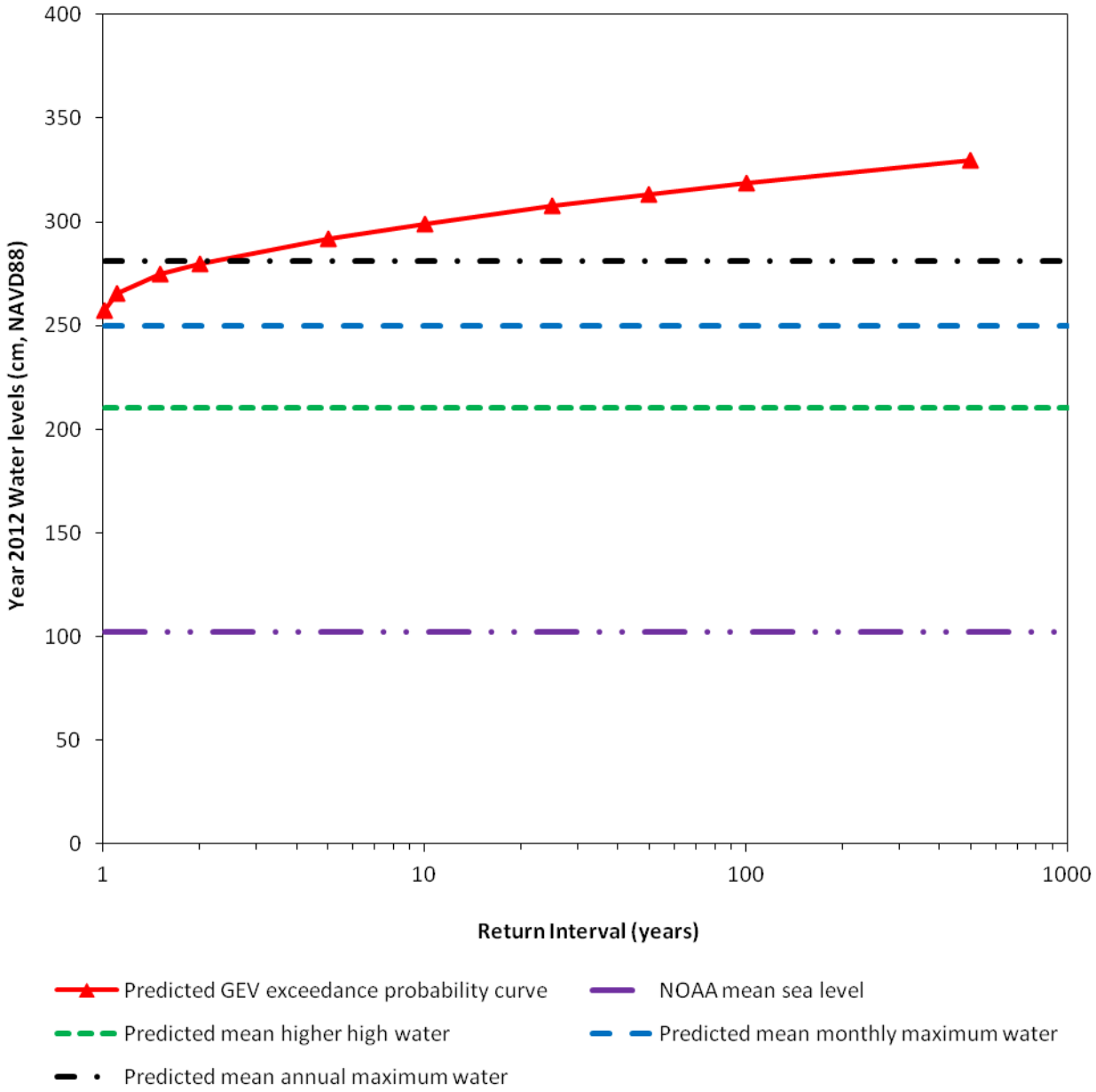

Figure 7-2 Humboldt Bay Year 2012 existing sea levels scenario bay-wide average water levels. The generalized extreme value (GEV) probability curve, mean higher high water, mean monthly maximum water, and mean annual maximum water are from 2D model predictions. Mean sea level is the average of all Humboldt Bay NOAA tide gauges mean sea level tidal datum (1983-2001 NTDE) adjusted to year 2012 by adding the 2.28 mm/yr ReMSL rise rate (Burgette et al., 2009) over 20 years (4.56 cm).

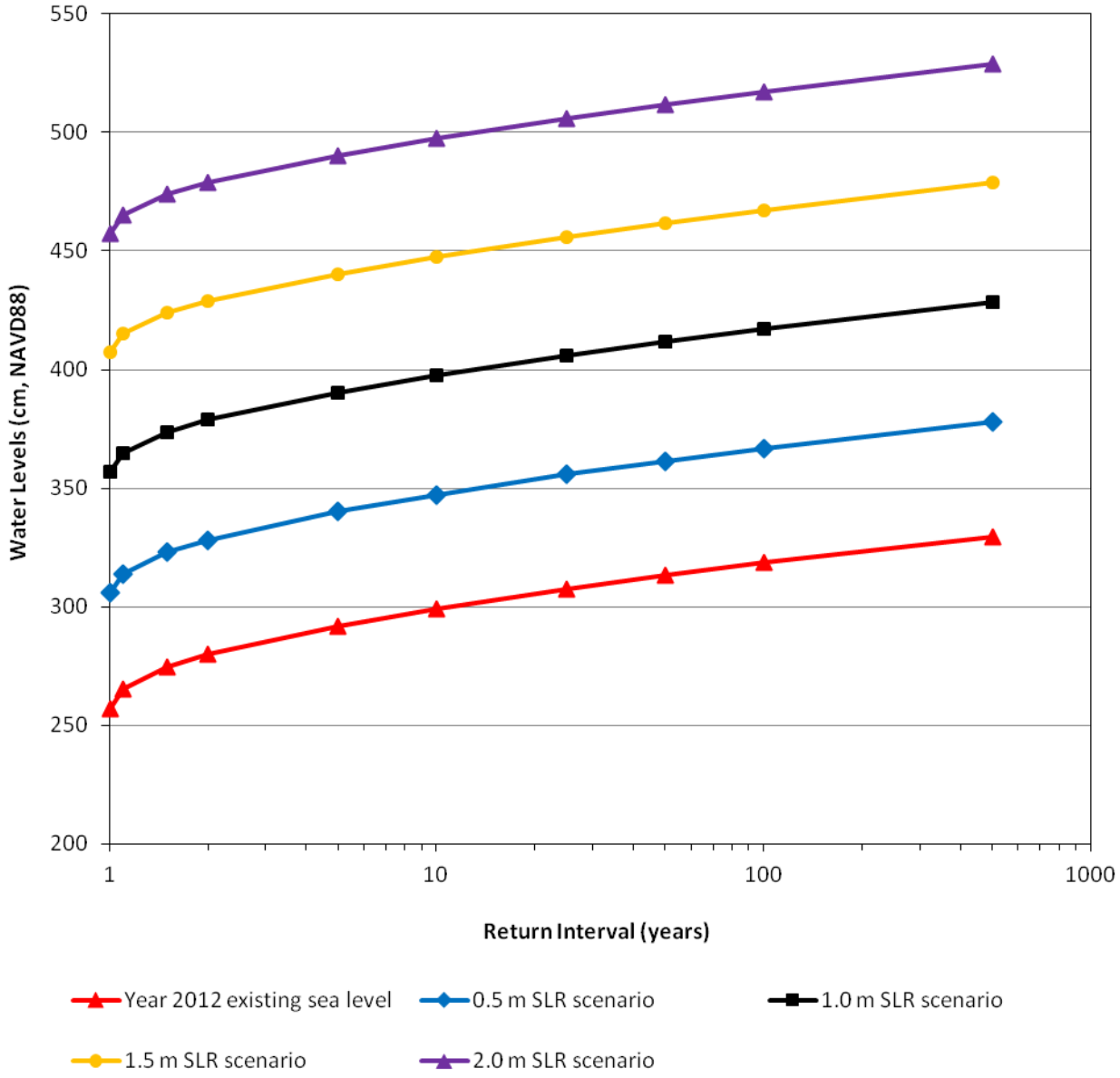

Figure 7-3 Humboldt Bay bay-wide average annual extreme high water level exceedance probability curves for Year 2012 existing sea levels and the 0.5, 1.0, 1.5 and 2.0-m SLR scenarios relative to year 2000. All generalized extreme value (GEV) exceedance probability curves are from the 2D model predictions.

Areas Vulnerable to Inundation for Existing and Future Sea Levels

Nearly 3,600 hectares of former tidelands surrounding Humboldt Bay have been reclaimed and converted to other land use since the 1880s (Laird, 2013). Most of these reclaimed tidelands have been either filled, or leveed and drained and converted to various urban or agricultural uses. Figure 7-4 shows the areas vulnerable to inundation from the Year 2012 existing mean monthly

maximum water (MMMW) level, and the U.S. Coast and Geodetic Survey 1870s mapped shoreline (Laird, 2007). The areas vulnerable to inundation from the existing MMMW level coincide well with the historic 1870s shoreline, and likely represent a large portion of the reclaimed former tidelands around Humboldt Bay. It appears that a significant portion of the Elk River delta area, located across from the bay entrance, is outside the historic 1870 shoreline but still vulnerable to inundation from the existing MHHW level. This may be because this area was not mapped consistent with other tributary deltas, such as Freshwater Creek.

Many of the former tideland areas are protected by levees and relatively low elevation railroad or road grades, such as Highway 101. Many of the bay levees are actively eroding, unmaintained and at relatively low elevations, and are therefore subject to overtopping by extreme high tides and storm events (Laird, 2013). Although currently protected against typical high tide levels, the poor condition of the bay levee system leaves much of the former reclaimed tideland areas highly vulnerable to inundation if the levees were to be breached or overtopped. Figure 7-5 shows areas vulnerable to inundation from MHHW and the 100-yr extreme high water level for Year 2012 existing sea levels, and Figure 6-4 shows the areas vulnerable to inundation from the 100-yr extreme event for year 2012 and the 2.0-m SLR scenario. If the existing levees or other barriers used to protect these vulnerable areas were to fail or breach, many of these areas would not only flood during extreme events, such as the 100-yr event, but also during typical high tides.

Although there is over a 1 m difference in elevation between MHHW and the 100-yr extreme high water level (Figure 7-2), the areas vulnerable to inundation from the 100-yr event do not increase significantly when compared to the MHHW inundation footprint for existing conditions (Figure 7-5), or to the 100-yr event for the 2.0-m SLR scenario (Figure 6-4). This is the result of two distinct topographic features: the low ground elevations of current vulnerable areas, and the landscape bounding Humboldt Bay and the adjoining tributary and slough channels. Most of the reclaimed former tidelands were not filled, and, on average, were likely at or near MHHW to MMMW elevations at the time they were reclaimed. Humboldt Bay is bounded by sand dunes to the west, coastal mountains to the east, and bluffs to the south, all of which limit the inundation extent of extreme high water events and the effects of sea level rise. The largest change in inundation extent is in the north to north-east end of Humboldt Bay, between Mad River Slough and the Mad River, where no significant bounding topographic barriers exist. The areas west of Eureka along the bay also show increases in the 100-yr inundation (Figure 6-4 and Figure 7-5), which are composed of reclaimed tideland areas that were filled. Overall, the lateral extent of inundation from existing and future sea levels appears limited by the natural and anthropogenically altered topographic landscape surrounding Humboldt Bay.

The greatest threats of tidal flooding to the vulnerable areas are by: (1) levee breaching or failure (Laird, 2013), which would allow water to flood into these areas over a range of water levels, and (2) overtopping the levees and railroad/road grades by extreme high water level events (e.g. 100-yr event). With sea level rise, the threat of levee failure will increase over time, and in addition, the frequency of extreme events overtopping levees and grades will also increase.

Figure 7-4 Mean Monthly Maximum Water (MMMW) inundation coverage (green) for Year 2012 existing sea levels and the 1870 historical shoreline (black line) coverage from Laird (2007).

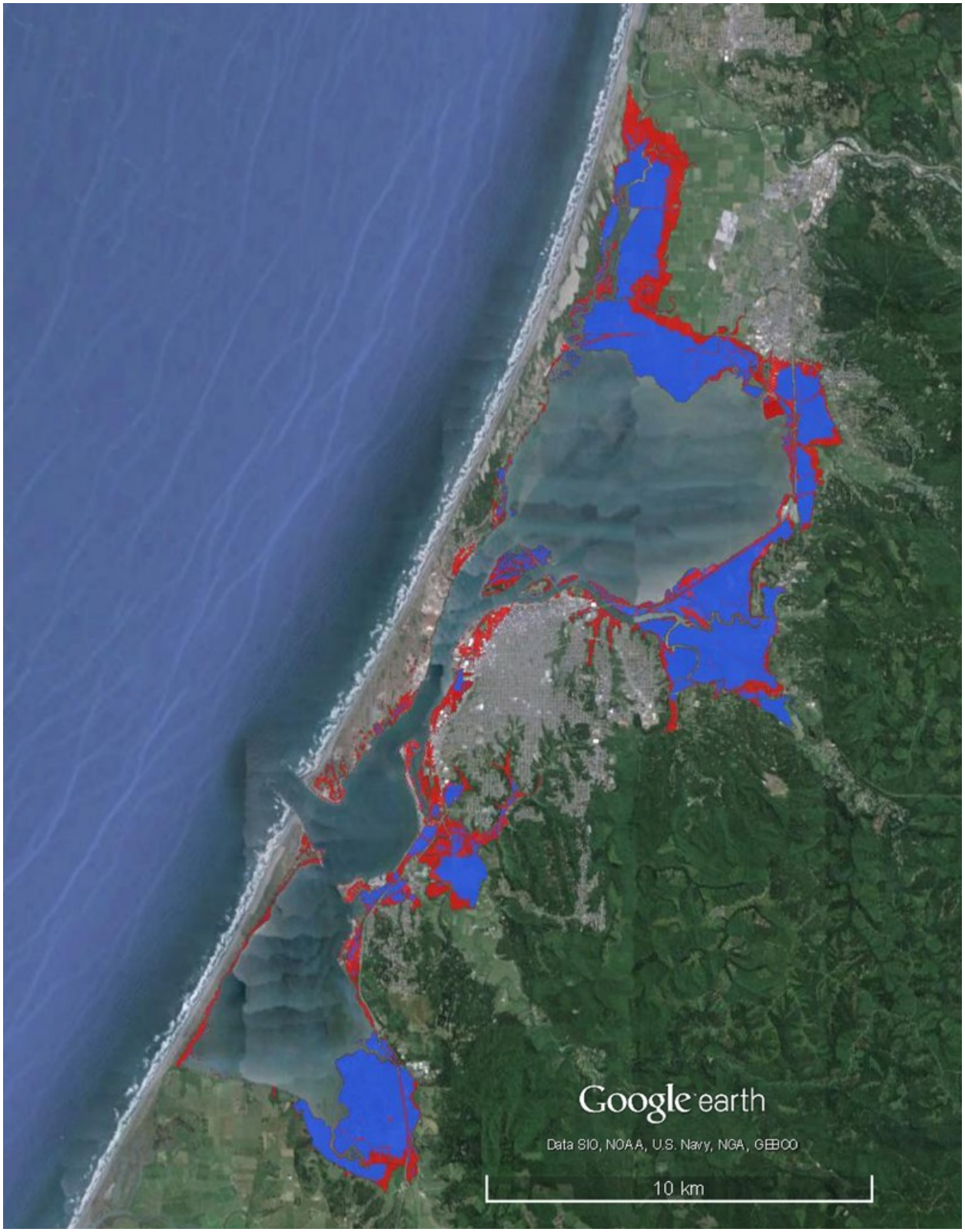

Figure 7-5 Areas surrounding Humboldt Bay vulnerable to inundation from mean higher high water (MHHW) (blue) and 100-yr extreme high water levels (red) for Year 2012 existing sea levels.

Interpretation of Inundation Vulnerability Maps

The inundation vulnerability maps show areas surrounding Humboldt Bay vulnerable to tidal inundation from existing and future sea levels that are currently protected from tidal inundation by the bay's shoreline. Although the inundation maps show areas vulnerable to inundation, not areas currently inundated, the maps can be used to illustrate when specific water levels associated with a SLR scenario may overtop a levee or barrier protecting a vulnerable area, allowing tidal flooding.

As an example, Figure 7-6 shows the areas surrounding the Arcata Wastewater Treatment Facility (WWTF) ponds that are vulnerable to inundation from the 100-yr extreme high water level for Year 2012 existing sea levels and the 0.5-m SLR scenario. The existing 100-yr event water level (A in Figure 7-6) did not show that the outer WWTF levees will be overtopped, since the levee tops are at a higher elevation than the water level, and are visible through the inundation coverage. Consequently, the inside of the WWTF ponds will not flood during the existing 100-yr event, even though the coverage shows them vulnerable to inundation. However, for the 0.5-m SLR scenario the levees would overtop from the 100-yr event at many locations (B in Figure 7-6), indicating that the ponds would flood during these conditions. Referring to Figure 7-1, the modified NRC (2012) high and low SLR projections indicate that 0.5 m of SLR are predicted to occur between year 2045 and 2089, respectively. Using the modified NRC projection, 0.5 m of SLR is likely to occur around year 2066.

Figure 7-6 Areas surrounding the Arcata Wastewater Treatment Facility (WWTF) ponds vulnerable to tidal inundation from the 100-yr extreme high water level events for year 2012 existing sea levels (A, blue inundation) and 0.5-m SLR scenario (B, red inundation). The year 2000 100-yr water level (A) would not inundate the top of the outer WWTF levees, indicating that the WWTF ponds would not be inundated; although the inundation map shows that the ponds would be vulnerable to inundation during the 100-yr event. The 100-yr event for the 0.5-m SLR scenario (B) shows that the top of the outer WWTF levees would be inundated at many locations, indicating that the ponds would be inundated for the 100-yr event with 0.5-m SLR.

8 Conclusions, Summary and Recommendation

Conclusions and Summary

This study has developed a hydrodynamic 2D model of Humboldt Bay to simulate water level responses to five SLR scenarios. The simulated SLR scenarios consisted of Year 2012 existing sea levels and four half-meter SLR increments of 0.5, 1.0, 1.5 and 2.0-m. Inundation vulnerability maps were produced to identify areas surrounding Humboldt Bay vulnerable to tidal inundation from existing and future sea levels. The results of this study have demonstrated:

1. Sea level rise will affect Humboldt Bay and the surrounding landscape in its existing condition.
2. Humboldt Bay water levels can be modeled in 2D using the EFDC modeling system.
3. The nontidal sea level models developed for the Crescent City tide gauge reproduce observed nontidal sea level heights and variability reasonably well using the three independent variables of wind, sea level pressure and ENSO variability. Predicted total hourly water levels (astronomical tide plus nontidal sea level) compare to tidal observations well.
4. The 100-yr HSLH series developed for the Crescent City tide gauge, which contains 639,011 hourly water level observations and 246,373 hourly predictions, can reproduce the gauge's observed water levels and variability.
5. The 2D hydrodynamic model driven solely by the 100-yr HSLH series developed for the Crescent City tide gauge can reproduce observed hourly water levels at three tide gauges in Humboldt Bay well, and also reproduce the daily maximum water level at five tide gauges.
6. The 100-yr HSLH series developed for the Crescent City tide gauge can be used to represent near shore ocean water levels, or still water levels, for the Humboldt Bay and Crescent City region.
7. Five SLR scenarios were assessed in this study: Year 2012 existing sea level and four half-meter SLR rise scenarios of 0.5, 1.0, 1.5 and 2.0-m. The four half-meter SLR scenarios are not tied to a specific future timeline, inherent to typical SLR projections.
8. The predicted water levels and inundation vulnerability maps for each SLR scenario represent conditions of SLR at any time in the future, assuming ground elevations of the Project DEM do not significantly change.
9. Twenty-five inundation vulnerability maps were produced for predicted Humboldt Bay water levels of MHHW, MMMW, MAMW, and the 10- and 100-yr extreme high water level events for the five SLR scenarios.
10. The tidal inundation maps show areas surrounding Humboldt Bay landward of MHW vulnerable to existing and future sea levels that are currently protected from inundation due to the natural shoreline, levees, railroad and/or road grades, or other such barriers.

11. The inundation vulnerability maps indicate areas vulnerable to inundation, not areas currently inundated.
12. A MHW map of Humboldt Bay was developed to show areas of the bay currently inundated below MHW, which coincides well with the Laird (2013) mapped shoreline.
13. The inundation vulnerability maps and MHW map are provided as kmz files, which can be opened in Google Earth, and shapefiles, which can be imported into GIS software such as ArcGIS.
14. The higher RSL rise rates observed in Humboldt Bay due to down trending VLM indicate that a global rise in sea levels will affect Humboldt Bay faster than other parts of U.S. west coast; and within the bay the southern end will be affected sooner than the northern portions of the bay.
15. The 100-yr extreme event is approximately 2 m higher than MSL, 1 m higher than MHHW, and 0.5 m higher than MAMW. The 2-yr extreme event is approximately equal to MAMW, and the 1-yr event is only slightly greater than MMMW.
16. The 1.1-yr extreme event under the 0.5-m SLR scenario is approximately equal to the existing condition 100-yr event.
17. Humboldt Bay water levels have increased approximately 0.5 m over the last 100 years due to a high RSL rise rate.
18. The reclaimed former tidelands around Humboldt Bay represent the most vulnerable areas to existing and future sea levels.
19. Many of the former tideland areas are protected by relatively low elevation levees and railroad/road grades, such as Highway 101. Many of the bay levees are actively eroding, unmaintained and at elevations subject to overtopping by extreme high tides and storm events (Laird, 2013).
20. If the levees or grades protecting the bay's existing vulnerable areas were to fail or breach, many of the low-lying areas would flood from daily high tides, while higher areas would flood from extreme events.
21. Sea level rise will increase the threat of levee failure, and increase the frequency of extreme events overtopping the levees and road and railroad grades protecting the bay's vulnerable areas.

Recommendations

Following are some recommendations regarding future sea level rise work for Humboldt Bay.

1. Incorporate the effects of internally generated wind waves into the modeling.
2. Include the tributary flooding into the modeling.
3. Include the effects of levee breaches and lateral flooding into the modeling.
4. Incorporate VLM directly into the modeling.

5. Incorporate the effects of internal wind waves, tributary flooding, lateral flooding, levee breaching, and VLM into the inundation vulnerability maps.
6. Conduct a detailed assessment of tidal wetland SLR vulnerability.
7. Conduct a detailed assessment of potential shoreline erosion.
8. Conduct a detailed engineering assessment of the Humboldt Bay levee system.

All of these considerations would provide improved information and assessments regarding the impacts of sea level rise in Humboldt Bay.

9 References

Anderson, J. K. 2010. A Three-Dimensional Hydrodynamic and Transport Model of Humboldt Bay. Poster presented at the Humboldt Bay Symposium, April 2010.

Blumberg, A. F., B. Galperin, and D. J. O'Connor. 1992. Modeling vertical structure of open-channel flow. *J. Hyd. Engr*., 118, 1119-1134.

Bromirski, P. D., A. J. Miller, R. E. Flick, and G. Auad. 2011. Dynamical suppression of sea level rise along the Pacific coast of North America: Indications for imminent acceleration. *J. Geophys. Res.*, 116, C07005, doi:10.1029/2010JC006759.

Burgette, R. J., R. J. Weldon II, and D. A. Schmidt. 2009. Interseismic uplift rates for western Oregon and along-strike variation in locking on the Cascadia subduction zone. *J. Geophys. Res.*, 114, B01408, doi:10.1029/2008JB005679.

Cayan D. R., P. D. Bromirski, K. Hayhoe, M. Tyree, M. D. Dettinger, and R. E. Flick. 2008. Climate change projections of sea level extremes along the California coast. *Climatic Change*, 87, 57–73.

Cayan, D., M. Tyree, M. Dettinger, H. Hidalgo, T. Das, E. Maurer, P. Bromirski, N. Graham, and R. Flick. 2009. Climate Change Scenarios and Sea Level Rise Estimates for California 2008 Climate Change Scenarios Assessment. California Climate Change Center. CEC-500-2009-014-F.

Church, J. A. and N.J. White. 2006. A 20th century acceleration in global sea level rise, *Geophysical Research Letters*, 33, L01602, doi:10.1029/2005GL024826.

Church, J. A., and N. J. White. 2011. Sea-level rise from the late 19th to the early 21st century. *Surv. Geophys*., 32, 585–602.

Church, J.A., P.U. Clark, A. Cazenave, J.M. Gregory, S. Jevrejeva, A. Levermann, M.A. Merrifield, G.A. Milne, R.S. Nerem, P.D. Nunn, A.J. Payne, W.T. Pfeffer, D. Stammer and A.S. Unnikrishnan. 2013. Sea Level Change. In: Climate Change 2013: The Physical Science Basis. Contribution of Working Group I to the Fifth Assessment Report of the Intergovernmental Panel on Climate Change [Stocker, T.F., D. Qin, G.-K. Plattner, M. Tignor, S.K. Allen, J. Boschung, A. Nauels, Y. Xia, V. Bex and P.M. Midgley (eds.)]. Cambridge University Press, Cambridge, United Kingdom and New York, NY, USA.

Cole, T. M. and S. A. Wells. 2011. CE-QUAL-W2: A Two-Dimensional, Laterally Averaged, Hydrodynamic and Water Quality Model, Version 3.71, User Manual. Department of Civil and Environmental Engineering, Portalnd State University, Portland, OR.

Compo, G. P., J. S. Whitaker, P. D. Sardeshmukh, N. Matsui, R. J. Allan, X. Yin, B. E. Gleason, R. S. Vose, G. Rutledge, P. Bessemoulin, S. Brönnimann, M. Brunet, R. I. Crouthamel, A. N. Grant, P. Y. Groisman, P. D. Jones, M. Kruk, A. C. Kruger, G. J. Marshall, M. Maugeri, H. Y. Mok, Ø. Nordli, T. F. Ross, R. M. Trigo, X. L. Wang, S. D. Woodruff, and S. J. Worley. 2011: The twentieth century reanalysis project. *Quarterly J. Roy. Meteorol. Soc*., 137, 1-28. DOI: 10.1002/qj.776.

Costa, S. L. 1982. The physical oceanography of Humboldt Bay. Proceedings Humboldt Bay Symposium. C. Toole and C. Diebel (ed.), HSU Center for Community Development, Arcata, CA.

Costa, S. L. and K. A. Glatzel. 2002. Humboldt Bay, California, entrance channel. Report 1: data review. U.S. Army Corps of Engineers, Engineer Research and Development Center, Coastal and Hydraulics Laboratory, Vicksburg, MS. ERDC/CHL CR-02-01.

Craig, P. M. 2013. User's Manual for EFDC_Explorer7.1: A Pre/Post Processor for the Environmental Fluid Dynamics Code (Rev 00). Dynamic Solutions-International, LLC, Edmonds, WA.

Flick R. E., K. Knuuti, and S. K. Gill. 2013. Matching mean sea level rise projections to local elevation datums. *J. Waterway, Port, Coastal, Ocean Eng.*, 139(2), 142–146.

Galperin, B., L. H. Kantha, S. Hassid, and A. Rosati, 1988: A quasi-equilibrium turbulent energy model for geophysical flows. *J. Atmos. Sci*., 45, 55-62.

Grinsted, A., J. C. Moore, and S. Jevrejeva. 2010. Reconstructing sea level from paleo and projected temperatures 200 to 2100 AD, *Clim. Dyn*., 34, 461-472.

Hamrick, J. M. 1992. A Three-Dimensional Environmental Fluid Dynamics Computer Code: Theoretical and Computational Aspects. The College of William and Mary, Virginia Institute of Marine Science, Special Report 317.

Hamrick, J. M., and W. B. Mills. 2000. Analysis of temperatures in Conowingo Pond as influenced by the Peach Bottom atomic power plant thermal discharge. *Environ. Sci. Policy*, 3, S197-S209.

Heberger, M., H. Cooley, P. Herrera, P. H. Gleick, and E. Moore. 2009. The Impacts of Sea-Level Rise on the California Coast. California Climate Change Center. CEC-500-2009-024-F.

IPCC. 2013a. Annex III: Glossary [Planton, S. (ed.)]. In: Climate Change 2013: The Physical Science Basis. Contribution of Working Group I to the Fifth Assessment Report of the Intergovernmental Panel on Climate Change [Stocker, T.F., D. Qin, G.-K. Plattner, M. Tignor, S.K. Allen, J. Boschung, A. Nauels, Y. Xia, V. Bex and P.M. Midgley (eds.)]. Cambridge University Press, Cambridge, United Kingdom and New York, NY, USA.

IPCC. 2013b. Summary for Policymakers. In: Climate Change 2013: The Physical Science Basis. Contribution of Working Group I to the Fifth Assessment Report of the Intergovernmental Panel on Climate Change [Stocker, T.F., D. Qin, G.-K. Plattner, M. Tignor, S.K. Allen, J. Boschung, A. Nauels, Y. Xia, V. Bex and P.M. Midgley (eds.)]. Cambridge University Press, Cambridge, United Kingdom and New York, NY, USA.

Jevrejeva, S., J. C. Moore, A. Grinsted, and P. L. Woodworth. 2008. Recent global sea level acceleration started over 200 years ago? *Geophys. Res. Lett*., 35, L08715.

Jevrejeva, S., J. C. Moore, and A. Grinsted. 2010. How will sea level respond to changes in natural and anthropogenic forcings by 2100? *Geophys. Res. Lett*., 37, L07703, doi:10.1029/2010GL042947.

Ji, Z.-G., M. R. Morton, and J. M. Hamrick. 2001. Wetting and drying simulation of estuarine processes. *Estuarine, Coastal and Shelf Science*, 53, 683-700.

Ji, Z. G. 2008. *Hydrodynamics and Water Quality, Modeling Rivers, Lakes, and Estuaries*. John Wiley & Sons, Inc., Hoboken, New Jersey.

Jin, K. R., J. M. Hamrick, and T. S. Tisdale. 2000. Application of a three-dimensional hydrodynamic model for Lake Okeechobee, *J. Hyd. Engr*., 106, 758-772.

Kalnay E, M. Kanamitsu, R. Kistler, W. Collins, D. Deaven, L. Gandin, M. Iredell, S. Saha, G. White, J. Woollen, Y. Zhu, A. Leetmaa, B. Reynolds, M. Chelliah, W. Ebisuzaki, W. Higgins, J. Janowiak, K. C. Mo, C. Ropelewski, J. Wang, R. Jenne, and D. Joseph. 1996. The NCEP/NCAR 40-year reanalysis project. *Bull. Amer. Meteor. Soc*., 77, 437-470.

Kaplan, A., M. Cane, Y. Kushnir, A. Clement, M. Blumenthal, and B. Rajagopalan. 1998. Analyses of global sea surface temperature 1856-1991. *Journal of Geophysical Research*, 103, 18, 567-18, 589.

Komar, P. D., J.C. Allan, and P. Ruggiero. 2011. Sea level variations along the U.S. Pacific Northwest Coast: tectonic and climate controls. *Journal of Coastal Research*: Volume 27, Issue 5: pp. 808 – 823.

Kominz, M. 2001. Sea Level Variations Over Geologic Time. In Encyclopedia of Ocean Sciences. Elsevier, 2605-2613.

Knowles, N. 2010. Potential inundation due to rising sea levels in the San Francisco bay region. *San Francisco Estuary and Watershed Science*, 8(1). Available at http://escholarship.org/uc/search?entity=jmie_sfews;volume=8;issue=1

Laird, A. 2007. Historical Atlas of Humboldt Bay and Eel River Delta. Prepared for Humboldt Bay Harbor, Recreation and Conservation District, Eureka CA. Trinity Associates, Arcata, CA.

Laird, A. 2013. Humboldt Bay Shoreline Inventory, Mapping and Sea Level Rise Vulnerability Assessment. Prepared for State Coastal Conservancy. Trinity Associates, Arcata, CA.

Mantua, N. J., S. R. Hare, Y. Zhang, J. M. Wallace, and R.C. Francis. 1997. A Pacific interdecadal climate oscillation with impacts on salmon production. *Bulletin of the American Meteorological Society*, 78, 1069-1079.

Meehl, G. A., T. F. Stocker, W. D. Collins, P. Friedlingstein, A. T. Gaye, J. M. Gregory, A. Kitoh, R. Knutti, J. M. Murphy, A. Noda, S. C. B. Raper, I. G. Watterson, A. J. Weaver and Z.-C. Zhao. 2007. Global Climate Projections. In: Climate Change 2007: The Physical Science Basis. Contribution of Working Group I to the Fourth Assessment Report of the Intergovernmental Panel on Climate Change [Solomon, S., D. Qin, M. Manning, Z. Chen, M. Marquis, K. B. Averyt, M. Tignor and H. L. Miller (eds.)]. Cambridge University Press, Cambridge, United Kingdom and New York, NY, USA.

Mellor, G. L. and T. Yamada. 1982. Development of a turbulence closure model for geophysical fluid problems. *Rev. Geophys. Space Phys*., 20, 851-875.

Mitchell, C. E., P. Vincent, R. J. Weldon, and M. A. Richards. 1994. Present-day vertical deformation of the Cascadia margin, Pacific northwest, United States: *J. Geophys. Res*. 99(B6), 12,257-12,277.

Moustafa, M. Z. and J. M. Hamrick. 2000. Calibration of the wetland hydrodynamic model to the Everglades nutrient removal project. *Water Quality and Ecosystem Modeling*, 1, 141-167.

National Oceanic and Atmospheric Administration (NOAA). 2013. Extreme Water Levels of the United States, 1893-2010. National Ocean Service Center for Operational Oceanographic Products and Services, Silver Spring, MA. NOAA Technical Report NOS CO-OPS 067.

National Research Council (NRC). 2012. Sea-Level Rise for the Coasts of California, Oregon, and Washington: Past, Present, and Future. The National Academies Press, Washington, DC.

Newman, M., G. P. Compo, and M. A. Alexander. 2003. ENSO-forced variability of the Pacific Decadal Oscillation. *J. Climate*, 16, 3853–3857.

Northern Hydrology & Engineering (NHE). 2009. Tidal wetland geometric relations in Humboldt Bay: Mad River Slough pilot study. Prepared for U.S. Fish and Wildlife Service. NHE, McKinlyville, CA.

Pacific Watershed Associates (PWA). 2014. Humboldt Bay Sea Level Rise Vulnerability Assessment: DEM Development Report, Final Draft. Prepared for Northern Hydrology & Engineering. PWA, McKinleyville, CA. PWA Report No. 14100351, February 2014.

Parris, A., P. Bromirski, V. Burkett, D. Cayan, M. Culver, J. Hall, R. Horton, K. Knuuti, R. Moss, J. Obeysekera, A. Sallenger, and J. Weiss. 2012. Global Sea Level Rise Scenarios for the US National Climate Assessment. NOAA Tech Memo OAR CPO-1. 37 pp.

Patton, J. R., T. B. Williams, J. K. Anderson, R. Burgette, and T. Leroy. 2014. Tectonic land level changes and their contribution to sea-level rise, Humboldt Bay region, Northern California: 2014 status update. Prepared for U.S. Fish and Wildlife Service Coastal Program. Cascadia GeoSciences, McKinleyville, CA.

Peltier, W. R. 1990. Glacial Isostatic Adjustment and Relative Sea Level Change. In Sea Level Change, R. Revelle ed., National Academy Press, Studies in Geophysics Series, pp. 73-87, Washington, DC.

Peltier, W.R. 2002. Global glacial isostatic adjustment: paleo-geodetic and space geodetic tests of the ICE-4G(VM2) model. *J. Quat. Sci*., 17, 491–510.

Peltier, W.R. 2009. Closure of the budget of global sea level rise over the GRACE era: the importance and magnitudes of the required corrections for global glacial isostatic adjustment. *Quaternary Science Reviews* (2009), doi:10.1016/j.quascirev.2009.04.004.

Pfeffer, W. T., J. T. Harper, and S. O'Neel. 2008. Kinematic constraints on glacier contributions to 21st-century sea-level rise. *Science*, 321, 1340-1343.

Philip Williams & Associates, Ltd. 2009. California Coastline Erosion Response to Sea Level Rise Analysis and Mapping, Final Draft. Prepared for Pacific Institute. Philip Williams & Associates, Ltd., San Francisco, CA. PWA Ref. #1939.00.

Rahmstorf, S. 2007. A semi-empirical approach to projecting future sea-level rise. *Science*, 315, 368-370.

Ray, R. D., and B. C. Douglas. 2011. Experiments in reconstructing twentieth-century sea levels. *Prog. Oceanogr*., 91, 496–515.

Rhein, M., S.R. Rintoul, S. Aoki, E. Campos, D. Chambers, R.A. Feely, S. Gulev, G.C. Johnson, S.A. Josey, A. Kostianoy, C. Mauritzen, D. Roemmich, L.D. Talley and F. Wang. 2013. Observations: Ocean. In: Climate Change 2013: The Physical Science Basis. Contribution of Working Group I to the Fifth Assessment Report of the Intergovernmental Panel on Climate Change [Stocker, T.F., D. Qin, G.-K. Plattner, M. Tignor, S.K. Allen, J. Boschung, A. Nauels, Y. Xia, V. Bex and P.M. Midgley (eds.)]. Cambridge University Press, Cambridge, United Kingdom and New York, NY, USA.

Rosati, A. K. and K. Miyakoda. 1988. A general circulation model for upper ocean simulation. *J. Phys. Ocean,* 18, 1601-1626.

Russell, N.and G. Griggs. 2012. Adapting to Sea Level Rise: A Guide to California's Coastal Communities. Prepared for the California Energy Commission Public Interest Environmental Research Program. University of California, Santa Cruz.

Schlosser, S., B. Price-Hall, A. Eicher, A. Hohl, D. Mierau, and G. Crawford. 2009. Humboldt Bay Initiative: Adaptive Management in a Changing World. Available at http://ca-sgep.ucsd.edu/sites/ca-sgep.ucsd.edu/files/advisors/humboldt/files/HBI%20StratPlan2009.pdf

Schlosser, S., and A. Eicher. 2012. The Humboldt Bay and Eel River Estuary Benthic Habitat Project. California Sea Grant Publication T-075, 246 p.

Smagorinsky, J. 1963. General circulation experiments with the primitive equations, Part I: the basic experiment. *Mon. Weather Rev*., 91, 99-164.

Smolarkiewicz, P. K. and T. L. Clark. 1986. The multidimensional positive definite advection transport algorithm: further development and applications. J. *Comp. Phys*., 67, 396-438.

Smolarkiewicz, P. K. and W. W. Grabowski. 1990. The multidimensional positive definite advection transport algorithm: non-oscillatory option. *J. Comp. Phys*., 86, 355-375.

Smolarkiewicz, P. K. and L. G. Margolin. 1993. On forward-in-time differencing for fluids: extension to curvilinear framework. Monthly Weather Rev., 121, 1847-1859.

Tetra Tech. 2007a. The Environmental Fluid Dynamics Code, User Manual, USEPA Version 1.01. Tetra Tech, Inc., Fairfax, VA.

Tetra Tech. 2007b. The Environmental Fluid Dynamics Code, Theory and Computation, Volume 2: Sediment and Contaminant Transport and Fate. Tetra Tech, Inc., Fairfax, VA.

Tetra Tech. 2007c. The Environmental Fluid Dynamics Code, Theory and Computation, Volume 3: Water Quality Module. Tetra Tech, Inc., Fairfax, VA.

Vermeer, M. and S. Rahmstorf. 2009. Global sea level linked to global temperature. Proceedings of the National Academy of Science of the USA, 106, 21527-21532.

Vimont, D. J., M. Alexander, and A. Fontaine. 2009. Midlatitude excitation of tropical variability in the Pacific: the role of thermodynamic coupling and seasonality. *J. Climate*, 22, 518–534.

Wolter, K., and M. S. Timlin. 1993. Monitoring ENSO in COADS with a seasonally adjusted principal component index. Proceedings of the 17th Climate Diagnostics Workshop, Norman, OK, NOAA/NMC/CAC, NSSL, Oklahoma Climate Survey, CIMMS and the School of Meteorology, University of Oklahoma: Norman, OK; 52–57.

Wolter, K., and M. S. Timlin. 1998. Measuring the strength of ENSO events – how does 1997/98 rank? *Weather* ,53, 315–324.

Wolter, K., and M. S. Timlin. 2011. El Niño/Southern Oscillation behaviour since 1871 as diagnosed in an extended multivariate ENSO index (MEI.ext). *Intl. J. Climatology*, 31(7), 1074-1087.

Zervas, C., S. 2009. Sea Level Variations of the United States 1854-2006. NOAA National Ocean Service Center for Operational Oceanographic Products and Services. NOAA Technical Report NOS CO-OPS 053. 78pp.

Zervas, C., S. Gill, and W. Sweet. 2013. Estimating Vertical Land Motion from Long-Term Tide Gauge Records. NOAA National Ocean Service Center for Operational Oceanographic Products and Services. NOAA Technical Report NOS CO-OPS 065. 78pp.

Zhang, Y., J. M. Wallace, and D. S. Battisti. 1997. ENSO-like interdecadal variability: 1900–93. *J. Climate*, 10, 1004–1020.

10 Glossary

100-yr HSLH series	100-yr long hourly sea level height series (detrended)
2D	two-dimensional
3D	three-dimensional
AR4	Fourth Assessment Report
AR5	Fifth Assessment Report
BFE	base flood elevation
CEINC	Coastal Ecosystems Institute of Northern California
CFL	Courant-Friedrich-Lewy criteria
CO_2	carbon dioxide
CO-OPS	Center for Operational Oceanographic Products and Services
CSZ	Cascadia subduction zone
DEM	digital elevation model
DSI	Dynamic Solutions International, LLC
EFDC	Environmental Fluid Dynamics Code
EFDC_DSI	DSI version of the EFDC model code
EFDC_DSI_OMP	DSI multi-threaded version of the EFDC model code
EFDC_EPA	EPA version of the EFDC model code
EFDC_Explorer7.1	DSI GUI for EFDC version 7.1
ENSO	El Niño-Southern Oscillation
EPA	U.S. Environmental Protection Agency
FEMA	Federal Emergency Management Agency
GIS	Geographic Information System
GMSL	global mean sea level
GPS	global positioning system
GUI	graphical user interface
HBSLRAP	Humboldt Bay Sea Level Rise Adaptation Planning
INT	intercept
IPCC	Intergovernmental Panel on Climate Change
MAMW	mean annual maximum water
MHHW	mean higher high water
MHW	mean high water
MMMW	mean monthly maximum water

MPDATA	multidimensional positive definite advective transport algorithm
MSL	mean sea level
NASA	National Aeronautics and Space Administration
NAVD88	North American Vertical Datum of 1988
NCAR	National Center for Atmospheric Research
NCEP	National Centers for Environmental Protection
NHE	Northern Hydrology and Engineering
NOAA	National Ocean and Atmospheric Administration
NOAA/OAR/ESRL/PSD	NOAA Office of Oceanic & Atmospheric Research, Earth System Research Laboratory, Physical Sciences Division
NTDE	National Tidal Datum Epoch
NTSLR	nontidal sea level residual
NWS	National Weather Service
PNW	U.S. Pacific northwest
PWA	Pacific Watershed Associates
R	correlation coefficient
ReMSL	regional mean sea level
RSL	relative (or local) sea level
SCC	State Coastal Conservancy
SD	standard deviation
SE	standard error
SLP	sea level pressure
SLR	sea level rise
STND	station datum at a specific tide gauge
SWS	Still water level
TIN	triangulated irregular network
TMDL	Total maximum daily load
TWL	Total water level
u_Vw	u- direction wind velocity component
USGS	United States Geological Survey
v_Vw	v- direction wind velocity component
VLM	vertical land motion
WL	water level

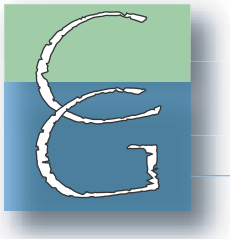

Cascadia GeoSciences

Apr-26-1992 M 7.2

Tectonic land level changes and their contribution to sea-level rise, Humboldt Bay region, Northern California

2014 Status Update

Jason R. Patton[1], Todd B. Williams[1], Jeff Anderson[2], Reed Burgette[3], Tom Leroy[4]

1. Cascadia GeoSciences jayp@cascadiageo.org toddw@cascadiageo.org
2. Northern Hydrology and Engineering
3. New Mexico State University
4. Pacific Watershed Associates

Executive Summary

Land subsidence in and around Humboldt Bay, California contributes to sea-level rise up to 2-3 times greater than anywhere else in California. Sea-level observations and highway level surveys confirm that land is subsiding in Humboldt Bay, in contrast to Crescent City where the land is rising. Rates of sea-level rise are 5.84 mm/yr in South Humboldt Bay (Hookton Slough), 3.76 mm/yr at Fields Landing, 4.61 mm/yr at the North Spit, 2.53 mm/yr at Samoa, and 3.39 mm/yr in Arcata Bay (Mad River Slough). Rates of land subsidence are -3.56 mm/yr in South Humboldt Bay (Hookton Slough), -1.48 mm/yr at Fields Landing, -2.33 mm/yr at the North Spit, -0.25 mm/yr at Samoa, and -1.11 mm/yr in Arcata Bay (Mad River Slough).

Introduction

We submit this report to the US Fish & Wildlife Coastal Program Coordinator as a semi-annual report for award F11AC01092 “Tectonic Land Level Changes and their Contribution to Sea Level Rise, Humboldt Bay Region, Northern California”.

Milestones achieved during 2013-2014 include the reanalysis of acquired historic tide gage data and inclusion of additional data in Humboldt Bay (US Army Corp. Eng., 2010) for the Fields Landing and Samoa historic tide gage locations. We completed leveling surveys at Trinidad Pier in support of CenCOOS deployments and procured a high precision tide gage slated for installation at the Trinidad dock.

In the coming year, our focus will move towards modeling regional tectonic deformation to fit the sea-level and land-level observations and prepare the results for a peer review journal. We will host an onsite visit to a tide gage location and prepare an online webinar to distribute our results to date.

Additionally, we hope to observe additional historic tide gage locations around Humboldt Bay.

Objectives & Background

This project characterizes the interseismic plate tectonic land-level change associated with the southern Cascadia subduction zone (CSZ), a major plate boundary fault system in the Pacific Northwest of the United States. We utilize tide gage, benchmark level, and Global Positioning System (GPS) observations to evaluate this tectonic vertical land motion.

The Gorda plate subducts beneath the North America plate at about 36 mm/yr to form the CSZ fault (McCaffrey, 2007; **Figure 1**). When the fault is locked, the plate deforms elastically, causing deformation and vertical land-level change (Mitchell et al., 1994; Flück et al., 1997; Wang, 2003). Since the Last Glacial Maximum (approximately 22 thousand years ago), global eustatic sea level has risen ~120 meters (Peltier, 2001). This rise is attributed to melting ice and changes in sea water temperature and salinity (Cazenave and Llovel, 2010). Local sea level change is a sum of the vertical change based on sea level rise and vertical land level changes (**Figure 2**; Nelson et al., 1996; Burgette et al., 2009). Understanding this ongoing phenomenon will allow us to quantify and predict future sea-level trends in Northern California. Results from this study will provide fundamental sea-level rise data for making management decisions as they apply to coastal landscapes and the species and ecosystems that inhabit the tidal prism, which are the most vulnerable to future sea-level rise. Quantifying future local sea-level change is the first step in planning strategies for coastal ecosystems.

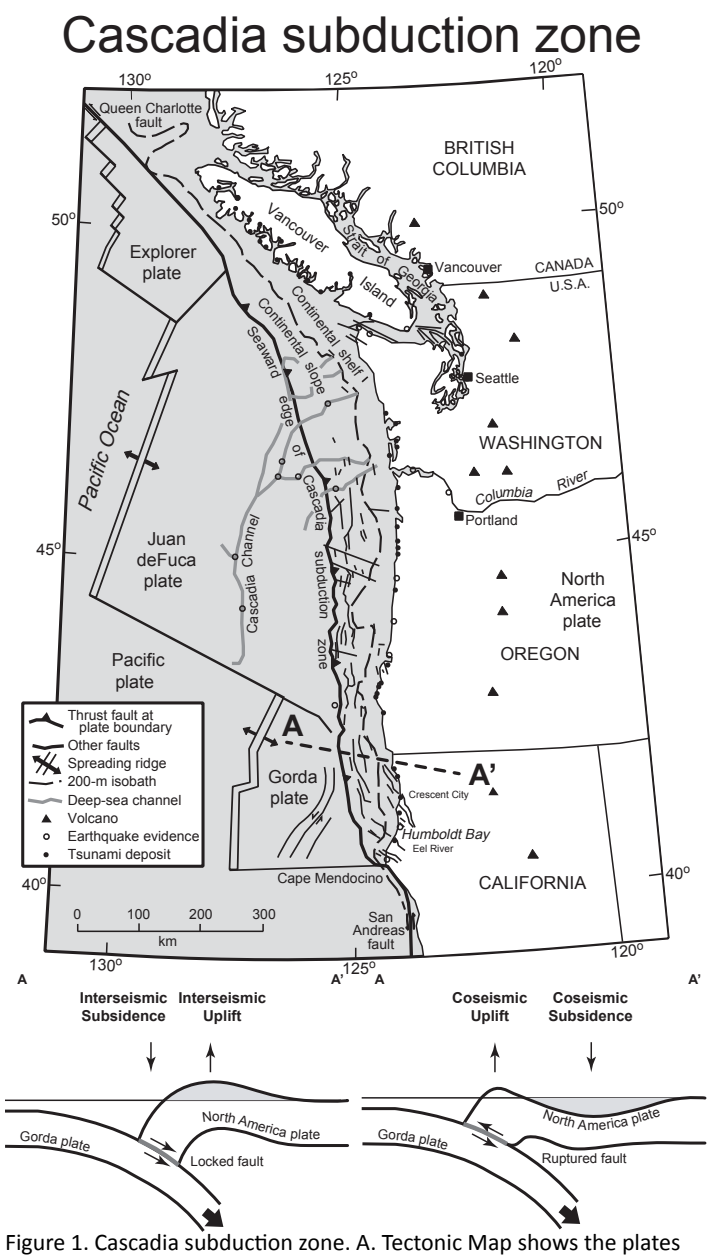

Figure 1. Cascadia subduction zone. A. Tectonic Map shows the plates and their boundary faults. The Cross section of B is designated by the dashed line A-A' (modified from Chaytor et al., 2004; Nelson et al., 2006). B. Generalized cross section across the subduction zone for the interseismic (in-between earthquakes) and coseismic (during earthquake) periods (modified from Plafker, 1972). The fault is locked during the interseismic period. Interseismic and coseismic vertical motion are inverse of each other.

Sea-level rise at the Humboldt Bay North Spit (NS) tide gage is much greater than any other gage in the Pacific Northwest (**Figure 3**). These NS gage records led previous researchers to discard these data as apparently anomalous, possibly due to localized site settlement (Verdonk, 2006). National Oceanic and

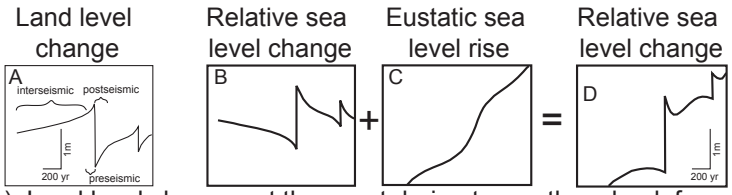

A) Land level changes at the coast during two eathquake deformation cycles with different amplitude
B) Relative sea level (RSL) changes produced by the cycles during a period of no change in regional sea level
C) A gradual rise in regional sea level during the cycles that does not include short term or small scale changes in local and regional sea level
D) RSL changes at the coast resulting from the sum of figures B and C

Figure 2. Tectonic land-level (as measured by relative sea-level) combine with regional sea-level rise to result in the water level observations recorded by tide gages (modified from Nelson et al., 1996).

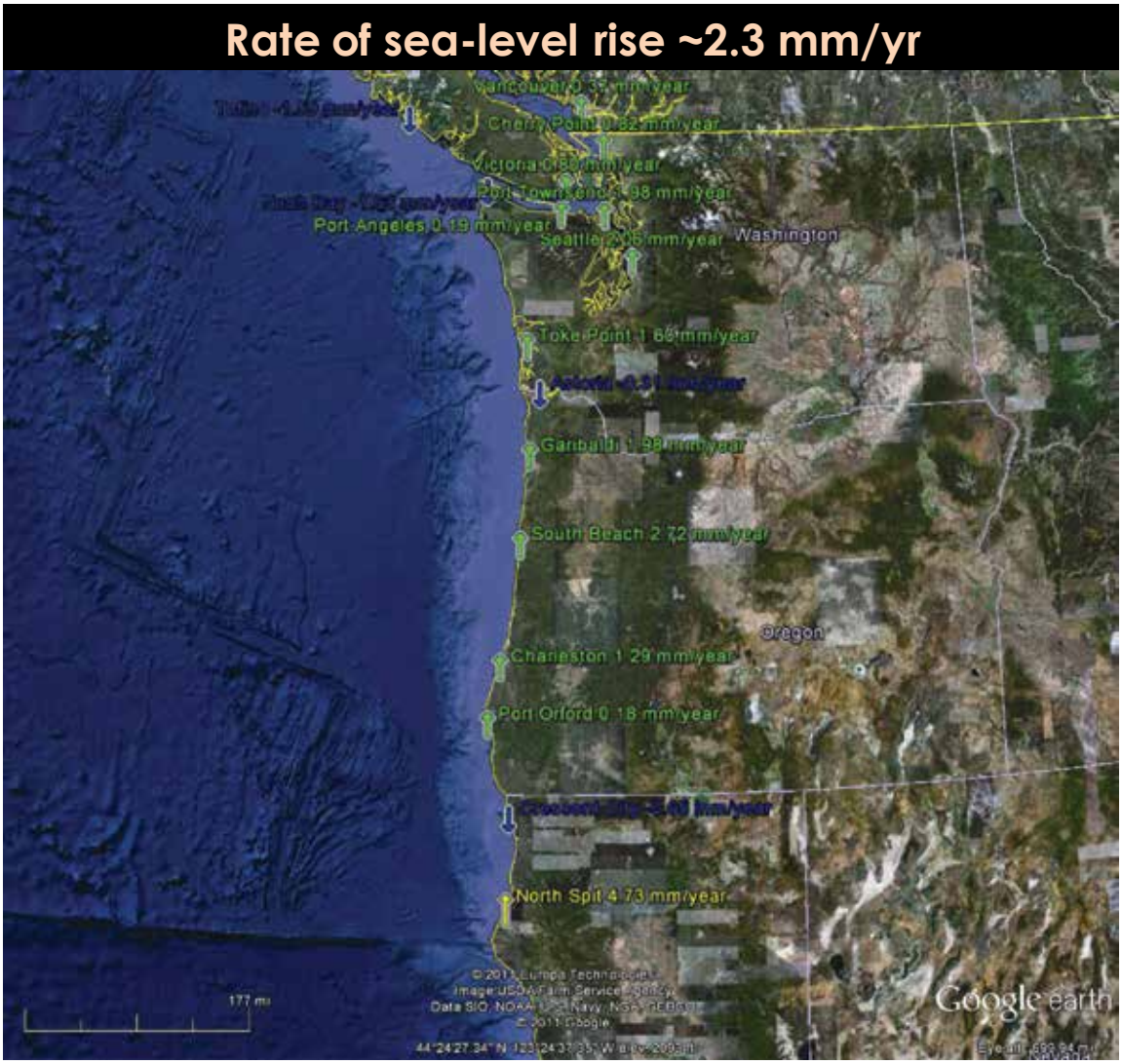

Figure 3. West coast sea-level trend variations from NOAA CO-OPS tide gages.

Atmospheric Administration Center for Operational Oceanographic Products and Services (NOAA Co-Ops) reports an observed sea-level rate of 4.7 mm/yr at the NS tide gage in Humboldt Bay (**Figure 3**). Sea level rise in the Pacific Northwest has been estimated to be 2.28 mm/yr (Burgette et al., 2009) and 2.38 mm/yr (Zervas et al., 2013). Based on satellite altimetry, global estimates of sea level rise range up to 3.4 mm/yr (Cazenave and Llovel, 2010). The discrepancy between regional sea level rise estimates and the NS tide gage observations suggests that there is subsidence of the land and the associated tide gage. At the next nearest tide gage in Crescent City (CC), California, sea-level is observed to be lowering at 0.65 mm/yr (Zervas et al., 2013), the result of upwards vertical land motion in Crescent City. When the NS tide gage was installed, 11 tidal benchmarks and associated temporary gaging stations were deployed from 1977 to 1980.

Utilizing a subset of these initial observation points, we analyze contemporary sea-level observations in Humboldt Bay to investigate Local relative to Regional sea-level rise. We also use first order leveling data collected by the National Geodetic Survey (NGS) to determine vertical land motion rates for the second half of the twentieth century (Burgette et al., 2012). Finally, we incorporate GPS observations into our analyses of vertical land motion for the past decade (Williams et al., 2002).

Methods and Results

We utilize water level observations in Humboldt Bay (North Spit, NS; Mad River Slough, MRS; Samoa SO; Fields Landing, FL; Hookton Slough, HS) as collected by the National Oceanic and Atmospheric Administration (NOAA 1977-1987), US Army Corps of Engineers San Francisco Office (USACE: TOWILL; 2010), and NHE (2008, 2012-13) to evaluate local trends in sea level compared to Crescent City, the longest operating tide gage in the region. The HS tide gage was installed within the Humboldt Bay National Wildlife Refuge (**Figure 4**). Initial results from the HS tide gage were presented in Cascadia GeoSciences (2013).We also use available first-order leveling data collected by the National Geodetic Survey (NGS) predominantly along the route of Highway 101 between Crescent City south through the Humboldt Bay region. We also use GPS observations from continuous GPS sites operated by the National Science Foundation program, EarthScope. We combine these nearshore water-level and onshore land-level observations to determine the land level and sea level trends around Humboldt Bay.

Sea-level Analysis Summary

Jeff Anderson at Northern Hydrology & Engineering (NHE) analyzed water level observations at tide stations for CC and five locations in Humboldt Bay (NS, MRS, SO, FL, and HS) to estimate the relative sea level (RSL) and vertical land motion (VLM) rates at these sites. RSL and VLM rate estimates for CC were determined directly from the water level observations due to the long record length (81 years). All of the tidal observations in Humboldt Bay are considered too short (less than 40 years) to allow direct estimates of RSL and VLM rates. Rates for these sites were determined following the general approach of Burgette et al. (2009), which uses the rates determined for the long-term CC site and the relative rates of differencing the short-term records in Humboldt Bay to the CC data. All rates were determined using least squares linear regression of the time series data.

Previous estimates of RSL and VLM rates for CC used the long-term monthly mean sea levels with

A.

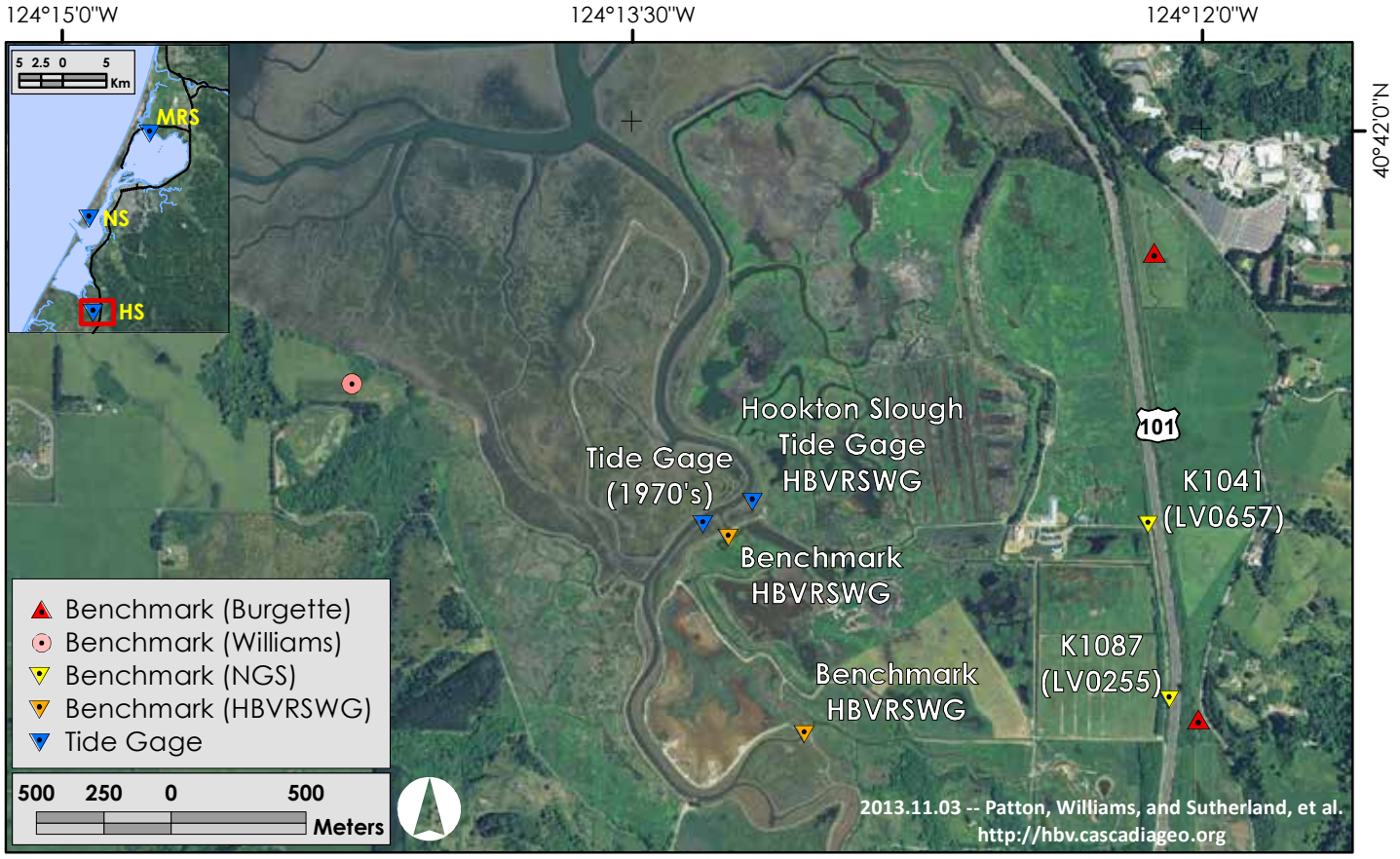

B.

Figure 4. A. Location Map Hookton Slough Tide Gage. B. Tide gage installation site photo.

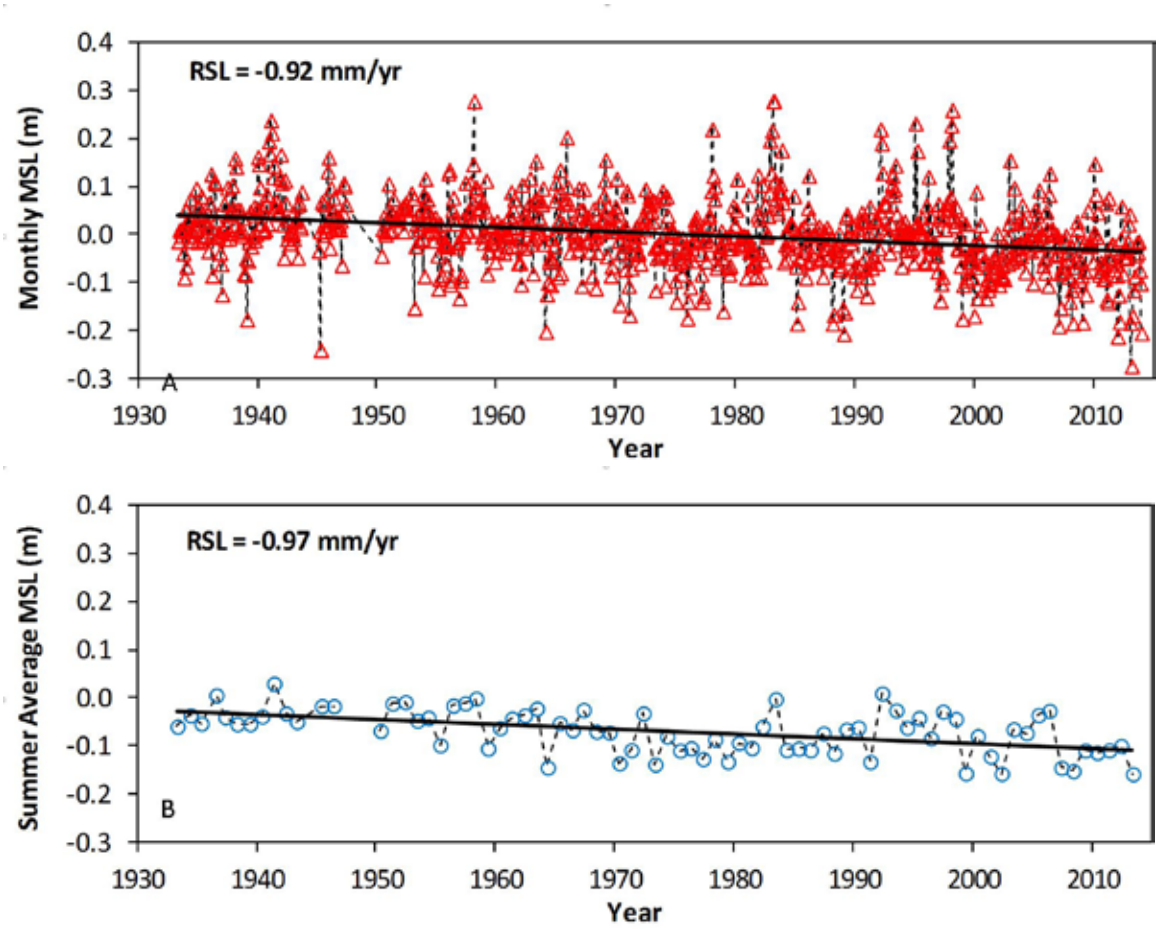

Figure 5. Tide gage results. Crescent City NOAA tide station (9419750) relative sea level trends using monthly mean sea levels with the average seasonal cycle removed (A), and summer 3-month average mean sea levels (B).

Table 1. Summary statistics of relative sea level trends for Crescent City (9419750) and North Spit (9418767) tide stations, and the vertical land motion estimate of North Spit relative to Crescent city using the differenced time series from the monthly mean sea levels with the average seasonal cycle removed, and the summer 3-month average mean sea levels. Note that the 95% confidence interval (CI) assumes independent observations.

Tide Station	Tide Analysis	RSL or VLM (mm/yr)	N	R^2	RMSE (m)	CI (mm/yr)
Crescent City	Monthly with average seasonal cycle removed	-0.92	905	0.083	0.070	± 0.20
Crescent City	Summer 3 month average	-0.97	77	0.244	0.039	±0.39
North Spit	Monthly with average seasonal cycle removed	3.85	429	0.263	0.067	±0.61
North Spit	Summer 3 month average	4.70	36	0.587	0.041	±1.38
North Spit minus Crescent City	Monthly with average seasonal cycle removed	5.75	428	0.909	0.019	±0.17
North Spit minus Crescent City	Summer 3 month average	5.58	36	0.942	0.014	±0.48

[1]RSL = relative sea level, N = count, R^2 = R squared of regression, RMSE = root mean square error of residual, and CI = 95% confidence interval assuming independent observations.

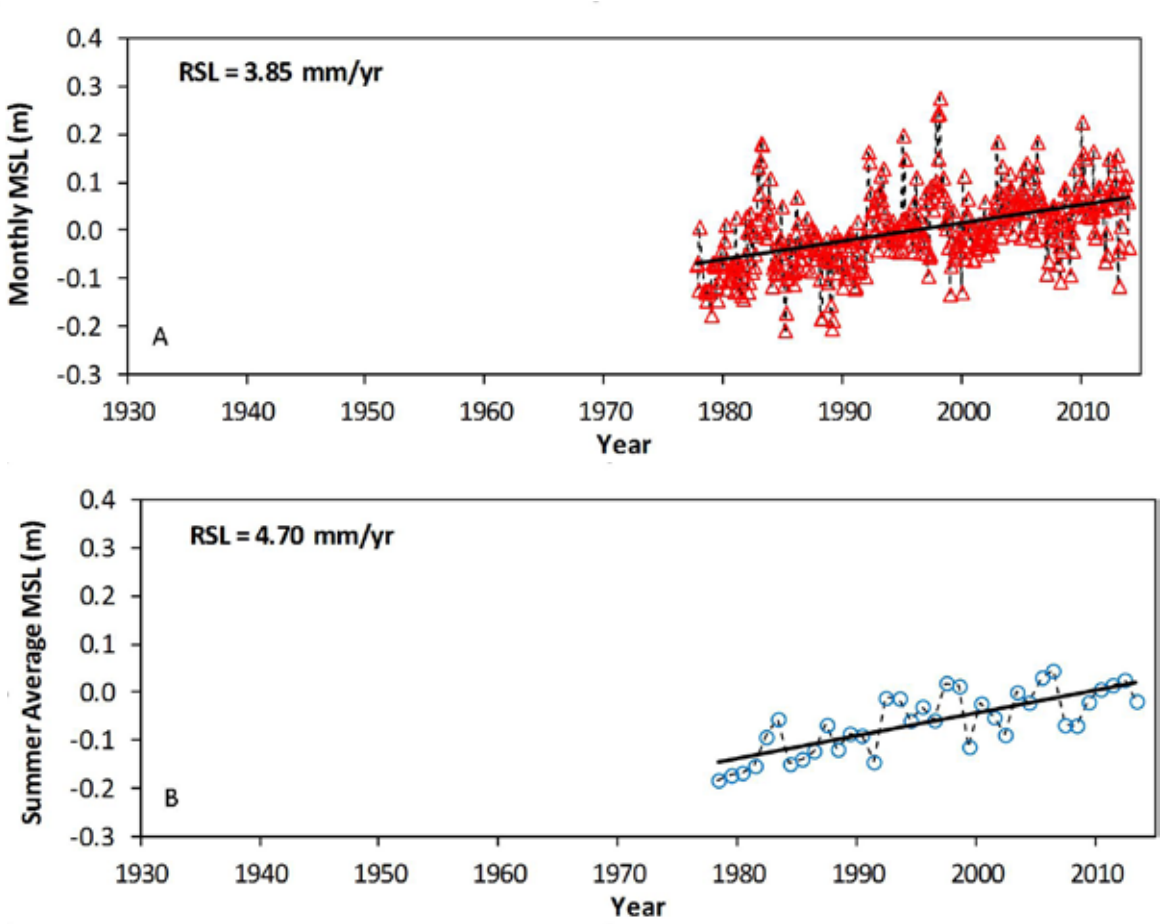

Figure 6. Tide gage results. North Spit NOAA tide station (9418767) relative sea level trends using monthly mean sea levels with the average seasonal cycle removed (A), and summer 3-month average mean sea levels (B).

Table 2. Summary of sea level rise and vertical land motion estimates for Humboldt Bay tide stations.

	SLR and VLM Rates (mm/yr)			
Tide Station (TS)	ReSL	RSL	TS - CC	VLM
Crescent City (CC)	2.28	-0.97		3.25
North Spit (NS)	2.28	4.61	5.58	-2.33
Mad River Slough (MRS)	2.28	3.39	4.36	-1.11
Samoa (SO)	2.28	2.53	3.50	-0.25
Fields Landing (FL)	2.28	3.76	4.73	-1.48
Hookton Slough (HS)	2.28	5.84	6.81	-3.56

[1]ReSL = regional sea level, RSL = relative sea level, and VLM = vertical land motion.

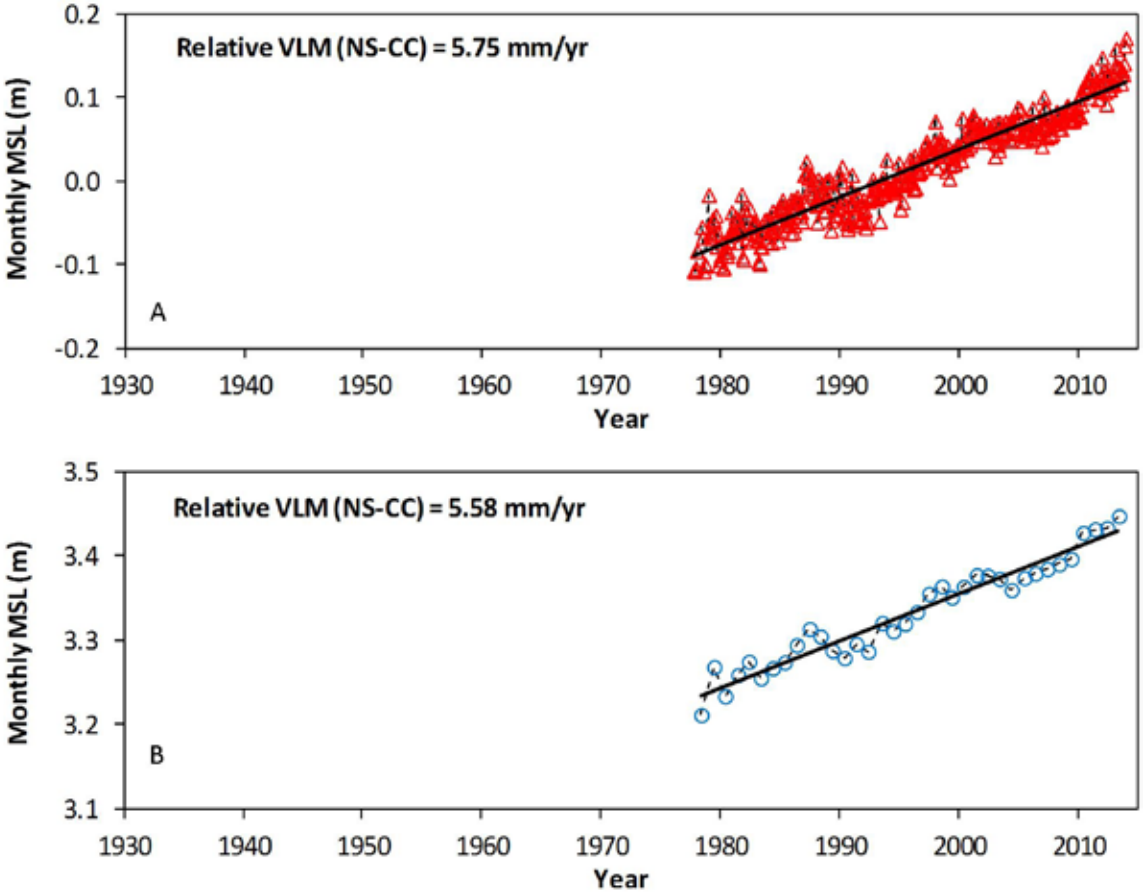

Figure 7. Differenced time series (North Spit minus Crescent City) representing the vertical land motion rate of North Spit relative to Crescent City using the monthly mean sea levels with the average seasonal cycle removed (A), and summer 3-month average mean sea levels (B).

the average seasonal cycle removed (Burgette et al., 2009; Zervas, 2009 and 2013). Recently, Komar et al. (2011) demonstrated that using the annual summer water levels provided the statistically best RSL trends for the Pacific Northwest coast. The annual summer water levels consist of the 3 month average centered on the unadjusted minimum monthly summer value. Both approaches were used to estimate the RSL rates for the CC and NS data (**Figures 5 and 6**), and the relative VLM of the differencing technique of NS minus CC (**Figure 7**). **Table 1** summarizes the rate trend statistics for CC, NS, and NS minus CC. For this assessment, the RSL and VLM rates for the CC station, and the NS minus CC relative VLM rate determined from the annual summer water levels were used.

The RSL rate for CC is -0.97 mm/yr, and assuming a regional eustatic sea level rate of 2.28 mm/yr (Burgette et al., 2009) gives a VLM estimate of 3.25 mm/yr (**Table 2**). The RSL and VLM rate estimates for NS are determined by using the 5.58 mm/yr relative VLM rate for NS minus CC (**Figure 7**), and the 3.25 mm/yr VLM for CC, which provides a VLM and RSL rate of -2.33 mm/yr and 4.61 mm/yr, respectively (**Table 2**). The estimated 4.61 mm/yr RSL rate is close to the annual summer RSL rate of 4.70 mm/yr (**Figure 6**).

Using this same method, 1970's era and contemporary (2008, 2010, 2012) observations of monthly mean sea levels are also differenced between the CC data for the remaining tide gage stations (MRS, SO, FL and HS) in Humboldt Bay (**Figures 8, 9, 10, and**

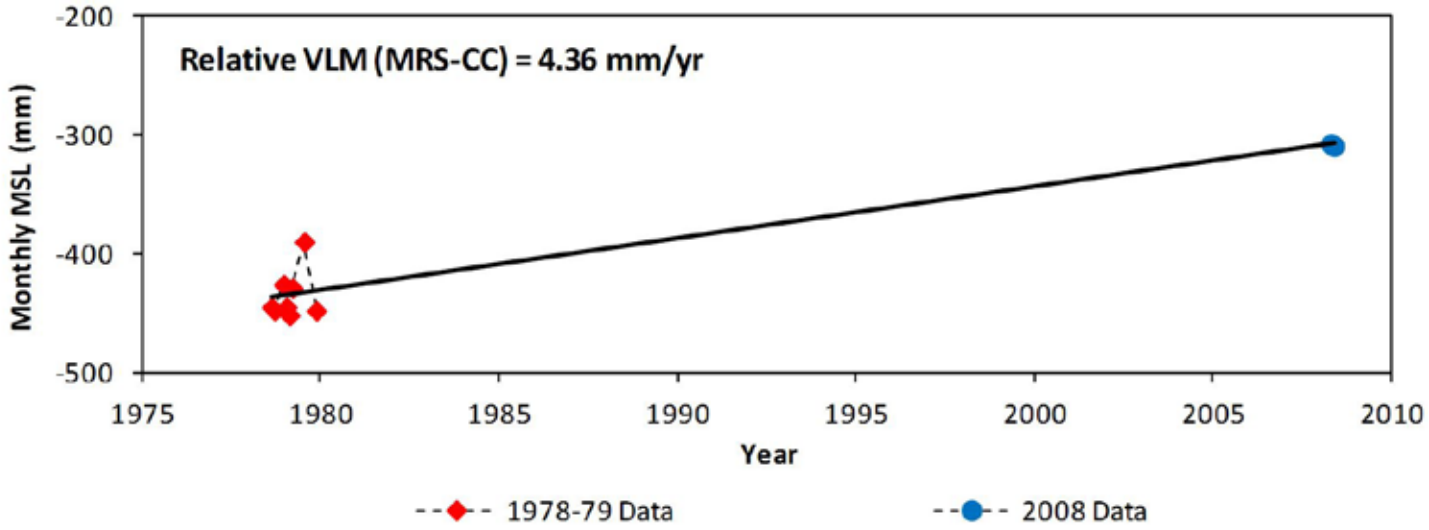

Figure 8. Differenced time series (Mad River Slough minus Crescent City) representing the vertical land motion rate of Mad River Slough relative to Crescent City using the monthly mean sea levels.

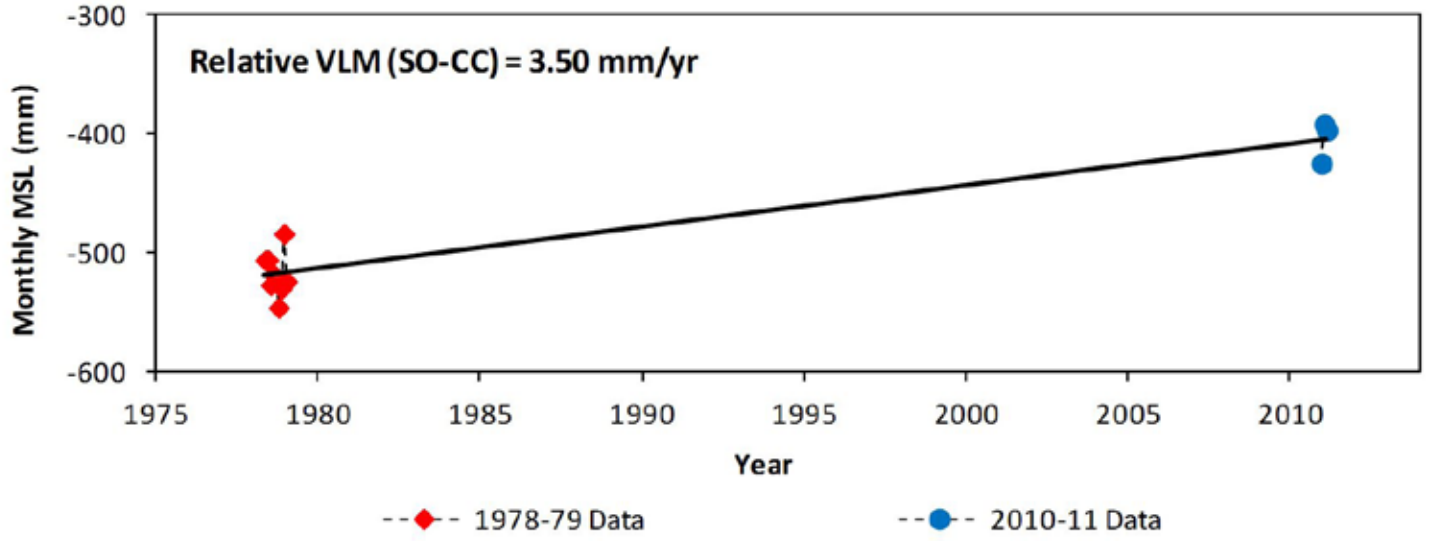

Figure 9. Differenced time series (Samoa minus Crescent City) representing the vertical land motion rate of Samoa relative to Crescent City using the monthly mean sea levels.

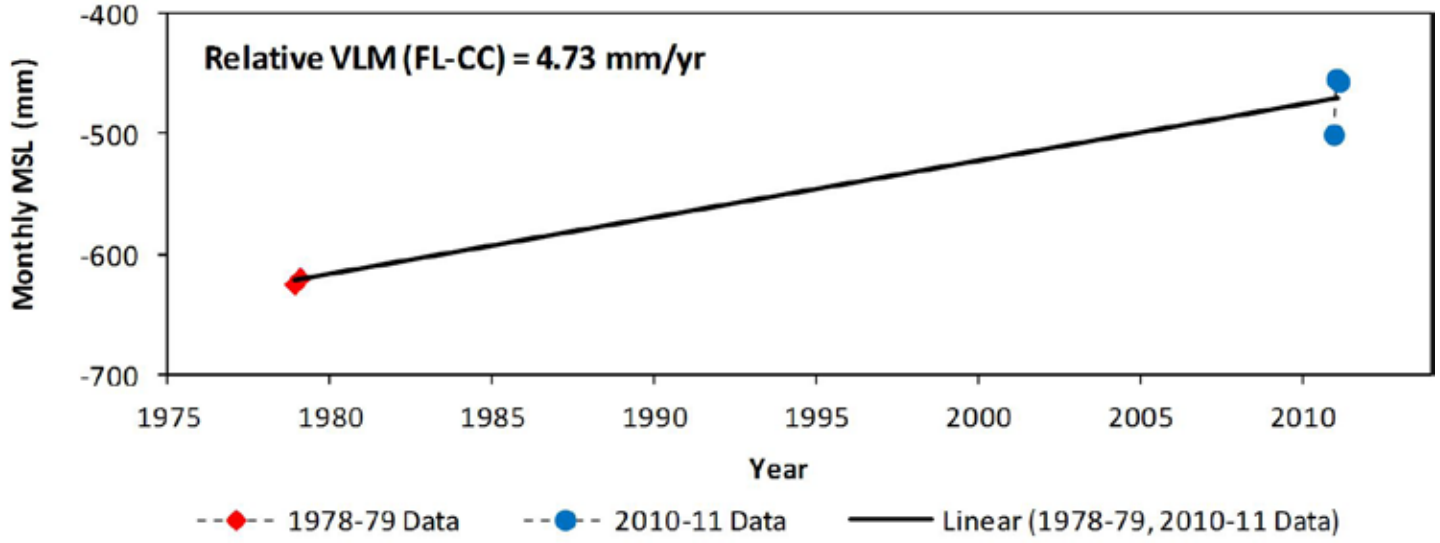

Figure 10. Differenced time series (Fields Landing minus Crescent City) representing the vertical land motion rate of Fields Landing relative to Crescent City using the monthly mean sea levels.

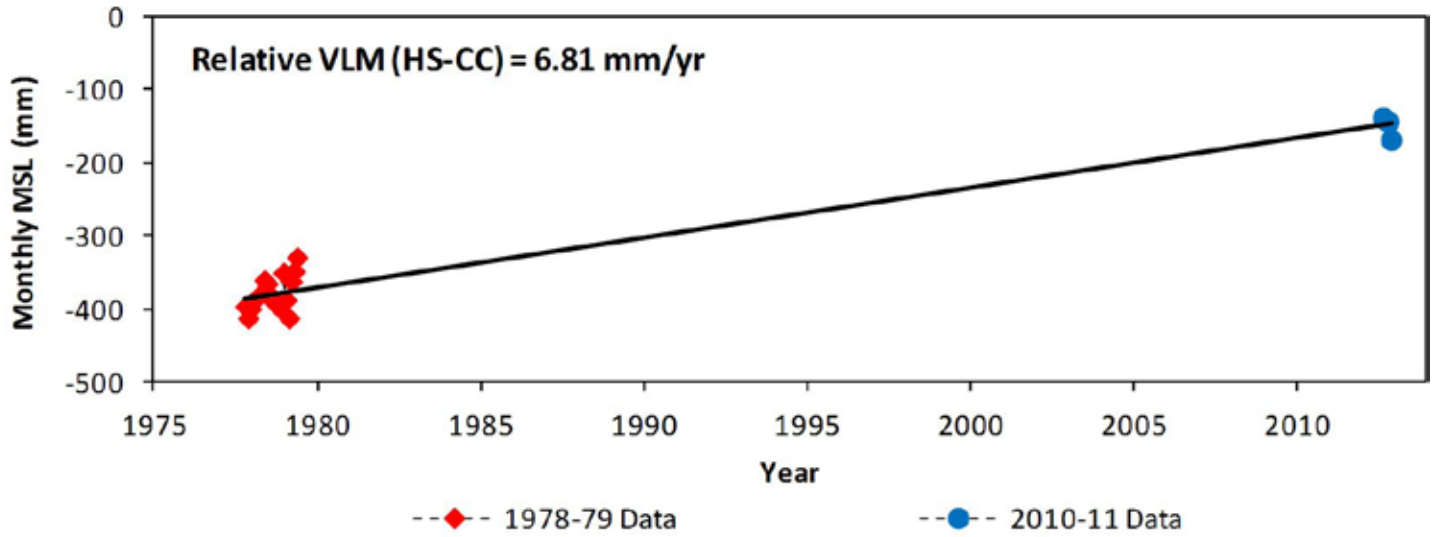

Figure 11. Differenced time series (Hookton Slough minus Crescent City) representing the vertical land motion rate of Hookton Slough relative to Crescent City using the monthly mean sea levels.

11). The RSL and VLM rates for the MRS, SO, FL, and HS are summarized in **Table 2**. Based on this assessment, we estimate VLM rates (mm/yr) of -2.33 (NS), -1.11 (MRS), -0.25 (SO), -1.48 (FL), and -3.56 mm/yr at HS (**Table 2**). Assuming a regional eustatic sea level of 2.28 mm/yr, gives a RSL rate (mm/yr) at NS of 4.61, 3.39 at MRS, 2.53 at SO, 3.76 at FL, and 5.84 at HS (**Table 2**).

Land level Analysis Summary

Dr. Reed Burgette at the University of Oregon analyzed the available first-order leveling data collected by the NGS, which were collected in 1931, 1945, 1968, and 1988. We analyzed the unadjusted line data, with orthometric, rod, level, temperature, astronomical, refraction, and magnetic corrections applied by the NGS as appropriate (Federal Geodetic Control Committee, 1984). The 1931 data pre-date the installation of the NS tide gage, and the surveyed benchmarks are confined to the route of Highway 101 between Crescent City south through the Humboldt Bay region. We also analyzed data from a spur route between Highway 101 and the NS tide gage that was first observed in 1945 as well as the regional lines observed in 1968 and 1988. We calculated tilt rates relative to Benchmark 60 in the Eureka downtown, which has a long history and appears to be locally stable. Run distance-dependent one sigma errors are propagated following the procedure of Burgette et al. (2009). In the Humboldt Bay area, leveling was completed between the NS tide gauge and the main leveling route along Highway 101 in 1945, 1968, and 1988. Relative uplift rates calculated from these epochs are all consistent within estimated random error, showing subsidence of North Spit at approximately 3 mm/yr relative to Arcata, and 1.5-2 mm/yr relative to benchmarks in the Old Town of Eureka. (**Figure 12; Burgette et al., 2012**). Uplift rates estimated from 1988-1968 leveling epochs are also consistent, in a regional sense, with the relative tidal rates between NS and CC as discussed in the previous section. There are discrepancies involving data observed in 1933, which we will investigate further with a misclosure analysis.

To verify the quality of the estimated relative uplift rates, we compare the relative rates from leveling between NS and CC to the relative uplift rates inferred

from the differenced tidal records. The rates from 1988-1968, which include the primary benchmarks at both gages, match within the estimated random error. We use the relative uplift rate between the NS primary benchmark and Benchmark 60, estimated from the 1988-68 epoch difference, to estimate the portion of NS to CC route not observed in 1933. The relative difference in uplift rate between Eureka (and by extension, NS) and Crescent City for the epoch differences involving the 1931 surveying are much lower than what is observed from the tidal records, when evaluated against the random error estimates. Similarly, uplift rates calculated from 1988-1931 along the route east from Arcata show a concave-up decay inland similar to what we observe to the north in Oregon (Burgette et al., 2009) but a strong subsidence (< -4 mm/yr) of the interior of area near Redding. In light of these discrepancies, we conclude that there may have been a systematic error that accumulated in the 1931 surveys in this area. Loop misclosure analysis may provide additional evidence of a problem localized in the 1931 epoch.

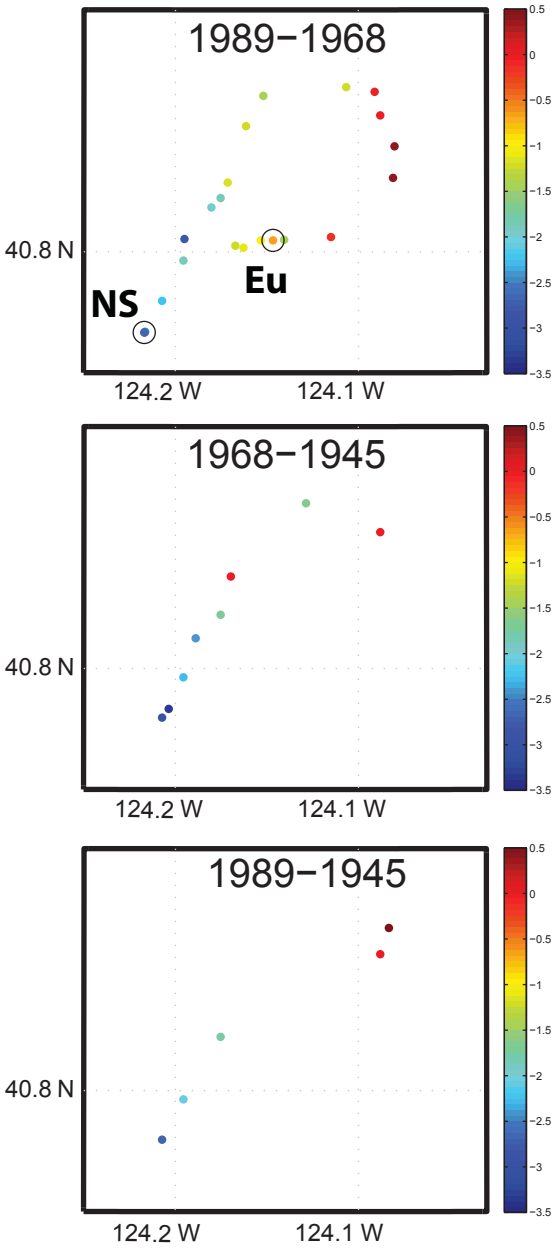

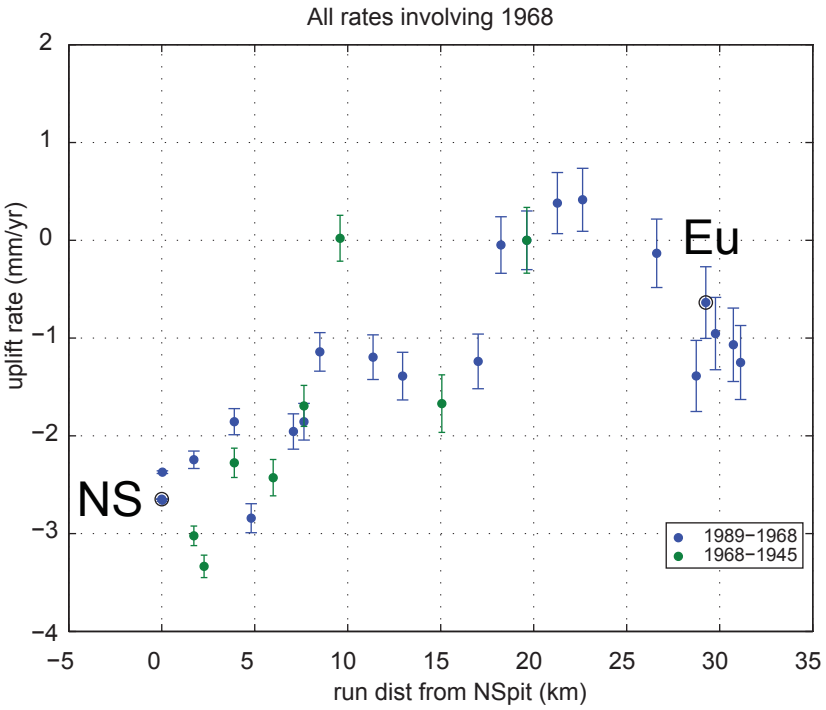

Figure 12 A. 1945, 1968, and 1989 benchmark leveling results plotted for central and northern Humboldt Bay (Burgette et al., 2012). Color represents vertical land motion rate in mm/year. Eu and NS benchmarks are circled.

Figure 12 B. Vertical land motion rates (mm/yr) for all rates that include the 1968 survey. Eu and NS benchmarks are circled.

Across the region, Humboldt Bay is subsiding while the surrounding areas are not (**Figure 13**). Rates of vertical land motion are estimated at -3.56 mm/yr in south Humboldt Bay, and 3.25 mm/yr in Crescent City. Uplift rate gradients are unaffected by the underlying basement material (bedrock versus fill/bay margins). South of Humboldt Bay there is uplift occurring in

Table 3. Land-level misfit between nearest Burgette level-loop data and tide gage.

Station	Nearest Surveymark Land-level (mm/yr)	Tide Gage Based Land-level (mm/yr)	Residual Land-level Misfit (mm/yr)
CC	2.33	3.25	0.92
NS	-2.69	-2.33	0.36
MRS	-1.58	-1.11	0.47
SA	-2.15	-0.25	1.90
FL	-1.94	-1.48	0.46
HS	-3.68	-3.56	0.12

the Fortuna-Scotia region, similar to the uplift rates north of Humboldt Bay. We compare vertical rates of motion derived from land-level surveys with those derived from our tide gage analyses. These compared rates are consistent, as evidenced by the small residuals in Table 3, except for station SO. Table 3 compares the land subsidence estimates based on both sea-level and land level measurements for Humboldt Bay and Crescent City.

In addition, continuously operating Global Positioning System (CGPS) stations operated by the National Science Foundation's EarthScope project provide another independent data set to determine rates of vertical land motion (**Figure 13**). In some cases, the 2004-2013 geodetic solutions agree with the patterns of subsidence and uplift from the leveling surveys, particularly at HS and CC (**Figure 13**). The GPS and land-level observations preclude localized settlement subsidence of tide gauge instruments and geodetic monuments as a significant mechanism for the gradients in subsidence in the Humboldt Bay region.

Discussion and Conclusions

Land-level derived uplift rates from 1968-1988 generally agree to within 1 mm/yr of tide gage derived rates for permanent and temporary sites within Humboldt Bay (1977-2012). Rates of local sea-level rise at CC, NS, MRS, SO, FL, and HS are -0.97, 4.61, 3.39, 2.53, 3.76, and 5.84 mm/yr, respectively. Rates of local land-level change at CC, NS, MRS, SO, FL, and HS are 3.25, -2.33, -1.11, -0.25, -1.48, and -3.56 mm/yr, respectively. The subsidence originally interpreted to be locally observed at NS is now found to extend over a 100 km^2 area in the Humboldt Bay region (**Figure 14**).

We conclude that tide gage, GPS, and land-level survey data provide independent observations of tectonic deformation in Northern California. Trends of sea-level rise at the NS tide gage, previously thought to be anomalous, are consistent with other observations in Humboldt Bay and resolvable when included in our regional analyses. The observed gradients in tectonic deformation directly control the variation of sea-level rise in this region. However, the detailed spatial variation of vertical land-level motion rates remain unresolved in many parts of the Humboldt Bay region. Below we list some tasks required to resolve this spatial variation in sea-level rise for the northern California region.

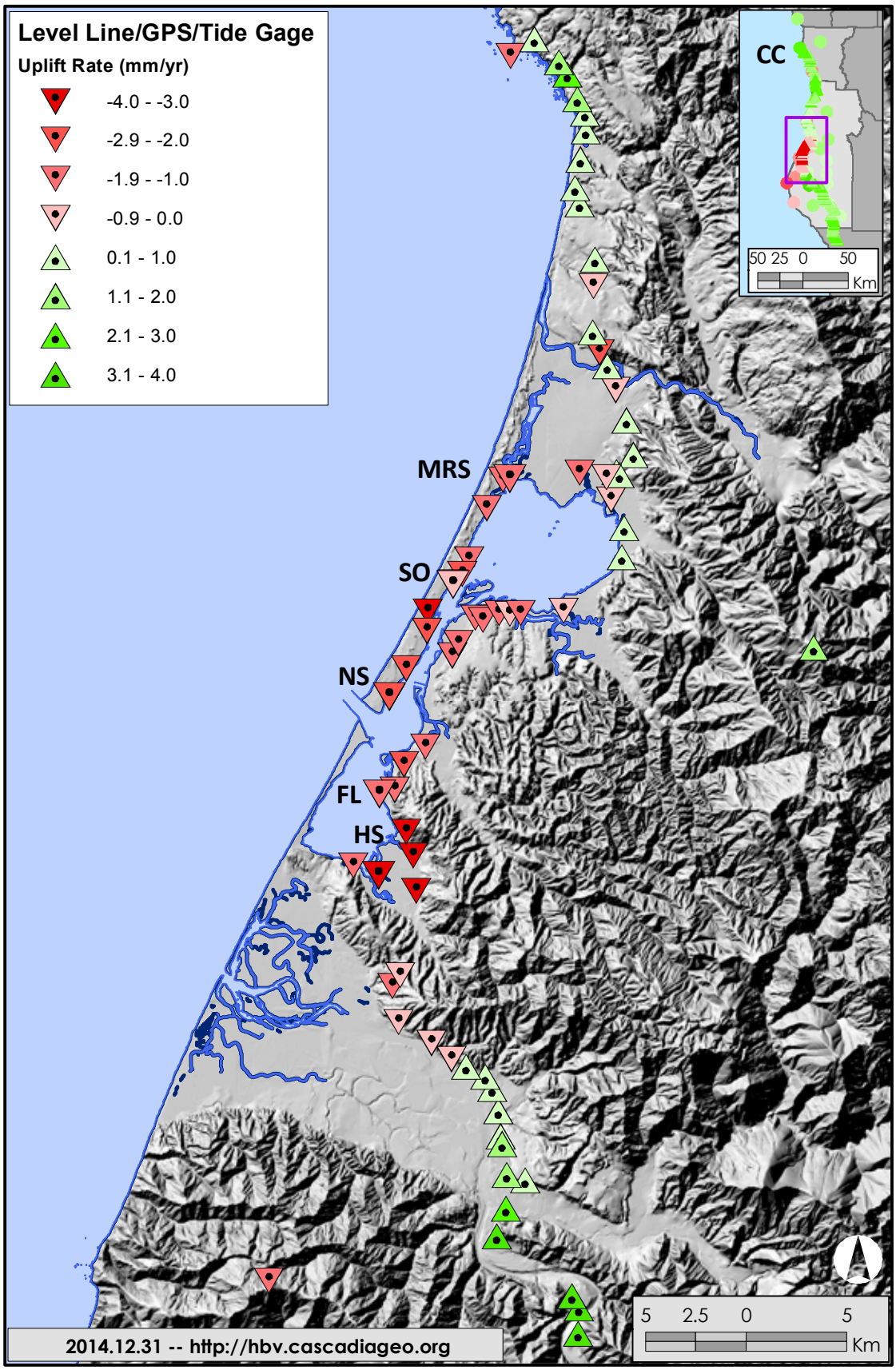

Figure 13. Summary of vertical land-level change in coastal northern California.

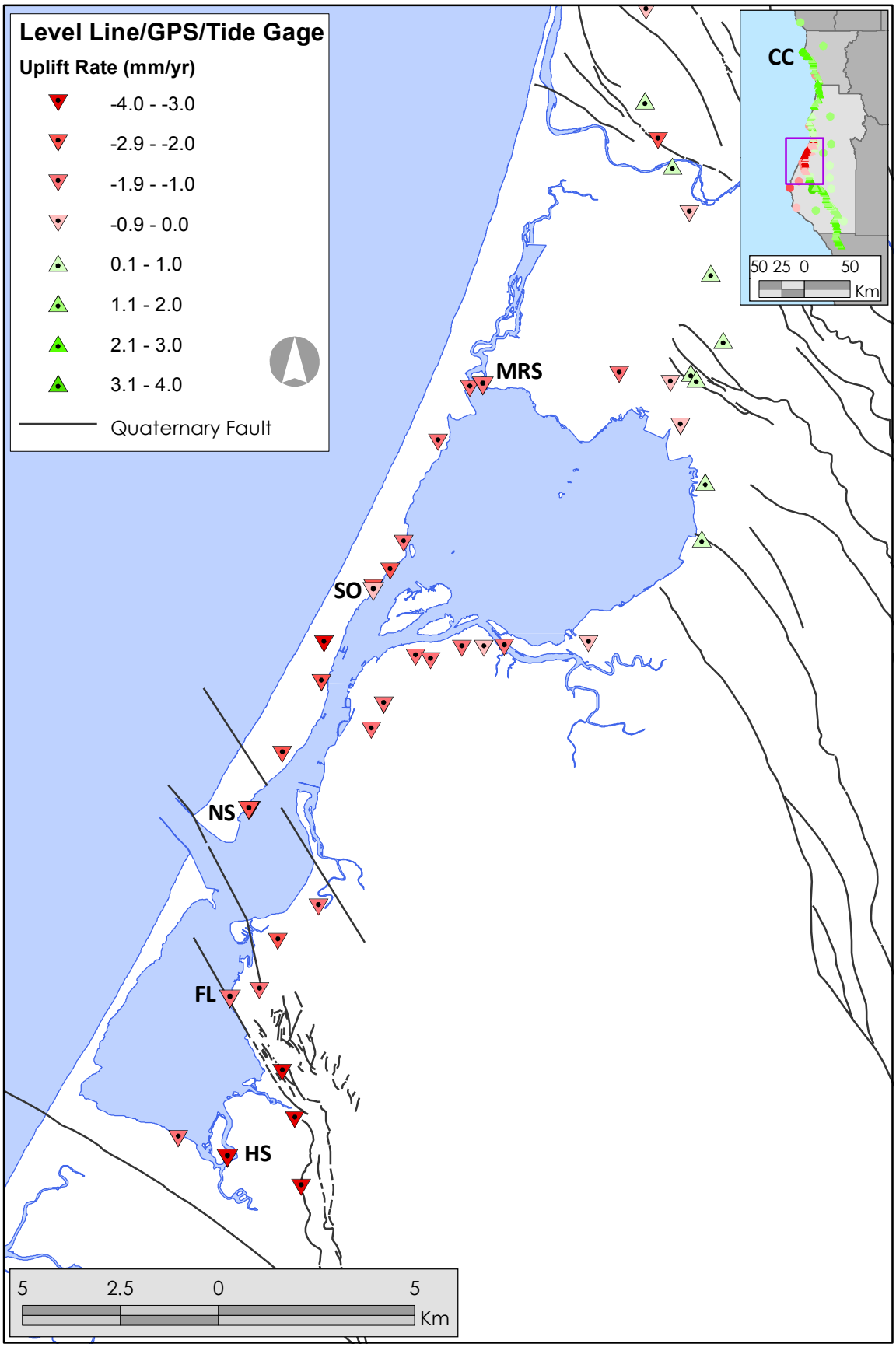

Figure 14. Summary of vertical land-level change in the Humboldt Bay region.

Future / Ongoing Work

- Installation of tide gage at Trinidad
- Installation of tide gage and complete leveling surveys at the Chevron dock in support of CENCOOS
- Support the NHE redeployment of the tide gage at MRS (water level observations, high precision level survey)
- Begin modeling uplift / subsidence in regards to plate tectonic processes
- Incorporate regional subsidence / uplift rates with Pacific Northwest estimates established by Weldon and Burgette at Univ. of Oregon
- Prepare GIS products as deliverables to USFWS, PLCC, and stakeholders (raster and vector data)
- Prepare peer reviewed journal article
- Conduct an onsite visit to a tide gage with USFWS, PLCC, and stakeholder coordinators
- Conduct a webinar in support of education and outreach to USFWS, PLCC, and stakeholders
- Acquire additional water level instrumentation for future deployments in Eureka
- Seek funding for GPS instrumentation at the NS tide gage, working with UNAVCO, Inc.

References

Burgette, R.J., Weldon, R.J., and Schmidt, D.A., 2009. , Interseismic uplift rates for western Oregon and along strike variation in locking on the Cascadia subduction zone, Journal of Geophysical Research, Vol. 114, B01408, doi: 10.1029/2008JB005679.

Burgette, R., Weldon, R., Schmidt, D., Williams, T.B., 2012. Constraints on interseismic locking along the southern Cascadia subduction zone from historic and recent leveling and sea level observations, presented at 2012 Fall meeting, AGU, San Francisco, CA, 3-7 Dec.

Cascadia GeoSciences, 2013. Tectonic land level changes and their contribution to sea-level rise, Humboldt Bay region, Northern California 2013 Status Update submitted to U.S. Fish and Wildlife Service regarding award F11AC01092.

Cazenave, A. and Llovel, 2010. Contemporary Sea Level Rise, Annu. Rev. Mar Sci., v. 2, pp. 145-173.

Chaytor, J. D., Goldfinger, C., Dziak, R. P., and Fox, C. G., 2004. Active deformation of the Gorda plate: Constraining deformation models with new geophysical data: Geology, v. 32, no. 4, p. 353-356.

Federal Geodetic Control Committee, 1984. Standards and Specifications for Geodetic Control Networks, Rockville, Maryland, pp. 34.

Flück, P., Hyndman, R. D., and Wang, K., 1997. Three-dimensional dislocation model for great earthquakes of the Cascadia subduction zone Journal of Geophysical Research, B, Solid Earth and Planets, v. 102, no. 9, p. 20,539-520,550.

Komar, P.D., Allan, J.C., and Ruggiero, P., 2011. Sea Level Variations along the U.S. Pacific Northwest Coast: Tectonic and Climate Controls, Journal of Coastal Research, v. 27, no. 4, pp. 808-825.

McCaffrey, R., Qamar, A., King, R. W., Wells, R. W., Khazaradze, G., Williams, C., Stevens, C., Vollick, J. J., and Zwick, P. C., 2007, Fault locking, block rotation and crustal deformation in the Pacific Northwest: Geophysical Journal International, doi: 10.1111/j.1365-246X.2007.03371.x.

Mitchell, C. E., Vincent, P., Weldon II, R. J., and Richards, M. A., 1994. Present-day vertical deformation of the Cascadia margin, Pacific northwest, U.S.A.: Journal of Geophysical Research, v. v. 99, p. p. 12,257-212,277.

Nelson, A. R., Shennan, I., and Long, A. J., 1996. Identifying coseismic subsidence in tidal-wetland stratigraphic sequences at the Cascadia subduction zone of western North America: J. Geophys. Res., v. v. 101, no. no. B3, p. p. 6115-6135. Northern Hydrology and Engineering, 2009, Tidal Wetland Geometric Relations in Humboldt Bay: Mad River Slough Pilot Study, prepared for U.S. Fish & Wildlife Service, 31p.

Nelson, A. R., Kelsey, H. M., and Witter, R. C., 2006. Great earthquakes of variable magnitude at the Cascadia subduction zone: Quaternary Research, v. 65, p. 354-365.

Peltier, W. R., 2001, On eustatic sea level history: Last Glacial Maximum to Holocene: Quaternary Science Reviews, p. 377-396.

Plafker, G., 1972. Alaskan earthquake of 1964 and Chilean earthquake of 1960: implications for arc tectonics: J. Geophys. Res., v. v. 77, p. p. 901-925.

Verdonk, D., 2006. Contemporary vertical crustal deformation in Cascadia, Tectonophysics, Volume 417, Issues 3–4, Pages 221–230.

Wang, K., Wells, R., Mazzotti, S., Hyndman, R. D., and Sagiya, T., 2003. A revised dislocation model of interseismic deformation of the Cascadia subduction zone Journal of Geophysical Research, B, Solid Earth and Planets v. 108, no. 1.

Williams, T. B., Kelsey, H. M., and Freymueller, J. T., 2002. GPS-derived strain in northwestern California: Termination of the San Andreas fault system and convergence of the Sierra Nevada–Great Valley block contribute to southern Cascadia forearc contraction: Tectonophysics, v. 413, p. 171-184.

Zervas, C., Gill, S., and Sweet, W., 2013. Estimating Vertical Land Motion from Long-Term Tide Gauge Records, Technical Report National Ocean Service (NOS) CO-OPS 065, 22p.

Contributors

Cascadia GeoSciences

Dr. Jason R. Patton, Todd B. Williams, Diane Sutherland, Jay Stallman, Tom Leroy

Northern Hydrology

Jeff Anderson, Corin Pilkington

Pacific Watershed Associates

Tom Leroy, Whelan Gilkerson, Ed Southwick

Humboldt State University

Dr. Mark Hemphill-Haley, and numerous HSU Geology student volunteers

Kyle R. Weiss, Department of Environmental Resources Engineering

University of Oregon

Drs. Ray Weldon, Reed Burgette

Northern Hydrology & Engineering

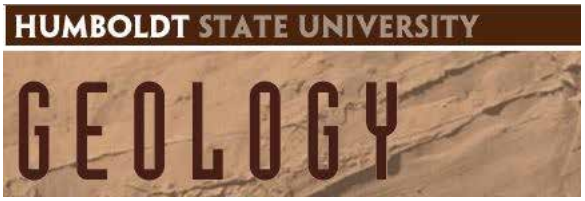

ESA PWA

550 Kearny Street
Suite 900
San Francisco, CA 94108
415.896.5900 phone
415.896.0332 fax

www.esassoc.com

memorandum

date July 21, 2014

to Rob Holmlund (GHD)

from Louis White, PE

subject Climate Data Projections for Caltrans District 1 Climate Change Pilot Study

1. Introduction

This memorandum describes climate change data sets that were compiled and processed for use in the Caltrans District 1 Climate Change Pilot Study (D1CCPS). The purpose of the project is to evaluate the vulnerability of Caltrans transportation assets in District 1 to various climate change impacts and develop adaptation strategies for the most vulnerable assets. The various climate change data sets prepared for this project, and included in the GIS geodatabase, will be combined with an inventory of Caltrans assets in District 1 to evaluate the vulnerability of those assets. This analysis is based on existing information and does not include any additional modeling. Data was processed to create metrics to describe the level of exposure of the assets to a particular climate change impact relative to a threshold or trigger at specific time intervals.

The following sections describe the information that is included in the geodatabase and the metrics used to characterize exposure of each climate stressor and hazard.

The work that is described in this memorandum was conducted by James Gregory, PE, Elena Vandebroek, PE, Pablo Quiroga, Louis White, PE, and with review by Jeremy Lowe.

2. Definition of Terms and Climate Change Background

The science of climate change and modeling of future scenarios has been extensively described (IPCC, 2013). In general, global temperature is driven by concentrations of greenhouse gases (GHGs) such as carbon dioxide, methane, and water vapor which absorb energy radiating from Earth back into space. Global emissions of greenhouse gases have rapidly increased following the industrial revolution in the mid-1700s primarily due to the burning of fossil fuels such as coal, oil, and natural gas. Emissions continue to grow as nations modernize and consume greater amounts of fossil fuels. Acknowledging this pattern, many national and statewide initiatives have been advanced to curb GHG emissions as well as respond to the anticipated impacts of climate change already underway.

Present day concentrations of carbon dioxide (CO_2) in Earth's atmosphere represent the highest ever measured, which is a key driver of increasing global temperatures, precipitation patterns, and rising sea levels. The anticipated rise in temperatures is expected to continue beyond year 2100, even if the CO_2 emissions are reduced by 2050 (Figure 1). The increased global temperature acts to warm ocean temperatures, and also has been shown to increase the rate of melting of the large ice sheets near the poles. Sea level rise (SLR) results from a combination of melting of land-based ice and thermal expansion of the oceans due to increased temperatures. The magnitude of the impact of global warming on climate change is influenced by various complex interactions in the earth-ocean-atmosphere system. Many processes and feedbacks must be accounted for in order to realistically project climate changes resulting from particular GHG emission scenarios. These complications are the source of much of the debate which has occurred about the likely magnitude and timing of climate changes due to the enhanced GHG effect.

The following sections provide background and descriptions of several terms that are used in this memorandum to describe climate change data and climate modeling.

2.1. Emissions Scenarios

Projecting potential climate trends and extremes requires first establishing future scenarios of GHG emissions that will influence future climate patterns. Due to the high level of uncertainty in the evolution of these factors, a series of qualitative storylines describing the evolution of possible trajectories of heat-trapping GHG emissions were developed by the International Panel on Climate Change (IPCC) for the IPCC Fourth Assessment Report (AR4) (IPCC 2007). These were used to guide climate change modeling efforts in AR4 upon which most of the available climate impact modelling has been based. The IPCC's (2000) special report on emissions scenarios (SRES) provides six scenario groups of plausible global emissions pathways, with no assigned probabilities of occurrence. Two of these scenarios, A2 and B1, have been selected to represent medium-high and relatively low (or "best-case") emissions projections respectively (Cayan et al. 2012). These emissions scenarios are defined as follows:

- **A2**. Medium-high emissions resulting from continuous population growth coupled with internationally uneven economic and technological growth. Under this scenario, emissions increase through the 21st century and by 2100 atmospheric carbon dioxide (CO2) levels are approximately three-times greater than pre-industrial levels.

- **B1**. Lower emissions than A2, resulting from a population that peaks mid-century and declines thereafter, with improving economic conditions and technological advancements leading to more efficient utilization of resources. Under this scenario, emissions peak mid-century and then decline, leading to a net atmospheric CO2 concentration approximately double that of pre-industrial levels. This scenario is often referred to as a "best-case" scenario.

2.2. General Circulation Models (GCMs)

General circulation models (GCMs) are used for predicting climate change. They model how the atmosphere, oceans, land surface, and ice interact to create weather and climate over long periods of time (decades and centuries) over the whole globe. GCMs subdivide the Earth's surface, atmosphere, and oceans into a 3D grid of thousands of cells. Standard physical equations for the transfer of heat, water, and momentum are solved for each grid cell to predict temperature, precipitation, and winds. Many relevant processes are well represented at the

scale of these grid cells, such as the large-scale westerly flow of moisture from the Pacific Ocean. Due to the spread of climate projections over the various models, data is often averaged over multiple GCMs to avoid biasing towards any one model.

To identify the GCMs that best suited to predicting climate phenomena in the State of California, Cayan et al. (2012) selected six models from AR4 based on data availability and on historic skill in representing climate patterns in California, including seasonal precipitation and temperature, annual variability of precipitation, and the El Niño/Southern Oscillation (ENSO) phenomenon. Data was obtained for six GCMs considered representative of climate trends in California. Each model has multiple runs with 16 total runs for the A2 scenario, and 17 total runs for the B1 scenario. Runs represent different initial conditions in the GCMs. The six models selected for the assessment were:

1. The NCAR Parallel Climate Model (PCM);

2. The NOAA Geophysical Fluids Dynamics Laboratory (GFDL) model, Version 2.1;

3. The NCAR Community Climate System Model (CCSM);

4. The Max Plank Institute 5th generation ECHAM model (ECHAM5/MPI OM);

5. The medium-resolution model from the Center for Climate System Research of the University of Tokyo and collaborators (MIROC 3.2); and

6. The French Centre National de Recherches Météorologiques (CNRM) models.

Data for a series of climate stressors downscaled to the 12-kilometer (7.5-mile) scale has been archived and made available for public use on the World Climate Research Programme's (WCRP) Coupled Model Intercomparison Project Phase 3 (CMIP3) website (http://gdo-dcp.ucllnl.org). This data has been widely applied for evaluating climate trends in California. The CMIP3 archive presents compiled data from a joint effort between the US Department of the Interior's Bureau of Reclamation, Lawrence Livermore National Laboratory, Santa Clara University, Scripps, Climate Central, and the USGS. This archive includes downscaled geographic gridded data for temperature and precipitation for a number of GCMs and emissions scenarios as well as daily hydrologic projections of precipitation and other hydrologic stressors derived from the downscaled GCM data. We acknowledge the modeling groups, the Program for Climate Model Diagnosis and Intercomparison (PCMDI) and the WCRP's Working Group on Coupled Modelling (WGCM) for their roles in making available the WCRP CMIP3 multi-model dataset. Support of this dataset is provided by the Office of Science, U.S. Department of Energy.

The CMIP3 dataset represents GCM data developed for AR4 driven by the SRES emissions trajectories. The downscaled GCM data has been used to develop additional datasets including surface water projections (USBR, 2011), and fire risk projections (Westerling, A. L., Bryant, B. P. 2008). For the Fifth Assessment Report (AR5), the IPCC has developed new emissions scenarios called Representative Concentration Pathways (RCPs). There are four RCPs which represent different amounts of anticipated radiative forcing by the end of the century. The emissions trajectories and GHG concentrations for the RCPs deviate from the previous scenarios. The RCPs have been used to develop new GCM output and a downscaled dataset for Phase 5 of the CMIP (CMIP5) has been published online by the WCRP. This dataset was not used for this report for two primary reasons

1. The most recent statewide assessment of climate change in California used CMIP3 data and emissions scenarios. To remain consistent with existing projection information for California the CMIP3 data was also used for this report.

2. The downscaled CMIP5 dataset is currently available for temperature and precipitation projections only. Secondary datasets such as hydrologic projections have yet to be developed using CMIP5 data.

As further data becomes available for CMIP5, projection information should be updated to reflect the most recent climate projection information.

2.3. Downscaling

GCMs are designed to represent climate change processes at the global scale. Models can show differences in the rate of climate change at different locations, but only on the continental scale. The size of the GCM grid cells, and thus the spatial resolution of the climate projections, is limited by the computing power necessary to solve the equations for all of the grid cells at hourly (or shorter) time steps for runs which may span 100 years or more. Thus, the climate models at the time of the latest IPCC report in 2007 produced output at spatial scales of roughly 120 to 180 miles.

Particularly in mountainous regions, such as the California coastal ranges and the Sierra Nevada, this scale is too coarse to capture the many important effects of topography on climate. For example, because the elevations of mountain ranges are averaged with the elevation of adjacent valleys, the Sierra Nevada, as represented in the GCMs, tops out at around 6,000 feet. The scale of GCM output is also too coarse to use as input for many models predicting environmental impacts, such as basin-scale hydrologic and water system models, or wildlife habitat models. Therefore, techniques to reduce the spatial scale of the GCM output (that is, downscaling) are needed for most user applications.

- **Statistical downscaling**. Statistical relationships between the regional circulation and aspects of the local climate (e.g., temperature, precipitation, wind) are used to apply GCM results to a particular place.

- A **regional climate model** (RCM) uses output from a general circulation model, but simulates processes at much higher resolution over the particular region. A RCM is very much like a GCM, except that it uses much finer resolution and covers a limited area. So a regional model may have a 10-mile grid spacing over specific regions, compared with 120 to 180 miles for a GCM.

When making use of downscaled climate projections, as with the underlying GCM output, a range of projections should be considered rather than one or two. In the case of statistical downscaling, several GCM projections are typically downscaled using the same method. Likewise with RCM downscaling, it is important to consider projections produced by multiple RCM-GCM combinations.

2.4. Uncertainty

Natural sources of uncertainty are inherent in climate processes due to fluctuating and chaotic processes, but the act of modeling using numerical algorithms and its required assumptions introduces two more main sources of uncertainty: method uncertainty and emissions uncertainty. The three types of uncertainty that appear in this memorandum are as follows:

- **Method uncertainty** is introduced from differences in model algorithms, techniques, and how the climate processes are considered. GCMs simulate climate phenomenon using a three-dimensional grid typically run with a spatial resolution of hundreds of kilometers. Smaller scale processes such as cloud interactions must be spatially averaged and this is managed differently between GCMs. Physical climate interactions such as ocean circulation, and water vapor and heat transport can be handled differently between models. The consequence of this is that GCMs may produce differing results for the same emissions pathway. For this reason, it is standard to evaluate multiple GCMs to estimate the range of potential changes in climate conditions.

- **Emissions uncertainty** is a function of the future pathways of global emissions which are, by definition, hypothetical, and based on assumptions of population growth, socioeconomic composition, and technological innovation. The emissions pathways are projections, not predictions, of possible future conditions and how those conditions relate to carbon emissions worldwide. It is standard to choose multiple emissions scenarios to estimate the range of projected climate conditions. However, measured global emissions have exceeded nearly all of the projected emissions pathways developed under AR4 (Le Quéré et al. 2010).

- **Natural variability** also influences climate trends lending another source of uncertainty. Even without external forcing from increasing greenhouse gases, climate variability will occur over space and time due to natural interactions within the climate system. This natural variability will continue in the future while external forcing will also induce variability. The two sources of variability lead to uncertainty in estimating the impact of radiative forcing on climate patterns independent of natural variations.

3. Geodatabase of Climate Information

The GIS geodatabase attached includes a series of raster files containing climate data processed from downscaled CMIP3 data. Datasets of temperature, precipitation, and runoff for 1950-2100 at a spatial resolution of 12 km by 12 km (7.5x7.5 miles) were downloaded from the CMIP3 archive for the A2 and B1 emissions scenarios. The timestamp for these online datasets is August, 2011. The datasets in the geodatabase developed for this project are horizontally referenced to the World Geodetic System of 1984 (WGS 1984). The climate datasets in the geodatabase and key parameters are summarized in Attachment 1 and described in more detail below.

3.1. Temperature

Daily maximum air temperature data was obtained from the CMIP3 archive and processed to illustrate average trends, as well as projections of extreme conditions. The annual average of daily maximum temperature for District 1 is projected to increase by approximately 4.1°F and 6.7°F for the B1 and A2 emissions scenarios, respectively, by 2100 (Figure 2). This time series represents a spatial average of temperatures across all of District 1 and is presented as a 10-year moving average to remove noise. The solid line represents an ensemble average of the results over all model runs, and the shading indicates the range in projections due to method uncertainty between models. The general trend is that the average temperatures in District 1 will increase over the coming century. Changes in the annual average of the daily maximum temperature are similar for all four counties, and close to the District 1 average (Table 1).

TABLE 1
CHANGE IN ANNUAL AVERAGE OF DAILY MAXIMUM AIR TEMPERATURE FROM HISTORIC AVERAGE (°F)

Year	2050		2100	
Emissions Scenario	A2	B1	A2	B1
District 1	3.3	3.0	6.7	4.1
Del Norte	3.2	2.8	6.7	4.0
Humboldt	3.3	2.9	6.7	4.0
Lake	3.5	3.2	6.9	4.4
Mendocino	3.4	3.0	6.7	4.2

For this study, extreme temperature is defined as the number of days per year exceeding 95° F, referred to here as "heat days." The two future conditions datasets (2050 and 2100) represent the change in number of heat days relative to a historic 30-year average (1970-2000) from the CMIP3 model data. This variable is averaged over a 30-year period (2035-2065 for 2050, and 2070-2100 for 2100) and then averaged over the GCMs.

The change in the number of projected heat days for 2050 and 2100 vary spatially throughout District 1, and tend to show a larger change for emissions scenario A2 compared to scenario B1 (Figures 3 and 4, respectively). Maps of the projected data show that inland areas have the greatest change in the number of extreme heat days, while little or no increase in the number of extreme heat days is expected in the coastal areas. Although the projections show an increase of approximately 15 to 20 extreme heat days per year by 2050, up to an additional 40 days per year are projected for inland areas. This is particularly the case in Lake County and the eastern portions of Mendocino and Humboldt Counties. A greater increase in heat days is projected for the A2 emissions scenario as compared to the B1 emissions scenario.

Method uncertainty introduced by the different model runs indicates that the number of additional heat days for the district could be significantly higher or lower (Figure 5). The number of extreme heat days presented in Figures 3 and 4 correspond to an average of all model runs, which tends to hide the model disagreement. The time series in the top panel of Figure 5 shows a running 30-year average of the additional number of heat days per year, where the solid line represents the average of all models, and the shaded areas correspond to the spread of the model projections. Note that this data is for a district average, as compared to the spatial data shown in the preceding figures. The lower panel of Figure 5 presents box plots that illustrate the distribution of model projections, where the blue box indicates the 25^{th} percentile of the model projections, the red box indicates the 75^{th} percentile, and the outer limits represent the maximum and minimum model projections.

3.2. Precipitation

Daily maximum precipitation data was obtained from the CMIP3 archive and processed to illustrate average trends, as well as projections of extreme conditions. The relative change of the total annual precipitation compared to the historic average is projected to decrease by approximately 2% to 7% for the B1 and A2 emissions scenarios, respectively, by 2100 (Table 2). The values in Table 2 represent a spatial average of precipitation across all of District 1 and was estimated using a 30-year moving average to remove noise in the signal. Figure 6 presents a time series graphic of the modeled precipitation data, where the solid line represents an ensemble average of the results over all model runs and the shading indicates the range in projections due to method uncertainty between models. The time series is presented using a 10-year moving average. The general trend of

the data indicates that the changes in total annual precipitation in District 1 over the coming century are very uncertain, as shown by the wide range of model projections. However, the GCM averaged relative change in the total annual precipitation as a spatial average over each county yields similar results close to the District 1 average (Table 2).

TABLE 2
PERCENT CHANGE IN TOTAL ANNUAL PRECIPITATION FROM HISTORIC AVERAGE (%)

Year	2050		2100	
Emissions Scenario	A2	B1	A2	B1
District 1	-4.1	-0.5	-6.5	-2.0
Del Norte	-3.0	0.0	-5.6	-0.6
Humboldt	-3.9	-0.4	-6.5	-1.8
Lake	-5.1	-1.2	-6.8	-3.0
Mendocino	-4.6	-0.8	-6.8	-2.6

The District 1 average of the total annual precipitation for the ensemble average of models was compared to a selected "wet" model (PCM) and a selected "dry" model (GFDL) to illustrate the range in projections (Table 3). The results of the wet model indicate an increase in the total annual precipitation of up to approximately 9% greater than the historic average (for B1 scenario at 2100), while the dry model shows a decrease of up to approximately 15% (for A2 scenario at 2100). These results indicate that careful interpretation and selection of future climate projections need to be considered when applying to assessing the vulnerability of assets as well as the selection of an appropriate emissions scenario.

TABLE 3
PERCENT CHANGE IN TOTAL ANNUAL PRECIPITATION FOR DIFFERENT MODELS

Year	2050		2100	
Emissions Scenario	A2	B1	A2	B1
Model Average	-4.1	-0.5	-6.5	-2.0
Wet Model	-0.7	7.1	-1.3	8.6
Dry Model	-5.0	1.1	-15.1	-8.3

Note: Data represents spatial average over all of District 1

For this study, extreme precipitation was characterized by the 98th percentile daily precipitation event over 30-year periods for 2050 and 2100. The 2050 timeframe was estimated based on the period from 2035 to 2064; the 2100 timeframe was estimated based on the period from 2070 to 2099. The 98th percentile is a statistical measure of the extreme occurrence which may be exceeded 2% of the time over a given period. The 98th percentile is used as an indication of the extreme events for this study rather than the 100-year recurrence because:

- The projections of extreme precipitation are highly uncertain due to modeling, downscaling, and may not be in agreement with the historical observations of precipitation;

- The use of recurrence requires an assumption of "stationarity[1]," in which the precipitation patterns are not changing.

However, the magnitude of the relative changes of the 98th percentile values may be correlated to changes in the 100-year event as an indication of changes in extremes. For example, an increase in the 98th percentile precipitation may be indicative of an increase of the 100-year event by a similar amount.

Maps of the ensemble average of extreme precipitation generally show a decrease for the A2 scenario (Figure 7) and a slight increase for the B1 scenario (Figure 8). However, Figures 7 and 8 represent the ensemble average over all models, which tend to indicate a low degree of change although the different models tend to show a significant amount of change.

Similar maps were generated to show the range in projected changes in extreme precipitation resulting from the wet and dry models. The wet model projects a District-wide increase in extreme precipitation for both emissions scenarios A2 (Figure 9) and B1 (Figure 10). The dry model projections show a significant decrease in extreme precipitation event for the A2 emissions scenario (Figure 11). However, results from the B1 emissions scenario for the dry model show that a decrease in extreme precipitation is limited to the southern portion of District 1 by 2050, and then expanding northward by 2100 (Figure 12). A general conclusion that can be made from these figures is that the projections of extreme precipitation are greater in the B1 emissions scenario than the A2 scenario.

The projections of changes in precipitation have a large amount of uncertainty due to disagreement between the different models (Figure 13). The box and whisker plots in Figure 13 show the distribution of the model projections for extreme precipitation as a District average for 2050 and 2100. The black diamond represents the 98th percentile value for the wet model, and the gray diamond represents the 98th percentile value for the dry model. Generally, the model agreement on projecting the extreme precipitation decreases for the A2 emissions scenario, as shown by the increasing spread of values. A similar range in values is projected for the B1 scenario, except that the majority of models tend to be greater than the average A2 values. A range in the percent change, from negative to positive, is projected for both the A2 and B1 emissions scenarios. However, the spatial distribution, as illustrated in the maps in Figures 7 through 12, is an important consideration in applying the projected changes to evaluate the vulnerability of the assets.

3.3. Runoff

Similar to the precipitation, daily maximum runoff data was obtained from the CMIP3 archive and processed to illustrate average trends, as well as projections of extreme conditions. Daily runoff projections were calculated using a simple water balance model that is driven by the projections of precipitation and temperature. The relative change of the total annual runoff compared to the historic average is projected to decrease by approximately 2% to 4% for the B1 and A2 emissions scenarios, respectively, by 2100 (Figure 14). This time series represents a spatial average of runoff across all of District 1 and is presented as a 10-year moving average to remove noise. The solid line represents an ensemble average of the results over all model runs, and the shading indicates the range in projections due to method uncertainty between models, which is noticeably large. The general trend

[1] Stationarity is defined as a quality of a process in which the statistical parameters, such as the mean and standard deviation, of the process do not change with time.

indicates that the changes in total annual precipitation in District 1 over the coming century are very uncertain, as shown by the wide range of model projections. The relative change in the total annual runoff is similar for Del Norte, Humboldt and Mendocino Counties, which are close to the District 1 average, although Lake County values tend to suggest relatively greater amount of runoff (Table 2). The table also suggests that, on average, runoff decreases for the A2 emissions scenario, but increases for the B1 emissions scenario.

TABLE 4
PERCENT CHANGE IN TOTAL ANNUAL RUNOFF FROM HISTORIC AVERAGE (%)

Year	2050		2100	
Emissions Scenario	A2	B1	A2	B1
District 1	-3.1	2.6	-4.1	2.2
Del Norte	-3.1	1.9	-4.3	2.6
Humboldt	-3.1	2.4	-4.2	2.1
Lake	-3.0	4.2	-1.9	3.9
Mendocino	-3.3	3.0	-4.5	1.8

The average percent change in total annual runoff for District 1 exhibits similar characteristics to the precipitation, in that there is a wide range in projections that show increase up to 150-200% and decrease up to 150-200% (Figure 14). The uncertainty is due to the different results from the several models used in the projections. The results are greatly affected by the different emissions scenarios, which project an increase in runoff by 2100 for the B1 scenario, and a decrease by 2100 for the A2 scenario (Table 4). However, the spatial results show a decrease in the total annual runoff from the historic values when averaged over all GCMs, particularly by 2100 (Figure 15).

The District 1 average of the total annual runoff for the ensemble average of models was compared to a selected "wet" model (PCM) and a selected "dry" model (GFDL) to illustrate the range in projections (Table 5). The results of the wet model indicate an increase in the total annual precipitation of up to approximately 30% greater than the historic average (for B1 scenario at 2100), while the dry model shows a decrease of up to approximately 15% (for A2 scenario at 2100). These results indicate that careful interpretation and selection of future climate projections need to be considered when applying to assessing the vulnerability of assets as well as the selection of an appropriate emissions scenario, and that method uncertainty poses a major challenge to providing management recommendations.

TABLE 5
PERCENT CHANGE IN TOTAL ANNUAL RUNOFF FOR DIFFERENT MODELS (%)

Year	2050		2100	
Emissions Scenario	A2	B1	A2	B1
Model Average	-3.1	2.6	-4.1	2.2
Wet Model	3.6	19.5	6.4	29.9
Dry Model	-3.3	5.7	-14.5	-10.4

Note: Data represents spatial average over all of District 1

For this study, extreme runoff was characterized by the 98th percentile daily runoff event over 30-year periods for 2050 and 2100, similar to how extreme precipitation is characterized and described above. The 2050 timeframe was estimated based on the period from 2035 to 2064; the 2100 timeframe was estimated based on the period from 2070 to 2099. Maps of the ensemble average of extreme runoff generally show a decrease for the A2 and B1 scenarios (Figures 15 and 16, respectively).

Similar to the analysis of extreme precipitation, maps were generated to show the range in projected changes in extreme runoff resulting from the wet and dry models. The wet model shows little changes District-wide for the A2 scenario (Figure 17), but suggests that areas in Lake County, northern portions of Mendocino County, and most of Humboldt and Del Norte Counties, may experience an increase in extreme runoff for the B1scenario (Figure 18). The dry model projections are somewhat different, and, by 2050, show a decrease to no change in extreme runoff north of Mendocino County, but a significant increase in extreme runoff throughout Lake County and most of Mendocino County for the A2 emissions scenario (Figure 19). However, by 2100, the dry model results suggest a District-wide decrease in the extreme runoff for the A2 scenario. Results from the B1 emissions scenario for the dry model show an increase in runoff by 2050, followed by a decrease by 2100 (Figure 20).

The projections of changes in runoff have a large amount of uncertainty due to disagreement between the different models (Figure 21). The box and whisker plots in Figure 21 show the distribution of the model projections for extreme runoff as a District average for 2050 and 2100. The black diamond represents the 98th percentile value for the wet model, and the gray diamond represents the 98th percentile value for the dry model. Generally, the model agreement on projecting the extreme precipitation decreases for the A2 emissions scenario, as shown by the increasing spread of values. A similar range in values is projected for the B1 scenario, overall, except that the majority of models tend to be greater than the average A2 values. A range in the percent change, from negative to positive, is projected for both the A2 and B1 emissions scenarios. However, the spatial distribution, as illustrated in the maps in Figures 15 through 20, is an important consideration in applying the projected changes to evaluate the vulnerability of the assets.

3.4. Fire Risk

3.4.1. Cal-Adapt Data

The projected fire risk data was obtained through Cal-Adapt.org. The data provided through Cal-Adapt represents projected increase in burned area as a ratio relative to existing fire risk for three GCMs for the A2 and B1 emissions scenarios averaged for 30-year time periods ending in 2020, 2050, and 2085. The three GCMs available for the Fire Risk data are:

1. The NCAR Parallel Climate Model (PCM);
2. The NOAA Geophysical Fluids Dynamics Laboratory (GFDL) model, Version 2.1;
3. The French Centre National de Recherches Météorologiques (CNRM) models.

The data provided in the geodatabase represents an average over the three GCMs for the 2050 and 2085 periods. The Cal-Adapt fire risk data projects an increase in fire risk for the whole district by 2100 (Figure 22).

3.4.2. Department of Water Resources Fire Exposure Data

A separate set of projections of wildfire exposure for early-, mid- and late-century were provided by the California Department of Water Resources (DWR). Fire exposure was estimated by DWR (2013) to evaluate vulnerability of their assets throughout the state, and was based on an extensive study of fire risk projections for California (Krawchuk and Moritz 2012). The Krawchuck and Moritz (2012) study estimated the change in probability of one or more fires occurring within a 30-year time period for three future periods (2010-2039; 2040-2069; and 2070-2099) as compared to the historic period (1971-2000). The future projections of wildfire risk were completed using two GCMs (PCM and GFDL), two emissions scenarios (A2 and B1), and two land use projections (business-as-usual and smart-growth. The final results of projected wildfire risk report the maximum modeled probability to represent a conservative estimate of future wildfire. DWR selected curves of five exposure categories from very low to very high to relate the future change in probability to existing probability of fire risk. For this study we used the exposure rating curves developed by DWR (2013).

The wildfire exposure data for mid- and late-century in District 1 is shown in Figure 23, and indicates that fire exposure increases for most areas by 2100, particularly the inland areas of Lake and Mendocino Counties.

3.5. Landslides

Projections of future landslide risk due to climate change are not available for the District 1 area. Existing information on the risk of deep-seated landslides is available from the California Geologic Survey (Wills et al. 2011). The study classifies deep-seated landslide susceptibility as a function of slope class and rock strength, with increasing susceptibility with slope and in weaker rocks. Much of District 1 is classified as high susceptibility to deep-seated landslides. We are not aware of any studies or date that indicates how the susceptibility may change due to climate change factors such as increased temperature and changes in precipitation.

Shallow landslides, including debris flows, are highly correlated to extreme rainfall events, and may be of the most interest to Caltrans in terms of hazards related to climate change. We understand that numerical and empirical models of shallow landslide susceptibility have been developed by researchers and geologists; however we are unaware of available data for District 1. Efforts to map existing and projected shallow landslide susceptibility for District 1 should be considered as a tool to aid in planning and design.

3.6. Sea Level Rise

Four datasets for sea level rise and coastal erosion were compiled for this project: coastal erosion and flood data from the Pacific Institute (2009) sea level rise study for the coast of California, data from Trinity Associates (2013) shoreline inventory, mapping, and vulnerability rating for Humboldt Bay, recent sea level rise inundation modeling and mapping by Northern Hydrology and Engineering (NHE) (2014) developed for the Humboldt Bay sea level rise vulnerability assessment project, and sea level rise inundation mapping using NOAA's Coastal Viewer. These datasets are described further below.

3.6.1. Pacific Institute and PWA (2009)

The Pacific Institute (2009) study mapped coastal erosion and flood hazard zones along the coast of California from Santa Barbara County north to the Oregon border.

Storm Flood Zones

Storm flood zones were estimated for the California Coast for existing (year 2000) and future (2100) conditions that assume a sea level rise of 55-inches, in accordance with state guidance at the time (CCC 2011). This sea level rise projection also falls within the range recommended by the updated state guidance (CCC 2013). 2011) The storm flood mapping used a bathtub model approach mapping the 100-yr total water level[2] resulting from 55-inches SLR by 2100. This is an overestimate of the 100-year flood zone in inland areas and is generally more accurate near the coast where wave run-up is occurring. These flood zones do not consider coastal erosion or vertical land motion.

Figure 24 shows an example of the existing and future (2100) 100-year coastal flood zone near Point Arena in Mendocino County. The areas with the blue shading represent the existing flood zones, and the green areas represent flood zones for 2100 that consider sea level rise. Although the bathtub approach used in the study generally tends to provide an overestimate of the flood elevations, areas with river mouths, such as at the mouth of the Garcia River, may be more accurate due to the interactions of fluvial discharge, inlet morphodynamics, and the "perching" of the estuarine water bodies due to the littoral barrier.

Dune and cliff erosion

Dune and cliff erosion hazard areas resulting from low (0.6 meters or 24 inches by 2100) and high (1.4 meters or 55 inches by 2100) sea level rise for years 2025, 2050, and 2100 were also estimated and mapped for the California coast north of Santa Barbara. Some gaps in coverage exist in District 1: Crescent City harbor, ~11 miles of coast near the Del Norte/Humboldt County Line, and from the Mattole River to Humboldt/Mendocino County Line.

A coastal erosion hazard zone represents an area where erosion (caused by coastal processes) has the potential to occur over a certain time period. This does not mean that the entire hazard zone is eroded away; rather, any area within this zone is at risk of damage due to erosion during a major storm event. Actual location of erosion during a particular storm depends on the unique characteristics of that storm (e.g. wave direction, surge, rainfall, and coincident tide). As sea level rises, higher mean sea level will make it possible for wave run-up to reach the dune more frequently, undercutting at the dune toe and causing increased erosion. These hazard zones consider historic trends in erosion, increased erosion due to sea level rise, and potential erosion of a 100-year storm. Figure 24 presents an example of the dune and cliff hazard zone near Point Arena. The red, orange, and yellow areas represent the erosion hazard zones for 2025, 2050, and 2100, respectively. Similar zones extending up and down the coast are included in the geodatabase.

3.6.2. Humboldt Bay Sea Level Rise Adaptation Planning Project (2010-present)

The State Coastal Conservancy (SCC) is funding a multi-phased project to identify sea level rise vulnerabilities and adaptation strategies for Humboldt Bay. This effort began in 2010 after Governor Schwarzenegger issued Executive Order S-13-08, which identified the necessity to plan for sea level rise. The first phase of the project, titled the Humboldt Bay Shoreline Inventory, Mapping and Sea Level Rise Vulnerability Assessment, was completed in January 2013 by Trinity Associates. The 2013 report presented the results of the inventory and

[2] The total water level is the elevation that represents the vertical extent of wave runup plus storm surge. Here the 100-year total water levels were developed using existing FEMA base flood elevations. Where no FEMA flood study was available a 100-year total water level was estimates using engineering judgment.

mapping of existing shoreline conditions, assessed shoreline vulnerability to extreme high water events and sea level rise, and presented an inventory of land uses and infrastructure vulnerable to inundation from overtopping, breaching, and rising sea levels. A shoreline vulnerability rating, a quantitative measure of vulnerability was developed as an addendum to the shoreline vulnerability assessment (2013). Trinity Associates shoreline vulnerability rating and mapping is useful in locating shoreline segments that are likely to fail during extreme high water events and as sea levels approach a critical elevation threshold for shoreline structures such as dikes and railroad grade.

The second phase of the project, titled Humboldt Bay Sea Level Rise Adaptation Planning Project, is sponsored by the Coastal Ecosystems Institute of Northern California (CEINC). There are two components to this project: inundation modeling and mapping by NHE and an adaptation planning working group led by the Humboldt County Public Works and Humboldt Bay Harbor, Recreation and Conservation District, with members from the Local Coastal Program authorities, Coastal Commission and various local and state resource agencies and Wiyot Tribe. Trinity Associates is the adaptation planning consultant for this phase of the project. Preliminary inundation mapping provided by NHE are used and presented herein.

There are nearly 9,000 acres of diked former tidelands adjacent to Humboldt Bay. Inundation maps were generated for existing conditions to illustrate areas subject to flooding if shoreline structures such as earthen dikes are compromised. 100-year storm flood maps were also developed for Humboldt Bay for existing conditions and four sea level rise scenarios: 0.5 meters (1.6 ft), 1.0 meter (3.3 ft), 1.5 meters (4.9 ft), and 2.0 meters (6.6 ft). The mapping identifies areas adjacent to Humboldt Bay and the adjoining sloughs that are below the 100-year extreme water surface elevation. Figure 25 presents an example of the preliminary model results and mapping by NHE that shows inundation from 100-year extreme water level variations within different portions of the Humboldt Bay for existing conditions and for 1.5 meters of sea level rise. These maps are based on preliminary model results provided by NHE as part of the State Coastal Conservancy funded Phase II Humboldt Bay Sea Level Rise Adaptation Planning Project. The geodatabase also includes information on the following flood zones for existing and sea level rise scenarios: 100-yr, 10-yr, and mean higher high water[3] (MHHW). These elevations comprise the base tidal elevations used to assess shoreline vulnerability in the Humboldt Bay Sea Level Rise Adaptation Planning Project.

3.6.3. NOAA SLR Viewer Data

Sea level rise inundation mapping data is available online using the NOAA Coastal Services Center's Sea Level Rise and Coastal Flooding Impacts Viewer (SLR Viewer). The SLR Viewer is an online tool that is helpful in graphically presenting potential impacts of sea level rise to coasts of the United States of America. The SLR Viewer provides a simple visual tool with a user interface that illustrates the potential impacts of sea level rise on the coast. A slider bar is used to see how various levels of sea level rise will impact the area of interest. The base elevation of the data is the MHHW elevation, which is 6.52 ft NAVD[4] in the vicinity of Humboldt Bay. The SLR Viewer presents several levels of high tide inundation with 1-foot incremental increases in sea level rise. The inundated areas is presented in a map with shades of blue, where darker blue represents hydrologically connected

[3] Mean higher high water (MHHW) is a tidal datum that is calculated as an average of the higher high water height of each tidal day observed over the National Tidal Datum Epoch (approximately 19 years).

[4] NOAA NOS Station 9418767, North Spit, CA

greater depths, lighter blue represents hydrologically connected shallow areas, and green shading represents low-lying areas that are not hydrologically connected but may flood.

The data is limited in that several natural processes associated with sea level rise are not included. The data presented in the maps is based on projected water surface elevations and mapped onto a digital elevation model (DEM). The mapping represents a bathtub mapping effort for existing conditions, when in fact natural processes associated with sea level rise, including erosion, marsh migration, fluvial-tidal interactions, and lagoon dynamics, are not included in establishing the inundation limits. Furthermore, other processes including storm surge and waves could present additional flood pathways that are not considered in the mapping. The confidence of the mapping is not 100%, as with all sea level rise mapping exercises, and user should evaluate the uncertainties in the extent of mapped inundation resulting from errors in the elevation data and the tidal corrections. Other hydrologic features, such as canals, ditches and stormwater infrastructure, may not be included to completely capture the area's hydrology.

More information on the SLR Viewer is summarized in documentation that is available on the website.[5,6]

4. Summary of Sea Level Rise Guidance for Caltrans District 1

This section summarizes California state guidance on sea level rise adaptation planning and design. Federal guidance also exists (USACE 2011); however, the California guidance incorporates recent science specific to the West Coast and is tailored to California planning processes. In 2008, Executive Order S-13-08 directed state agencies to plan for sea-level rise and other climate change impacts. It also directed the California Natural Resources Agency, in coordination with other state agencies and the National Research Council (NRC) of the National Academy of Sciences, to assess sea level rise for the Pacific Coast and create official sea level rise estimates for state agencies in California, Oregon and Washington.

In March 2011[7], the Coastal and Ocean Working Group of the California Climate Action Team (CO-CAT) presented interim guidance to state agencies for incorporating the risks posed by sea level rise into project and program plans (OPC 2011). The guidance was targeted towards state agencies and non-state entities implementing projects or programs funded by the state or on state property.

In May 2011, Caltrans published specific guidance on when and how to implement sea level rise guidance in transportation planning and design (Caltrans 2011). The guidance included the sea level rise projections from the interim state guidance and stated that the Caltrans guidance would be revised when the NRC study (below) was complete. The guidance has not been updated as of May 2014.

In 2012, the National Research Council (NRC) released a report titled "Sea-Level Rise for the Coasts of California, Oregon, and Washington: Past, Present, and Future" (NRC 2012). This report provides global and regional sea level rise projections and likely ranges at four locations along the West Coast. The report splits the West Coast into two tectonic regions when incorporating vertical land motion into regional sea level rise

[5] NOAA 2012, Method Description: Detailed Methodology for Mapping Sea Level Rise Inundation, May 2012.
[6] NOAA 2014, Frequent Questions: Digital Coast Sea Level Rise and Coastal Flooding Impacts Viewer, March 2014.
[7] Prior to completion of the NRC 2012 report

estimates: North of Cape Mendocino (uplift, 1 ± 1.5 mm/year) and South of Cape Mendocino (subsidence, -1 ± 1.3 mm/year).

In March 2013, the Ocean Protection Council (OPC) staff presented an update to the interim guidance (OPC 2013). The purpose of the document remained the same but was updated to include the range of sea level rise projections NRC 2012 study. The guidance document seeks to enhance consistency across agencies as each develops its respective approach to planning for sea level rise. It will be updated regularly, to keep pace with scientific advances associated with sea level rise.

In October 2013, the California Coastal Commission released draft guidance to help local governments apply the OPC 2013 guidance in new and updated Local Coastal Programs and Coastal Development Permits (CCC 2013). The draft document is currently out for public comment, and is expected to be finalized in early summer 2014. A series of technical appendices provide examples, adaptation strategies, and detailed instructions for estimating local hazard conditions. This guidance recommends modifying the regional sea level rise projections in the vicinity of Humboldt Bay and the Eel River, where vertical land motion differs significantly from that assumed by NRC 2012 (and adopted in OPC 2013).

Caltrans District 1 includes regions north of Cape Mendocino, south of Cape Mendocino, and Humboldt Bay to the Eel River. Therefore, according to draft CCC 2013 guidance, three different sea level rise projections should be considered. Table 6 presents the range of sea level rise projections for each of these regions, as presented in OPC 2013 for North and South of Cape Mendocino and as estimated by ESA for Humboldt Bay according to CCC 2013 draft guidance[8].

TABLE 6
SEA LEVEL RISE PROJECTIONS FOR CALIFORNIA, RELATIVE TO YEAR 2000

Year	North of Cape Mendocino (OPC 2013)	South of Cape Mendocino (OPC 2013)	Vicinity of Humboldt Bay (ESA analysis, based on CCC 2013)
2030	-4 to 23 cm (-0.13 to 0.75 ft)	4 to 30 cm (0.13 to 0.98 ft)	13 to 33 cm (5 to 13 in)
2050	-3 to 48 cm (-0.1 to 1.57 ft)	12 to 61 cm (0.39 to 2.0 ft)	25 to 65 cm (9.8 to 25.7 in)
2100	10 to 143 cm (0.3 to 4.69 ft)	42 to 167 cm (1.38 to 5.48 ft)	66 to 177 cm (25.8 to 69.7 in)

5. Selection of Climate Stressors for Asset Exposure Analysis

Evaluation of the exposure of critical Caltrans transportation assets in District 1 to a range of climate stressors is a key component of the vulnerability assessment. As described in Section 2.4, many sources of uncertainty accompany the climate model outputs, including method uncertainty from climate models, implications of different emissions scenarios, and the natural and spatial variability of the projections. Therefore, this section screens the climate data to select climate stressor datasets that represent the "worst-case" scenarios in terms of asset exposure and that yield the most conservative results.

[8] Vertical land motion at North Spit was estimated by NOAA 2013 (-3.42 mm/yr ± 0.54 mm/yr). This estimate (including the uncertainty) was added to the regional sea level projections for Newport, OR (the nearest regional projection, assume vertical land motion removed) in NRC 2012 to give an estimate of relative sea level rise at North Spit.

5.1. Temperature

Evaluating the exposure of assets to temperature should consider the climate scenarios that project the greatest increase in the number of extreme heat days. The results shown by the box plot in Figure 5 suggest that the A2 emissions scenario yields the most conservative results with the greatest change in number of extreme heat days per year.

5.2. Precipitation

Although the projections of extreme precipitation show a wide range in relative change, the exposure analysis will focus on the dataset that shows the greatest increase in extreme daily rainfall event. The focus on the "wet" conditions will allow the exposure analysis to consider the potential impacts of flooding that may result from increased heavy precipitation events. Out of the three sets of model results, the "wet" model (PCM) run for the B1 emissions scenario yields the greatest change in the extreme daily rainfall. The wet model is represented by the black diamond in the box plot in Figure 13, and is consistent with projecting more wet conditions.

5.3. Runoff

Similar to the extreme precipitation, extreme runoff projections varied greatly across models and emissions scenarios. The greatest change in extreme daily runoff results from the "wet" model with the B1 emissions scenario. The wet model is represented by the black diamond in the box plot in Figure 21. Note that although the results vary considerably spatially, and that some specific areas may show large changes for a particular model or emissions scenario, the analysis is focused on the entirety of District 1 suggesting that the "wet" model with B1 emissions scenario best represents the extreme runoff condition.

5.4. Wildfire

Evaluation of the exposure of transportation assets to wildfire should be accomplished using the DWR (2013) dataset, which was previously screened by DWR to consider the "worst-case" conditions resulting from the A2 and B1 emissions scenarios. Furthermore, DWR already rated the exposure of the original fire risk projections made by Krawchuk and Moritz (2012) in a semi-quantitative scale that can easily be applied to this vulnerability assessment.

5.5. Sea Level Rise

Exposure of assets to sea level rise should be completed using separate datasets for areas along the open coast of District 1 and for the interior of Humboldt Bay. This is partly due to the availability of the data. For example, the Pacific Institute study covers most of the shoreline of District 1, while the Humboldt Bay Sea Level Rise Adaptation Planning Project is focused only on the shores of Humboldt Bay. These represent the best available data for this assessment. For more frequent events (i.e. daily to annual occurrences) we understand that data from the NOAA SLR Viewer will be used to assess the exposure of assets to flooding.

5.5.1. Open Coast

The Pacific Institute study data should be applied along stretches of the open coast in all available areas besides within Humboldt Bay. The conditions along the open coast are subject to large waves and elevated tides which result in flooding and erosion. Erosion hazard maps show the areas that may be impacted by increased erosion

from sea level rise at years 2050 and 2100. These zones can be applied to the exposure analysis to determine if an asset is impacted or not. Similarly, existing and future (year 2100) flood zones that represent the approximate 100-year flood elevation can be used to assess the exposure of the assets to potential coastal flooding. Intermediate conditions at year 2050 can be inferred from results of the existing and future extreme conditions.

5.5.2. Humboldt Bay

Flooding within Humboldt Bay should use the data developed by the Humboldt Bay Sea Level Rise Adaptation Planning Project that show areas of inundation resulting from different amounts of sea level rise. Specifically, extreme flooding in Humboldt Bay should consider the different projections of inundation of the simulated 100-year recurrence flood projections.

Because the inundation mapping was conducted for discrete amounts of sea level rise, and the exposure will be conducted for the planning horizons of 2050 and 2100, the following datasets should be used:

- Year 2050: Use the 0.5 meter projection with the 100-year recurrence water level to infer the extreme water level at 2050;

- Year 2100: Use the 1 and 1.5 meter projections of the 100-year recurrence water level to develop a range in the anticipated extreme water level at 2100.

This dataset represents the best available flood mapping that considers increased water surface elevation resulting from sea level rise. Assessing the range of potential sea level rise for 2100 is important because of the non-uniform rates of vertical land motion that are observed in Humboldt Bay, and suggest that areas along the southern shore of Humboldt Bay may be experiencing greater rates of relative sea level rise than in the north (Cascadia GeoSciences 2013). Site specific and design-level analyses may need to use sanctioned rates and estimates of sea level rise in accordance with the National Geodetic Survey and National Ocean Service.

5.5.3. NOAA SLR Viewer Data

We understand the SLR Viewer data will be used to assess frequent tidal inundation for existing and future conditions with sea level rise. Table 7 summarizes the recommended data mapping layers to be applied in evaluation of the asset exposure. The table presents three planning horizons: existing conditions at 2010; future conditions at 2050; and future conditions at 2100. For each of the three planning horizons we identify two inundation frequencies that can be used for the evaluation: daily high tide and annual high tide. Here, we assume that the MHHW elevation can be representative of the daily high tide without storm surge and without the effects of waves and wave runup. The annual high tide elevation was assumed to include an additional 2 feet of storm surge above the MHHW elevation, but does not include the effects of waves. We selected an annual storm surge of 2 feet as a conservative estimate based on review of tidal records at Point Arena, North Spit in Humboldt Bay, and at Crescent City.

TABLE 7
RECOMMENDED DATA LAYERS FOR EVALUATING INUNDATION FREQUENCY

Year	Frequency of Inundation	Assumptions	Mapping Layer
2010 (Existing)	Daily High Tide	MHHW	CA_EKA_slr_0ft
2010 (Existing)	Annual High Tide	MHHW + 2 feet of storm surge	CA_EKA_slr_2ft
2050	Daily High Tide	MHHW + 2 feet SLR	CA_EKA_slr_2ft
2050	Annual High Tide	MHHW + 2 feet SLR + 2 feet storm surge	CA_EKA_slr_4ft
2100	Daily High Tide	MHHW + 4 feet SLR	CA_EKA_slr_4ft
2100	Annual High Tide	MHHW + 4 feet SLR + 2 feet storm surge	CA_EKA_slr_6ft

Note: Assumes no wave action; assumes storm surge limited to 2 feet;

Applying the data layers listed in Table 7 to the asset exposure analysis will help to inform the level of impact that may occur for a range of inundation magnitudes. The level of impact to an asset will be a function of the level or frequency of inundation that occurs. For example, an asset that experiences shallow flooding approximately once per year may have a moderate impact, or in a “temporary closure” category of impacts. However, an asset that is flooded on a daily to monthly frequency likely implies a higher degree of impact, such as the “temporary closure” or “complete failure” categories.

Use of the NOAA SLR Viewer data is considered acceptable in the absence of other available data that considers other important factors, such as waves and erosion. The geomorphic changes to the shore associated with sea level rise play an important role in erosion hazard determination and flood routing, which have major implications on assessing vulnerability. In evaluating the vulnerability of the assets, the data should be used in combination with the separate sea level rise and erosion data sets provided. Additional assumptions were made by ESA regarding the degree of storm surge associated with a flood event with an approximately annual recurrence, but is based on tidal records in the vicinity of District 1. Further, the NOAA data does not include waves when it is known waves play an important role in coastal flooding along the exposed and open coast in California. Other interactions between fluvial and tidal processes, including the water surface elevation of coastal lagoons, should be considered a special case and may need additional site specific evaluation. We recommend associating the annual high tide inundation with the “reduced capacity” category of impacts and the daily high tide inundation with the “temporary closure” or “complete failure” impact categories.

6. References

California Ocean Protection Council (OPC) (2011). Resolution of the California Ocean Protection Council on Sea Level Rise. March 11, 2011.

California Ocean Protection Council (OPC) (2013). State of California Sea-Level Rise Guidance Document. March 2013 Update.

California Coastal Commission (CCC) (2013). California Coastal Commission Draft Sea-Level Rise Policy Guidance – Public Review DRAFT. October 14, 2013. Available at http://www.coastal.ca.gov/climate/SLRguidance.html. Accessed 2/20/2014.

Caltrans (2011). Guidance on Incorporating Sea Level Rise: For use in the planning and development of Project Initiation Documents. Prepared by the Caltrans Climate Change Workgroup, and the HQ Divisions of Transportation Planning, Design, and Environmental Analysis. May 16, 2011.

Cascadia GeoSciences (2013). Tectonic land level changes and their contribution to sea-level rise, Humboldt Bay region, Northern California.

Cayan, D. R., D. W. Pierce, T. Das, E. P. Maurer, N. L. Miller, Y. Bao, M. Kanamitsu, K. Yoshimura, M. A. Snyder, L. C. Sloan, G. Franco, and M. Tyree (2012). Probabilistic estimates of future changes in California temperature and precipitation using statistical and dynamical downscaling. Climate Dynamics, doi:10.1007/s00382-012-1337-9.

Department of Water Resources (DWR) (2013). Draft Fire Exposure Assessment Methodology and GIS Mapping Products. Prepared by DWR staff for Assessing Fire Exposure.

IPCC (2013). Summary for Policymakers. In: Climate Change 2013: The Physical Science Basis. Contribution of Working Group I to the Fifth Assessment Report of the Intergovernmental Panel on Climate Change [Stocker, T.F., D. Qin, G.-K. Plattner, M. Tignor, S.K. Allen, J. Boschung, A. Nauels, Y. Xia, V. Bex and P.M. Midgley (eds.)]. Cambridge University Press, Cambridge, United Kingdom and New York, NY, USA.

Krawchuk, M. A., and M. A. Moritz (Simon Fraser University; University of California, Berkeley) (2012). Fire and Climate Change in California. California Energy Commission. Publication number: CEC-500-2012-026.

Le Quéré, C., Raupach, M. R., and J. G. Canadell (2010). Recent Trends in CO_2 Emissions. RealClimate, June 14, 2010.

NOAA (2013). Estimating Vertical Land Motion from Long-Term Tide Gauge Records. Technical Report NOS CO-OPS 065. Silver Spring, Maryland. May 2013.

National Research Council (NRC) (1987). Responding to Changes in Sea Level: Engineering Implications. National Research Council. National Academy Press: Washington, D.C.

Northern Hydrology and Engineering (NHE) (2014). Humboldt Bay Sea Level Rise Adaptation Planning Project. Preliminary Sea Level Rise Inundation Mapping Products, April 2014.

NRC (2012). Sea-Level Rise for the Coasts of California, Oregon, and Washington: Past, Present, and Future. Prepublication. National Academy Press: Washington, D. C.

Pacific Institute (2009). The Impacts of Sea-Level Rise on the California Coast. California Climate Change Center, CEC-500-2009-024-D.

Trinity Associates (2013). Humboldt Bay Shoreline Inventory, Mapping and Sea Level Rise Vulnerability Assessment, prepared for the California State Coastal Conservancy, January 2013.

Trinity Associates (2013). Humboldt Bay Shoreline Inventory, Mapping and Sea Level Rise Vulnerability Assessment. Addendum: Shoreline Vulnerability Ratings, prepared for the California State Coastal Conservancy, July 2013. USACE (2011). Sea-Level Change Considerations for Civil Works Programs. US Army Corps of Engineers, EC 1165-2-212.

USBR (2011). West-Wide Climate Risk Assessments: Bias-Corrected and Spatially Downscaled Surface Water Projections. Technical Memorandum, Water and Environmental Resources Division, U.S. Bureau of Reclamation

Westerling, A. L., and Bryant, B. P. (2008) Climate Change and Wildfire in California. Climatic Change (2008) 87 (Suppl 1): s231-s249

Wills, C.J., Perez, F.G., and Gutierrez, C.I., (2011). Susceptibility to Deep-Seated Landslides in California. Map Sheet 58, California Geological Survey.

7. Figures

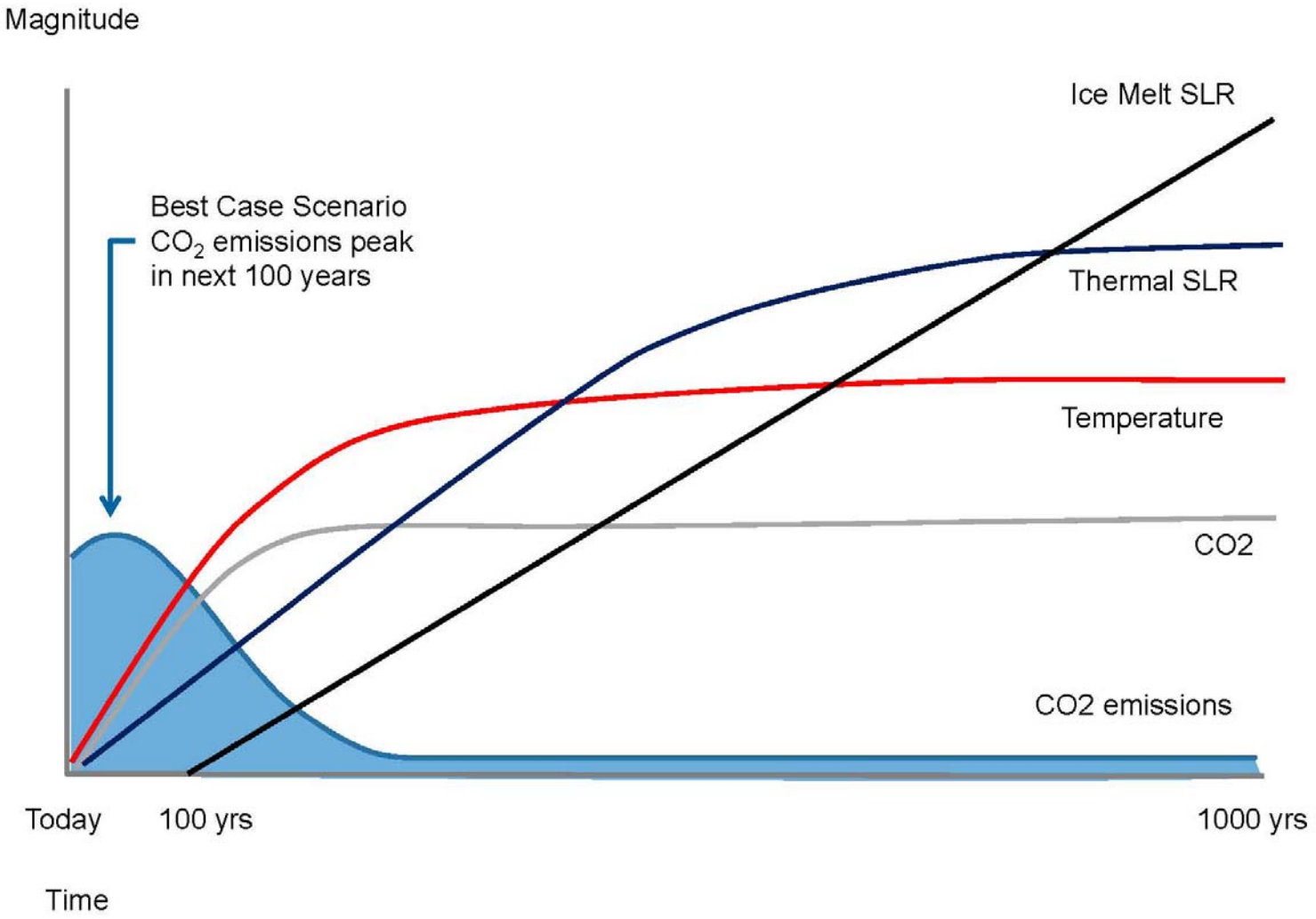

SOURCE: After IPCC 2007

Figure 1

Residual Climate Effects Continue Beyond 2100

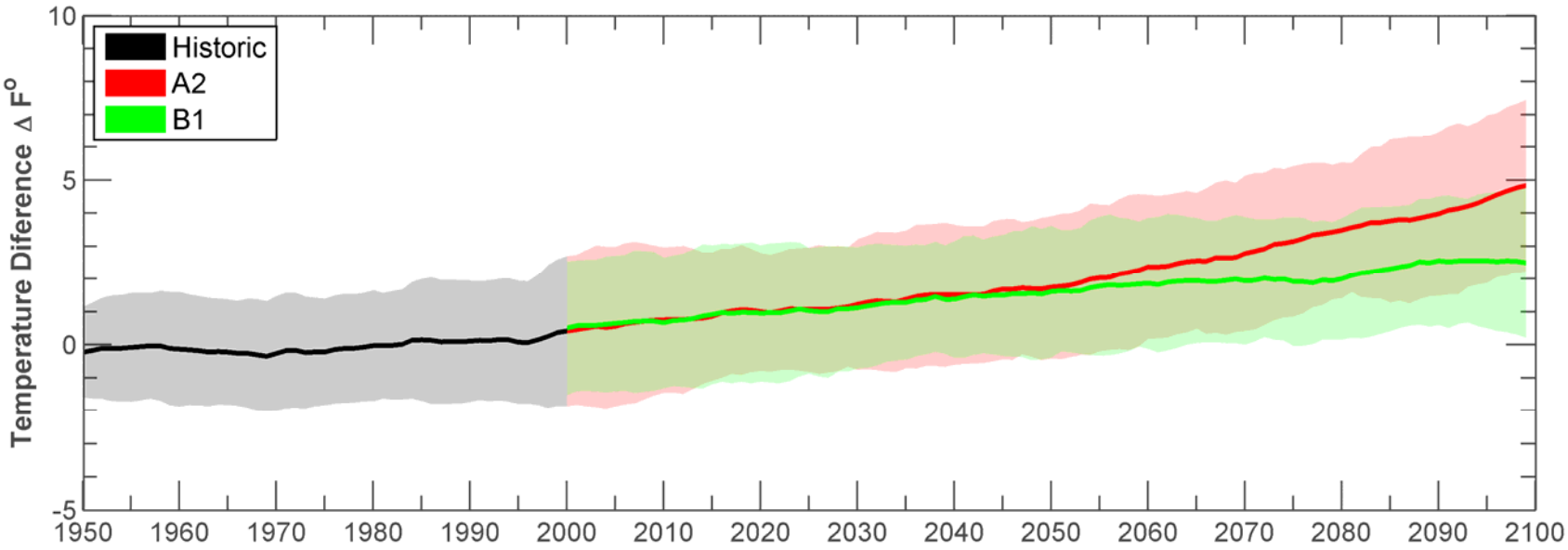

SOURCE: CMIP3

NOTES: 10-year moving average; spatially averaged over District 1;
solid lines are ensemble average;
shading represents range of individual GCMs

Figure 2

Change in Annual Average of Daily Maximum Temperature from Historic Average for A2 and B1 Emissions Scenarios

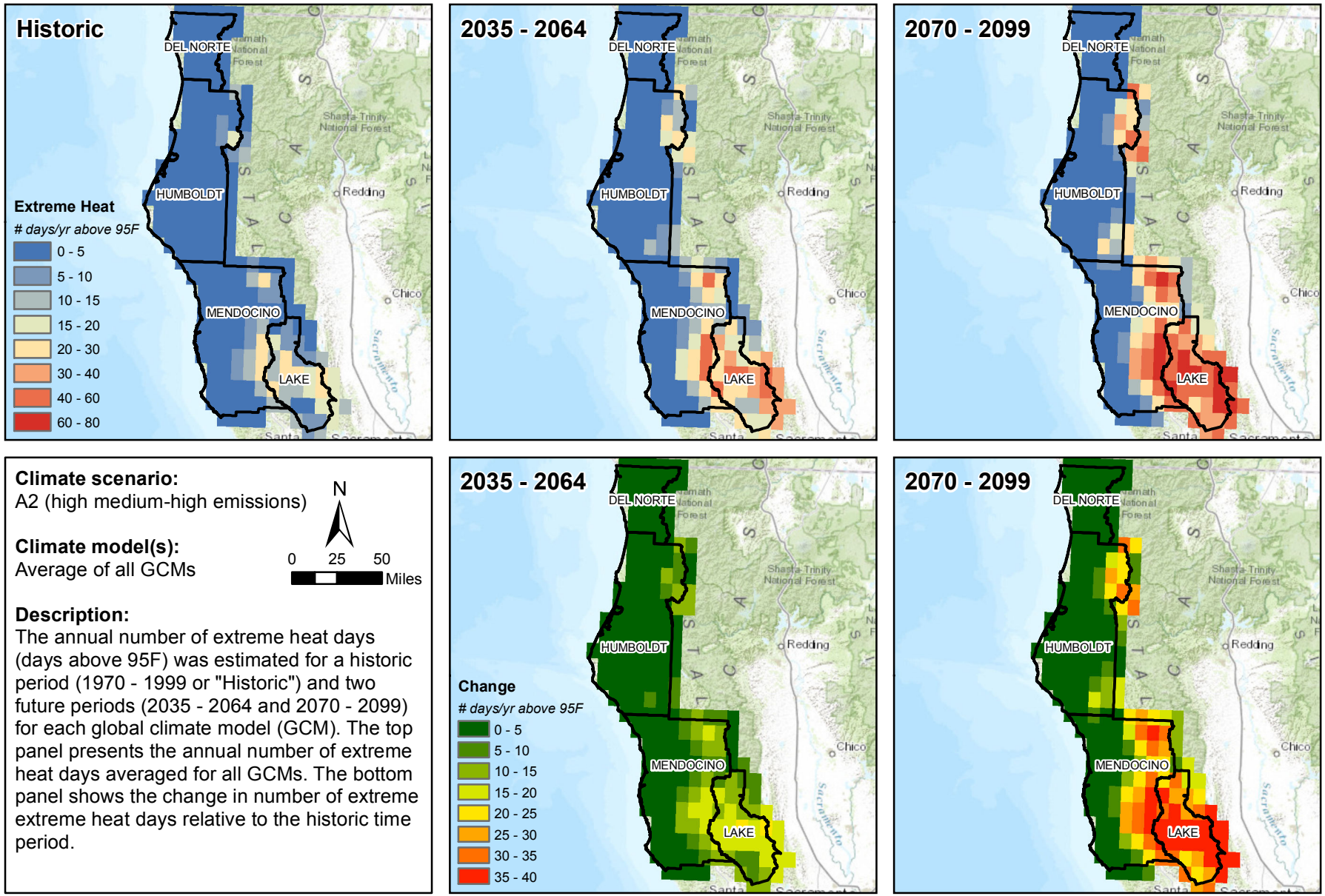

Climate scenario:
A2 (high medium-high emissions)

Climate model(s):
Average of all GCMs

Description:
The annual number of extreme heat days (days above 95F) was estimated for a historic period (1970 - 1999 or "Historic") and two future periods (2035 - 2064 and 2070 - 2099) for each global climate model (GCM). The top panel presents the annual number of extreme heat days averaged for all GCMs. The bottom panel shows the change in number of extreme extreme heat days relative to the historic time period.

G:\130588_HCAOG-ClimateChange\MXDs\Figures\Temperature_Above95F_16Jun2014.mxd

SOURCE: Cal Adapt, 2014

Figure 3
Extreme Temperatures: Days Above 95F for Scenario A2, All Models

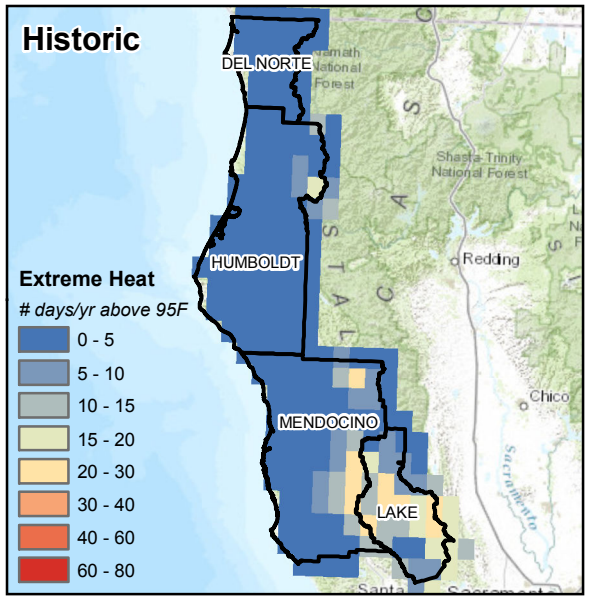

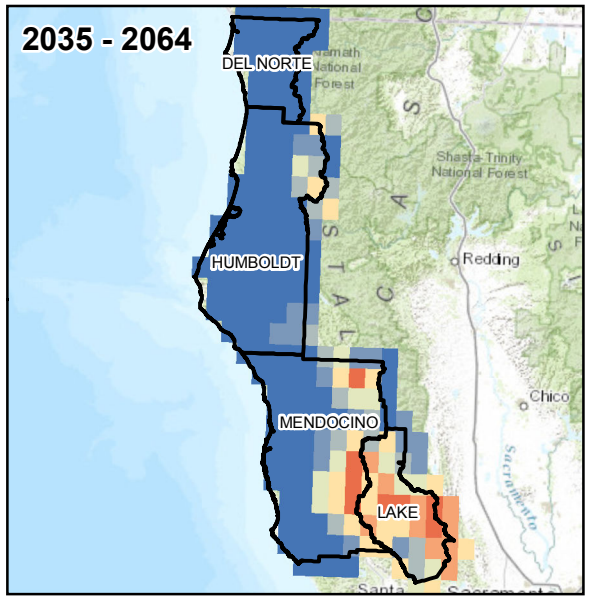

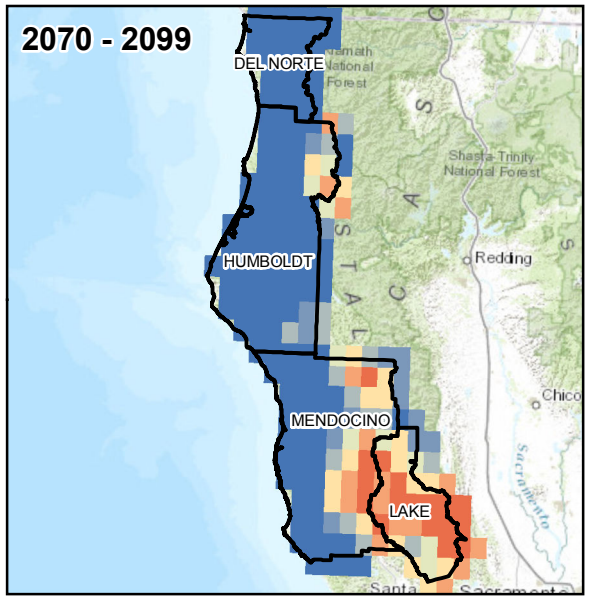

Climate scenario:
B1 (low emissions)

Climate model(s):
Average of all GCMs

N

0 25 50
Miles

Description:
The annual number of extreme heat days (days above 95F) was estimated for a historic period (1970 - 1999 or "Historic") and two future periods (2035 - 2064 and 2070 - 2099) for each global climate model (GCM). The top panel presents the annual number of extreme heat days averaged for all GCMs. The bottom panel shows the change in number of extreme extreme heat days relative to the historic time period.

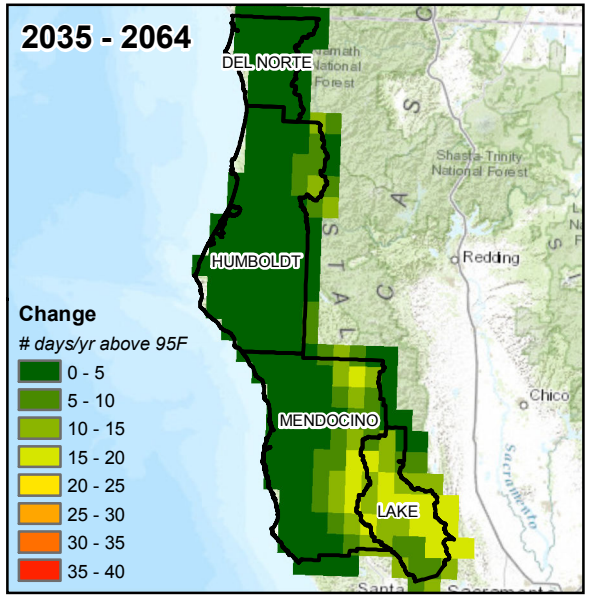

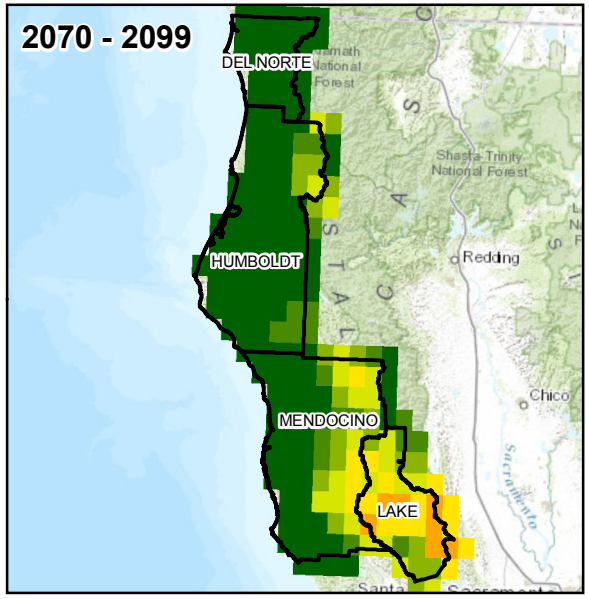

G:\130588_HCAOG-ClimateChange\MXDs\Figures\Temperature_Above95F_16Jun2014.mxd

SOURCE: Cal Adapt, 2014

Figure 4
Extreme Temperatures: Days Above 95F for Scenario B1, All Models

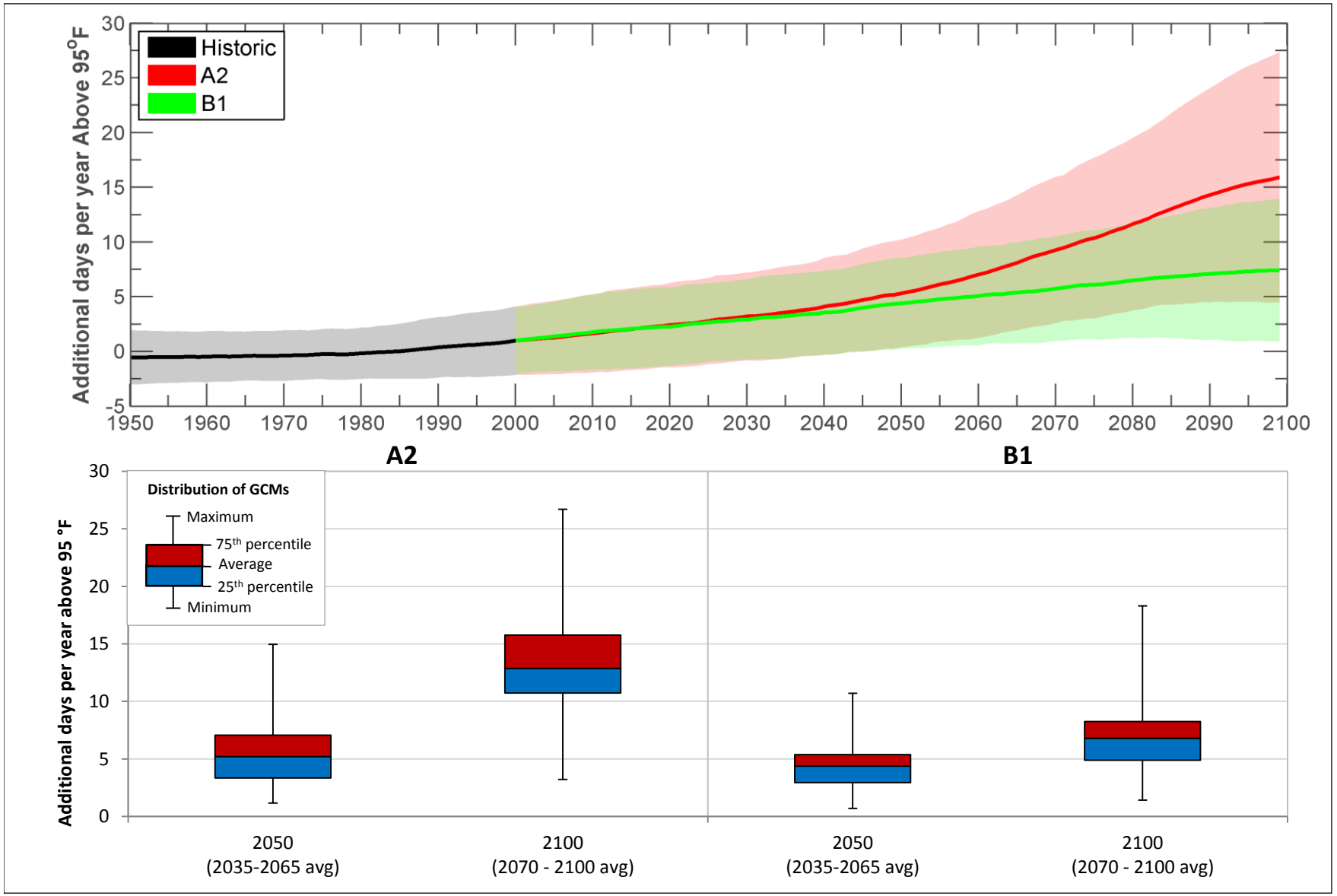

SOURCE: WCRP CMIP3 downscaled data
NOTE: The top plot shows a time series of the change in number of days per year exceeding 95 °F relative to a historic average (1970-2000). The range of GCMs is shown for historic (grey), A2 (red), and B1 (green) conditions. Solid lines represent an average of the GCMs. The lines are smoothed using a moving 30-year average. The bottom plot shows the range of GCMs for A2 and B1 emissions for 30-year averages for 2050 and 2100.

Figure 5

Change in Extreme Temperature Over Time for Multiple GCMs - District 1 Average

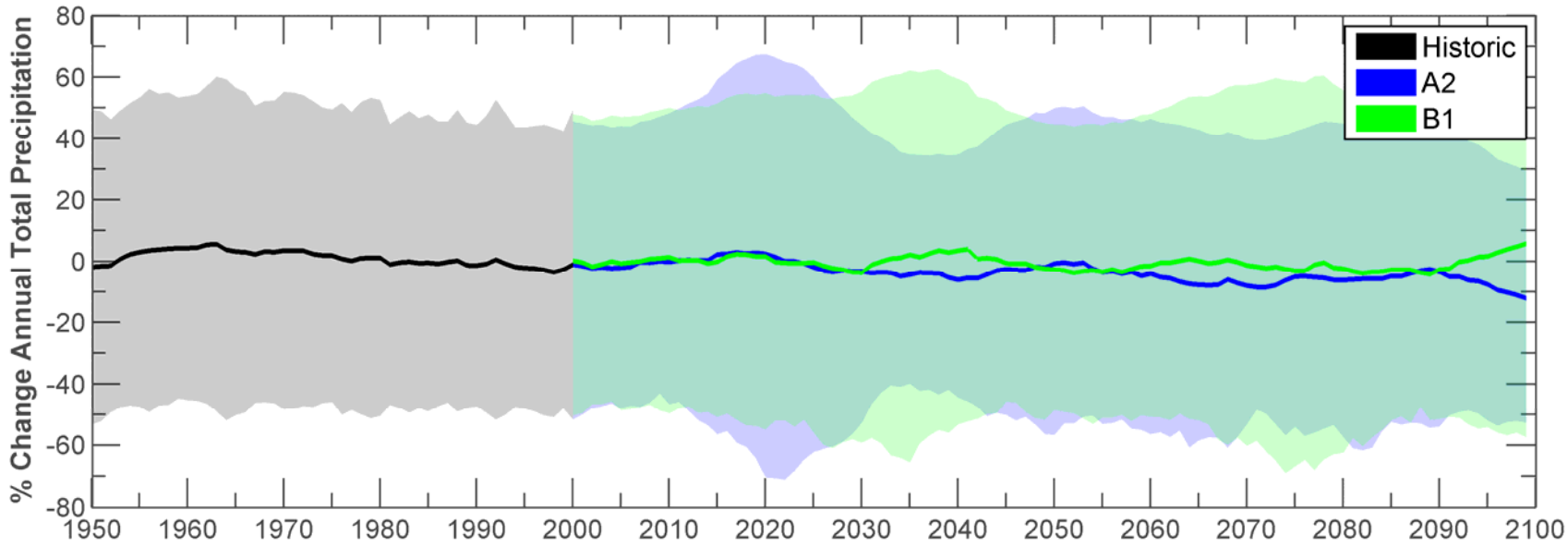

SOURCE: CMIP3

NOTES: 10-year moving average; spatially averaged over District 1;
solid lines are ensemble average;
shading represents range of individual GCMs

Figure 6

Percent Change of Total Annual Precipitation from Historic Average
for A2 and B1 Emissions Scenarios

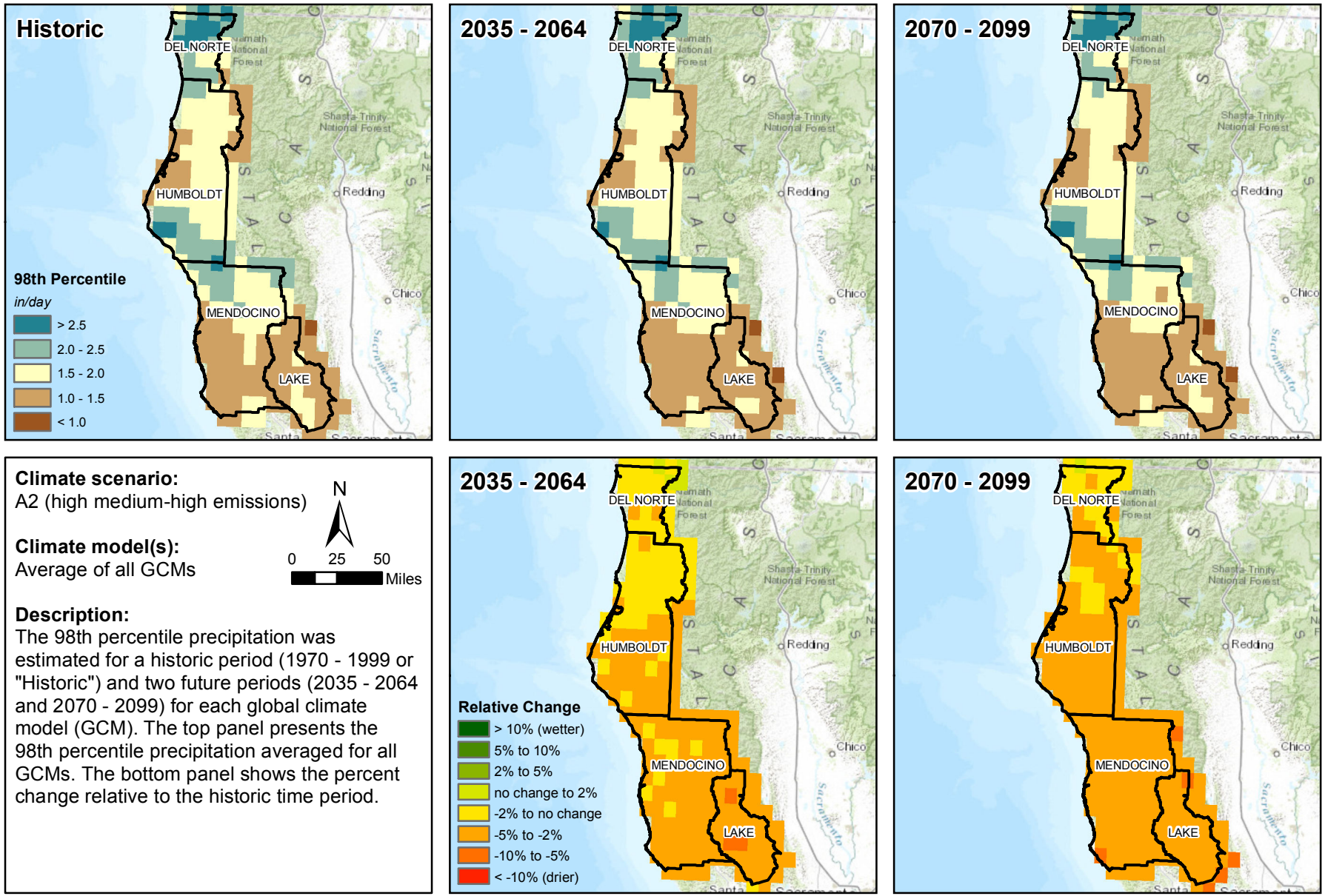

Climate scenario:
A2 (high medium-high emissions)

Climate model(s):
Average of all GCMs

N

0 25 50
Miles

Description:
The 98th percentile precipitation was estimated for a historic period (1970 - 1999 or "Historic") and two future periods (2035 - 2064 and 2070 - 2099) for each global climate model (GCM). The top panel presents the 98th percentile precipitation averaged for all GCMs. The bottom panel shows the percent change relative to the historic time period.

G:\130588_HCAOG-ClimateChange\MXDs\Figures\Precip_98Percentile_11Jun2014.mxd

SOURCE: Cal Adapt, 2014

Figure 7

98th Percentile Precipitation: Average Values and Relative Change for Scenario A2, All Models

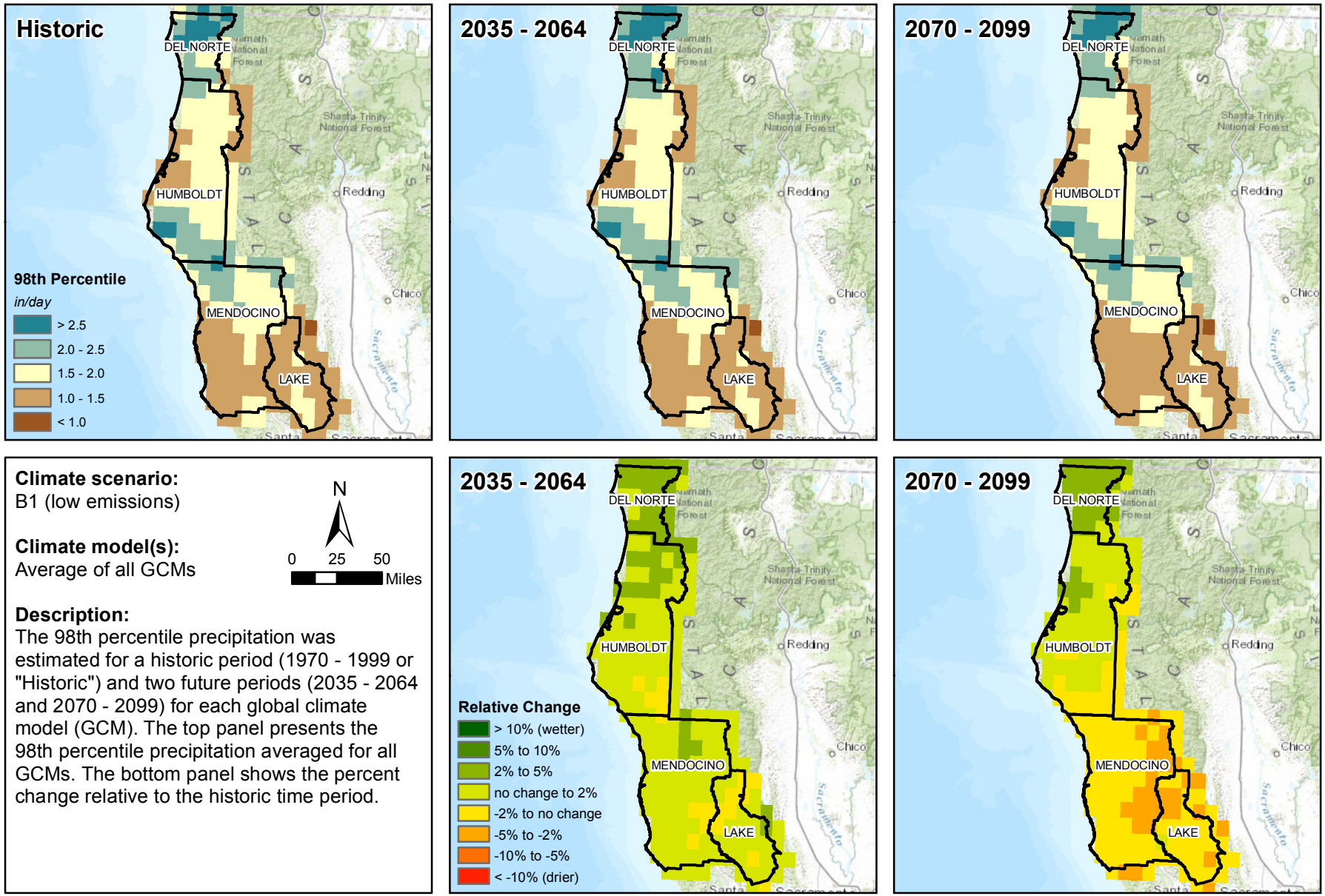

Climate scenario:
B1 (low emissions)

Climate model(s):
Average of all GCMs

N
0 25 50
Miles

Description:
The 98th percentile precipitation was estimated for a historic period (1970 - 1999 or "Historic") and two future periods (2035 - 2064 and 2070 - 2099) for each global climate model (GCM). The top panel presents the 98th percentile precipitation averaged for all GCMs. The bottom panel shows the percent change relative to the historic time period.

G:\130588_HCAOG-ClimateChange\MXDs\Figures\Precip_98Percentile_11Jun2014.mxd

SOURCE: Cal Adapt, 2014

Figure 8
98th Percentile Precipitation: Average Values and Relative Change for Scenario B1, All Models

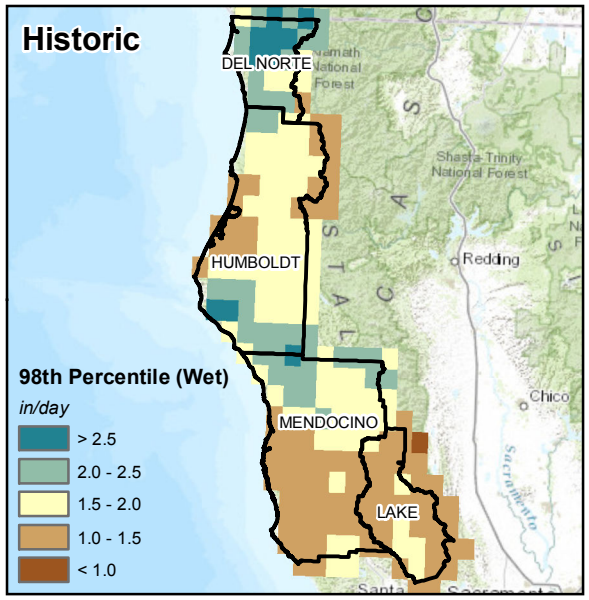

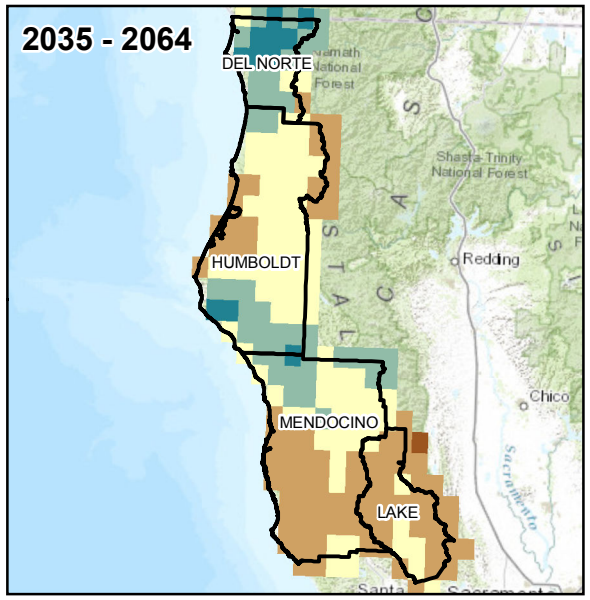

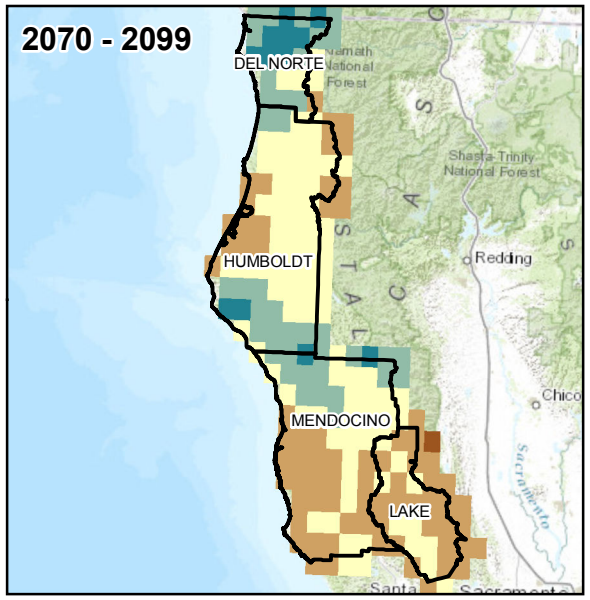

Climate scenario:
A2 (high medium-high emissions)

Climate model(s):
Wet GCM (PCM)

N

0 25 50
Miles

Description:
The 98th percentile precipitation was estimated for a historic period (1970 - 1999 or "Historic") and two future periods (2035 - 2064 and 2070 - 2099) for a wet global climate model (GCM). The top panel presents the 98th percentile precipitation for the wet GCM. The bottom panel shows the percent change relative to the historic time period.

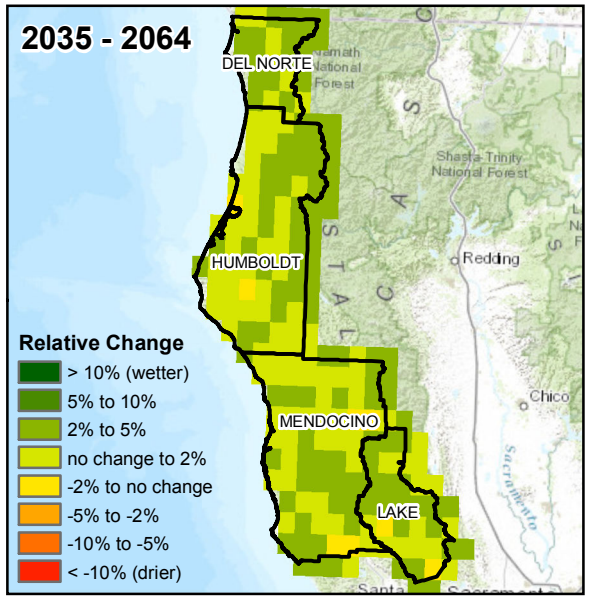

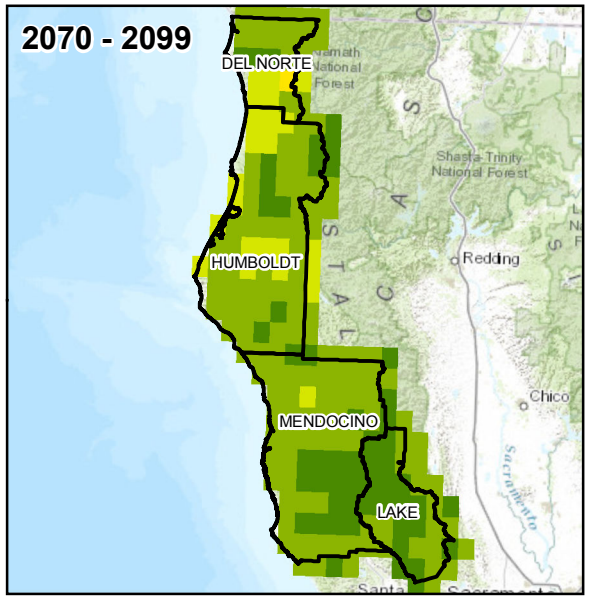

G:\130588_HCAOG-ClimateChange\MXDs\Figures\Precip_98Percentile_11Jun2014.mxd

SOURCE: Cal Adapt, 2014

Figure 9

98th Percentile Precipitation: Average Values and Relative Change for Scenario A2, Wet Model

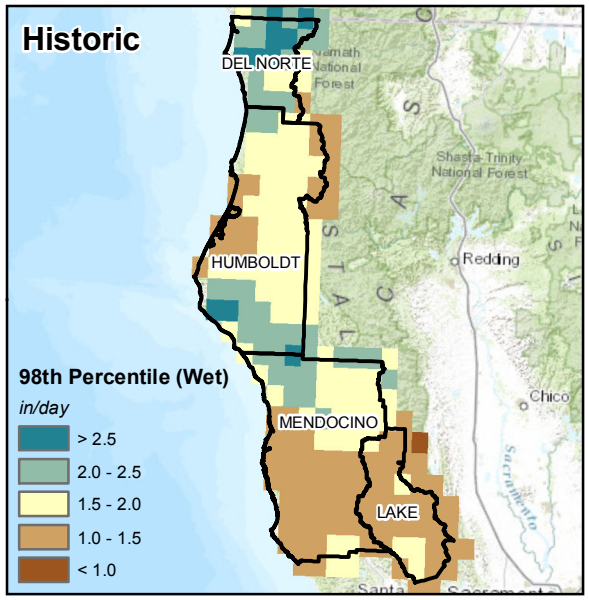

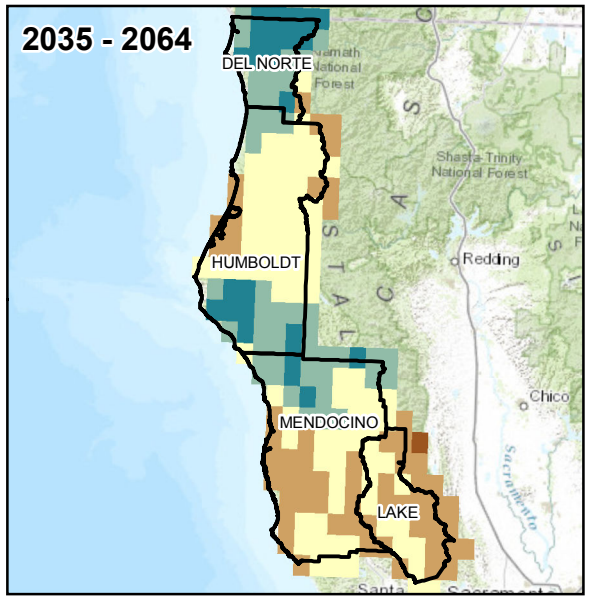

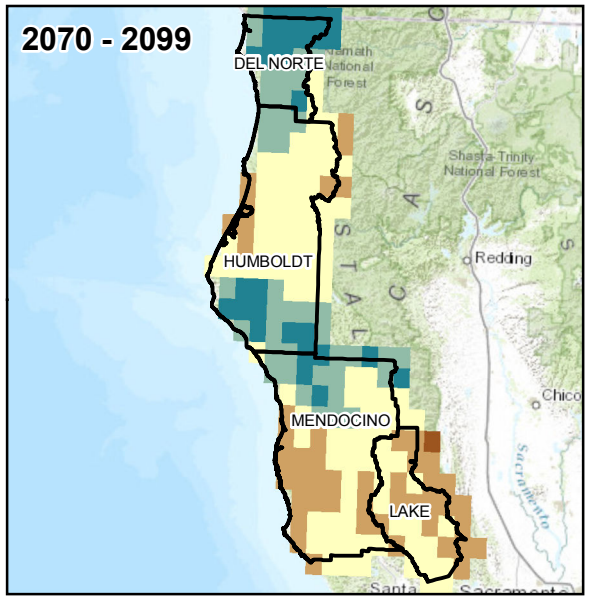

Climate scenario:
B1 (low emissions)

Climate model(s):
Wet GCM (PCM)

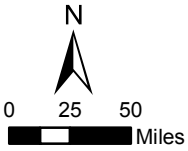

Description:
The 98th percentile precipitation was estimated for a historic period (1970 - 1999 or "Historic") and two future periods (2035 - 2064 and 2070 - 2099) for a wet global climate model (GCM). The top panel presents the 98th percentile precipitation for the wet GCM. The bottom panel shows the percent change relative to the historic time period.

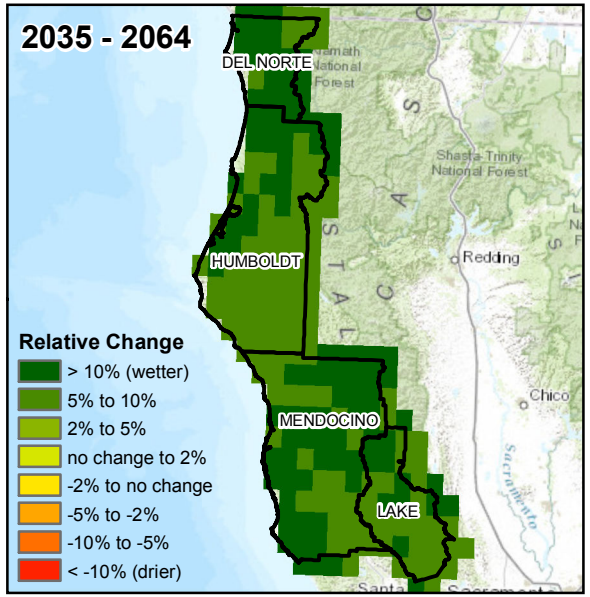

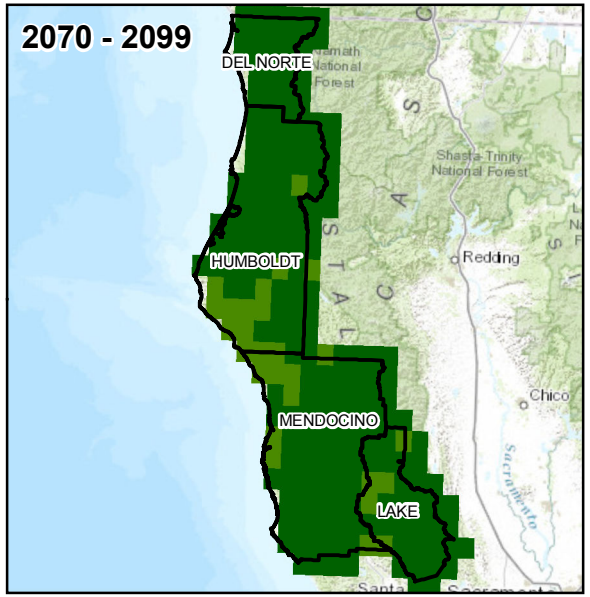

G:\130588_HCAOG-ClimateChange\MXDs\Figures\Precip_98Percentile_11Jun2014.mxd

SOURCE: Cal Adapt, 2014

Figure 10

98th Percentile Precipitation: Average Values and Relative Change for Scenario B1, Wet Model